Preparation of high surface area porous carbons using methane as the carbonaceous feedstock

By

Amos Ramatlhodi Keaoleboga Mosupi

A thesis submitted in partial fulfilment of the requirements for the degree of

Magister Scientiae in Chemistry

UNIVERSITEIT VAN PRETORIA
UNIVERSITY OF PRETORIA
YUNIBESITHI YA PRETORIA
Denkleiers • Leading Minds • Dikgopolo tša Dihlalefi

Faculty of Natural and Agricultural Sciences

University of Pretoria

Hatfield Pretoria

September 2022

Supervisor: Dr. Nicholas M. Musyoka

Co-Supervisor: Prof. Henrietta Langmi

Declaration

I, Amos Ramatlhodi Keaoleboga Mosupi declare that this thesis, entitled "***Preparation of high surface area porous carbons using methane as the carbonaceous feedstock***" which I hereby submit for the degree **Magister Scientiae (MSc)** in the Department of Chemistry, University of Pretoria, South Africa has not previously been submitted by me for a degree at any other tertiary institution.

Signature…… Date…….

Acknowledgement

I would like to acknowledge my supervisor Dr N. Musyoka and co-supervisor Prof H. Langmi. It is through their vision, dedication, and guidance that this project was a success.

I would like to thank Future Leader-African Independent Research awarded to N M Musyoka, HySA and CCU infrastructure and the CSIR for the financial support and University (UP) is also appreciated for providing facilities and support to make this project a success.

My gratitude is also extended to HySA and CCU team at CSIR, carbon group and laboratory for Microscopy and Microanalysis at university of Pretoria for the support. A big thank you to Dr Xoliswa Dyosiba for assistance throughout the study.

Dedication

This thesis is dedicated to my family

My grandmother (Mrs Ntswaki Peele), my mother (Mrs Motshabi Mosupi), my brothers (Mr Boitumelo and Omphemetse Mosupi), and my partner (Miss Refentse Morubisi).

I am thankful for the great support everyone of you has provided throughout this journey. It could not have been an easy journey without the words of encouragement, the wisdom you have shared with me. Thank you for believing in me.

Abstract

Research has recently focused on the adaptation of environmentally benign routes for porous materials synthesis. Porous carbon materials have found applications on gas storage, water purification, catalyst supports, and electrodes for electrochemical double-layer capacitors and fuel cells. Various methods using various carbon precursors have been used to synthesise porous carbon materials. Aim of this study is to develop solid carbons i.e., Templated carbons, MOF derived carbons and carbon nanotubes, using methane (CH_4) from biogas as a carbon precursor.

Biogas, a product of anaerobic digestion, is an attractive renewable energy source due to its continuous production and use cycle. Recently there has been great interests on value addition of biogas, concerning the utilisation of the main component methane (CH_4). In this work we focused on utilisation of simulated biogas (CH_4 and CO_2 mixture) and pure CH_4 for preparation of zeolite templated carbons (ZTC). ZTCs are known to have attractive properties such as high surface area, uniform pores and large pore volumes, and have found applications in gas storage and gas separation. When methane was utilised on both one-step and two-step process, the obtained ZTCs had higher surface area and hydrogen (H_2) adsorption as compared to the simulated biogas feedstock. The high surface area obtained was 2974 m^2/g while the best H_2 storage capacity at 1 bar was 2.77 %wt. Structural (XRD) and morphological (SEM and TEM) characterisation were found to be almost similar to the samples obtained when ethylene was used as a carbon source. The study has proven that sustainable source of feedstock in ZTCs production can be utilised to create value added products.

Metal organic frameworks (MOF) have great properties as porous materials; however, most types are known to have very low thermal stability which can be shortcoming for various applications. Carbonisation strategy can be employed to enhance thermal stability of this porous materials. Two MOFs types (MIL-88B & MIL-101) derived from acid mine drainage waters (AMD) were carbonised to generate carbons which were then tested for hydrogen adsorption and further used to grow carbon nanotubes (CNTs). For the growth of CNTs, CH_4 was used as carbon precursor. The obtained results shown that the MOF structures were completely carbonised and multiwalled carbon nanotubes (MWCNTs) were prepared. Surface area of MOF-derived carbons (MDC-88B and -101) was found to be 267 and 272 m^2/g with hydrogen adsorption of 0.58 wt% and 0.54 wt% respectively. The MWCNTs had a reasonable degree of graphitisation ($I_G/I_D = 1$). This study confirms that AMD derived MOFs can be used as catalyst for synthesis of CNTs and their derived carbons can be used for H_2 adsorption.

Keywords

Carbon nanotubes

Chemical vapour deposition

Matérial Institut Lavoisier (MIL)

Metal organic framework

Methane

MOF derived carbons

Zeolite 13X

Zeolite templated carbons (ZTC)

Achievements during masters study

The subject matter was presented at one conference:

Keaoleboga Mosupi, Ashton Swartbooi, Nqobile Mthembu, Henrietta W. Langmi, Nicholas M. Musyoka, Synthesis of carbon nanotubes over iron-based metal organic frameworks (MIL-88B & MIL-101), 1st sustainable bioenergy and processes conference, Cape Town, 13-15 December 2021

Keaoleboga Mosupi, Henrietta W. Langmi, Xoliswa Dyosiba, Nicholas M. Musyoka, Utilisation of methane as a carbonaceous feedstock the synthesis of high surface area zeolite templated carbons, SACI North section young chemist symposium, University of Pretoria (Pretoria), 28 October 2022

The following are being considered for journal article publications:

1. Keaoleboga Mosupi, Ashton Swartbooi, Nqobile Mthembu, Henrietta W. Langmi, Nicholas M. Musyoka. Synthesis of solid carbons using iron-based metal organic frameworks (MIL-88B & MIL-101)
2. Keaoleboga Mosupi, Henrietta Langmi, Xoliswa Dyosiba, Nicholas Musyoka. Utilisation of biogas(methane) as carbonaceous feedstock for preparation of high surface area zeolite templated carbons

Contents

List of figures

List of Tables

List of equations

Nomenclature

°C	Degree Celsius
BET	Brunauer-Emmett-Teller
CH_4	Methane
CNT	Carbon Nanotubes
CO_2	Carbon dioxide
CVD	Chemical Vapour Deposition
FA	Furfural Alcohol
FAU	Faujasite
H_2	Hydrogen
H_2BDC	Ditopic Terephthalic Acid
H_2O	Water
H_2S	Hydrogen sulphide
HF	Hydrofluoric acid
KOH	Potassium Hydroxide
LSX	low-silica X
MDC	MOF derived carbons
MIL	Material Institute Lavoisier
MOF	Metal Organic Framework
MWCNT	Multiwalled Carbon Nanotubes
N_2	Nitrogen
PSA	Pressure Swing Adsorption

SEM	scanning electron microscope
SWCNT	Single Walled Nanotubes
TEM	Transmission Electron Microscope
TGA	Thermogravimetric Analysis
TSA	Temperature Swing Adsorption
UiO	University of Oslo
XRD	X-ray Diffraction
ZSM-5	Zeolite Socony Mobil–5
ZTC	Zeolite Templated Carbon

Chapter 1

1. Introduction

1.1 General Introduction

Biogas, a product of anaerobic digestion, has many applications, one of which is its application as an energy source. Recently there have been great interests on value addition of biogas, concerning the utilisation of the main component methane (CH_4). Raw biogas is the product of several types of anaerobic species that decompose organic matter under controlled temperature, acidity, and moisture conditions. Various types of materials can be used as organic sources for the production of biogas, e.g. municipality solid waste, animal manure, algae, kitchen remains, crops straws and leaves after decomposition and fermentation under airtight (no oxygen) condition.[1] The constituents of biogas are CH_4, carbon dioxide (CO_2), hydrogen sulfide (H_2S), hydrogen (H_2), nitrogen (N_2), volatile organic compounds (VOCs), siloxanes, carbon monoxide (CO), ammonia (NH_3) and traces of water vapour. Biogas can be utilised in heat generation, electricity or mechanical energy, and as raw material in the chemical industry.

The use of biogas is mainly dependent on the high presence of CH_4, which has high calorific value as compared to other constituents. The higher the presence of CO_2 and N_2, the lower the calorific value of CH_4. Removal of harmful and/or toxic compounds including VOCs, siloxanes, CO and NH_3, which is regarded as "biogas cleaning" is the first step to biogas treatment. This is then followed by biogas upgrading which mainly focuses on the removal of CO_2. CO_2 is subsequently used as a precursor for many other applications such as methanol, dimethyl carbonate, methane synthesis, etc. The product of upgraded biogas, biomethane is then used as a source of fuel and can also serve as a carbonaceous feedstock to produce porous solid carbons.[2-4]

Since they can interact with atoms, ions, and molecules both at their surfaces and throughout the bulk of the material, porous solids are of interest for research. Pore diameters are used to categorise porous materials; for example, micropores are defined as pores smaller than 2 nm. Zeolite materials are mainly dominated by pores below 2nm and are good representatives of microporous material. Mesopores have pores sizes in the range of 2nm to 50nm. Mesoporous silica (M41S family) and Santa Barbara Amorphous (SBA) series of materials are examples of

this group. Pore sizes greater than 50 nm are classified as macropores. Amorphous aluminosilicates and porous glass represent the macroporous class. Distribution of sizes, shapes and volumes of the pores enables porous materials to perform desired functions for specific applications. Therefore, it is important to create uniformity within the pore size, shape and volume as it can lead to superior specific applications properties.[5] For example, zeolites, which are composed of uniform micropores, can separate molecules based on their size by selectively allowing a small molecule to enter the pores, while larger molecules are excluded. The presence of different pore sizes would reduce the ability of the solid to effectively separate molecules of differing sizes. Of other great importance apart from the pore spaces, is the composition of the material. For instance, organic molecules are selectively adsorbed from water by hydrophobic pure silica, whereas molecular sieves consisting of aluminosilicates, such as zeolites, are hydrophilic and can thus separate water from organic solvents. Zeolites also have the ability to adsorb gases however, they lack versatility for functionalisation, which is limited to only a few moieties.[6] Furthermore, the lack of pore size flexibility and the absence of hydrophobicity make them have very limited use.

1.2 Porous carbons

Carbon-based materials and their applications dates back to more than five decades when they were discovered from incomplete combustion of wood. Since then, various types of carbon homologues were discovered, including graphene, carbon fibers, graphite, carbon foam, fullerene, activated carbon, carbon nanotubes, etc. These materials have since been used in different areas including, but not limited to, electronics, aerospace applications, environment, catalysis, energy and so on.[7]Additionally, carbonaceous sorbents are easy to prepare and volumetric density of stored gases can drastically increase on this sorbents.[8] Available number of binding sites directly impacts total capacity of adsorbents thus influencing gas storage by physical adsorption. Applications of porous carbons depend on hydrophobic nature of their surfaces, high surface area, large pore volumes, and chemical robustness in both acid and base medium, good mechanical stability, and good thermal stability. These materials are also attractive because they are featherweight and generally easily available. They have various applications, including chromatography columns, water purification, storage of gases (e.g. natural gas, CO_2 and H_2), electrodes of an electric double-layer capacitor, catalyst support, and gas separation.[9-11] Different porous carbons have been tested as adsorbents such as metal organic frameworks (MOF) derived carbons (MDCs), carbon nanotubes (CNTs), activated

carbons, carbide-derived carbons, carbon fibres, zeolite template carbons (ZTCs) etc.[12-14] Although these materials have many attractive features, they must completely be wash out of contaminants produced during the activation/synthesis process, which is a drawback. Additionally, the molecular structure of activated carbon contains curved polycyclic aromatic molecules of different sizes and shapes which are stacked and connected in very complicated ways. Moreover, some activated carbons have low surface areas and wide pore size distributions, which are not good for gas storage. The control of the shape and the position of each macromolecule in activated carbons is very difficult and proven impossible. Carbon fibers and CNTs have similar low removal efficiencies, poor selectivity, and very small surface areas and pore volumes.[15] ZTCs are superior than carbide-derived carbons in terms of surface area and pore volume.[8, 16] High surface area, high pore volume, and uniform porosity are only a few of the beneficial characteristics of ZTCs and MDCs.

1.3 Problem statement

As mentioned above, biogas is a product of anaerobic digestion that can be applied as an energy source, amongst other applications. Recently, there has been increased interests in the valorisation of biogas with regards to utilisation of the principal component methane (CH_4). In the synthesis of various carbon materials there is a need to use carbon precursors. Glucose, sucrose, ethylene, propylene, acetronitrile and vinyl cyanide are commonly used carbon precursors in the synthesis of porous carbons, however, these carbon precursors tend to be very expensive. Methane, possibly from biogas, can provide a cheaper alternative synthesis of porous carbons such as ZTCs. For the longest time, porous materials have been used to separate and store different components from mixtures. The pore sizes and components that make up a porous material are of great importance towards selectivity of substances. The ability to control pores has played a major role in the storage of different gases such as H_2.[17] Simulated biogas and pure methane are tested as an alternative cheaper method for synthesis of ZTCs and CNTs in this study.

Although MOFs are great materials for gas storage, direct carbonisation of these materials results in higher surface areas, pore volumes, and thermal and chemical stabilities. In this study, MOFs derived from a waste feedstock (acid mine drainage waters (AMD)) are carbonised under inert conditions to obtained MDCs, thereby performing valorisation and potentially providing a cheaper route to synthesise MDCs.

Electronic, mechanical, and structural properties of CNTs have allowed CNTs to be used in various applications. High cost of production of CNTs due to preparation of different catalysts is still unresolved. There is a need to develop an effortless, general, and high-yield method for the oriented formation of CNTs from MDCs. MDCs in this study, contain iron which is a good metal for the synthesis of CNTs. The use of MDC from AMD-derived MOFs potentially provides a cheaper and general method for CNTs synthesis. The goal of this research is to synthesise high surface area porous carbons with potential for use in various applications such as H_2 storage.

1.4 Aims and objectives

Main objective: The main objective of the study is to develop porous carbon materials using methane as the carbonaceous feedstock.

To fulfil the main objective the following sub objectives have been set

- To synthesise ZTCs from methane using commercial zeolite 13X as a hard template via wet impregnation and chemical vapor deposition
- To determine the effect of various carbon sources on the structure of the synthesised ZTCs
- To synthesise MDCs from iron-based MOFs (MIL-88B and MIL-101) derived from AMD
- To synthesise carbon nanotubes from methane using MIL-88B and MIL-101 derived carbons as iron catalysts
- To characterize the developed materials to determine their physical properties using various techniques
- To test H_2 adsorption on the synthesised ZTCs and MDCs

1.5 Hypothesis

Zeolite templated carbons from biogas and methane as carbon precursors via chemical vapour deposition and MDCs will have high surface area and pore volume for gas storage. Multiwalled CNTs are synthesised from MDCs.

1.6 Thesis outline

Chapter 1 gives an introduction of the broad context of the focus of the study. This chapter describes the problem, presents the objectives, and highlights the aim of the study. It further hypothesises the outcomes of the study.

Chapter 2 discusses detailed literature review on various ways in which templated carbons can be synthesised. It further discusses modification of templated carbons. This chapter also reviews the synthesis of MDCs. Synthesis of CNTs, various purification methods and the types of CNTs are also discussed in this chapter.

Chapter 3 outlines the details of the experimental procedures carried out. The experimental conditions and parameters that were taken into consideration as well as the various techniques that were used to characterise the synthesised materials are discussed.

Chapter 4 discusses the results of ZTCs that were made from methane and ethylene as carbon precursors. The obtained carbons were thoroughly compared against each other based on the morphology and textual properties.

Chapter 5 discusses the results of solid carbons synthesised using iron-based MOFs (MIL-88B and MIL-101).

Chapter 6 presents the conclusions and findings that were obtained from the research, and discusses future work and recommendations.

Chapter 2

2. Literature review

2.1 Introduction

The chapter begins with general introduction to the structure and composition of zeolites. It further discusses literature on the synthesis of ZTCs. The second part of this chapter discusses the background and literature on synthesis of MDC. The third part discusses the literature on synthesis of CNTs, types of CNTs, and purification of CNTs.

2.2 Zeolites

Zeolites are crystalline porous aluminosilicates ($[SiO_4]^{4-}$ and $[AlO_4]^{5-}$ tetrahedra) with defined cavities, mobile cations and water molecules.[18-19] It is evident from the formulae that there is a negative charge which lies at each tetrahedron with aluminium as its centre. Within the channels of the zeolites there is water and/or hydrogen and/or sodium ions which compensate for the negative charge. The chemical formula of the zeolite can then be expressed as $M_{x/n}[(AlO_2)_x(SiO_2)_y].wH_2O$ where M is the cation usually the group I or II metals, n is the charge of the atom, x and y comprise the total number of tetrahedra per unit cell and w is the number of water molecules per unit cell. Natural zeolites are formed from volcanic activities, which are hydrothermal. They can be found in igneous, metamorphic and sedimentary rocks.[20] Among natural zeolites only a few (Clinoptilolite, Chabazite, Mordenite, Erionite, Ferrierite, Analcime and Phoilipsite) have several uses. Clinoptilolite occurs abundantly and due to its high acid resistant silica content, it is used in agriculture for soil amendment and feed additives.[21] Natural zeolites main disadvantage is that the pore diameters are too small (for example clinoptilolite has a diameter range of 0.30 – 4 nm), which prohibits adsorption of larger molecules. Additionally, zeolites deposits are non-renewable resources. To overcome these issues, zeolites can be prepared with different chemical compositions and framework structures and over 200 topologies are already reported.[22-23] Structures of zeolite A, zeolite Y, zeolite L and ZSM-5 are shown in Fig. 2.1. Due to the accessible cations that are located within the pores of the zeolite framework, zeolites can be used as ion exchangers. In laundry detergents, zeolites are used to exchange sodium ions for calcium and magnesium ions in order to soften the washing water.[24] They are also useful in adsorbing NH_4^+ ions from contaminated water.[25] The acidity and shape of zeolites makes them suitable for catalytic cracking of hydrocarbons such as heavy feedstocks and naphtha range.

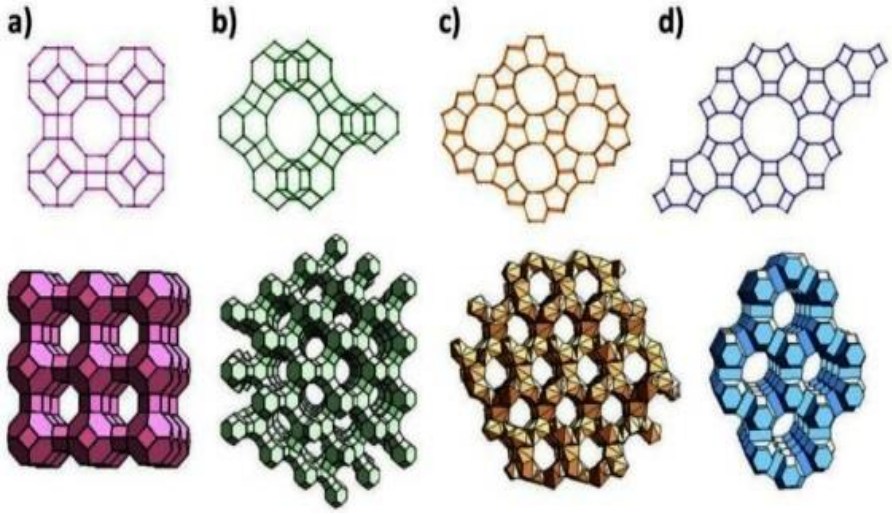

Figure 2.1: Representative zeolite frameworks (a) zeolite A; (b) zeolite Y; (c) Zeolite L; (d) ZSM-5 (silicalite) .[26]

Zeolites play a vital role in industrial gas separation and storage processes, which are based on adsorption at elevated pressures. Gas separation and storage by zeolites depends on different factors such as structural composition, and the presence of guest molecules or compounds in the pores and/or on the surface. The size, polarity, and molecular shape of the adsorbate also plays a role. Zeolites uses the molecular sieving effect, which is favoured by the distribution of uniform pore sizes of these materials. Separation can also occur through selective adsorption of molecules that consists of high energetic dipole and quadrupole. The electrical field created by cations (Na^+) has a strong interaction with molecules that have high quadrupole moments, CO_2 (-14.29 X 10^{-40} $C.m^2$) is an example of such molecules. Zeolites A, X, Y and other naturally occurring zeolites such as chabazites, clintopiles, ferrierites, mordenites have been used as CO_2 adsorbents. Siriwardane *et al.,*[27] showed that zeolites with the highest amount of sodium and surface area, have higher CO_2 adsorption capacity and adsorption rates. Harlick and Tezel[28] tested approximately 13 zeolites, which included 5A, 13X, NaY, ZSM-5, HiSiV-3000 for adsorption of CO_2 from flue gas. 13X has strong affinity towards CO_2 due to low Si/Al=2.2 ratio and high presence of sodium ions. The electrostatic field around sodium has strong selectivity towards CO_2. Cavenati and co-workers[29] concluded that zeolite 13X can be used to sequester carbon dioxide from flue gas as well as to purify CH_4 from biogas and/or natural gas since it preferentially adsorbs CO_2 over CH_4, O_2, and N_2.

Several studies have shown that zeolites can store small amounts of H_2 (<1 wt.%) at room temperature. However, better adsorption (>1 wt.%) can be achieved under cryogenic temperatures.[30-32] Langmi *et al.* [33] investigated H_2 storage on zeolites A, X, Y and RHO and

effects of cation exchange on these zeolites, maximum hydrogen storage (1.81 wt.%) was observed on zeolite NaY. Streb and Mazzotti [34] tested H_2 adsorption on pelleted zeolite 13X at various temperatures and up to 30 bar and achieved H_2 uptake of 3, 3.5 and 4 mol/kg at temperatures of 25 , 45, 65 °C. Clay derived zeolites were used by Musyoka *et al.* [35] to test H_2 adsorption and H_2 uptake of 0.3 wt.% was achieved. To combat the lack of high surface area of zeolites, carbonaceous materials such as ZTCs with pre-determined nanoporosity and high pore volumes can be used to improve gas adsorption. Such materials have high potential to achieve considerable amount and reversibility H_2 adsorption. Introducing a carbon precursor into the channels of the zeolite followed by carbonisation and ultimately acid etching of the zeolite results in ZTCs.

2.2.1 Zeolite 13X

In this study, zeolite 13X with the formula $Na_{86}[(AlO_2)_{86}(SiO_2)_{106}]\bullet H_2O$ is adopted as the sacrificial template. It is hydrophilic crystalline material and dominated by microporous. The sodium X zeolite type is made of β-cages and supercages (surrounded by the β-cages) as shown in Fig 2.2. Supercages have the inner diameter of ~ 7 Å and outer diameter of ~ 13 Å.[18] The pore structures of zeolite 13X are 3D and connected by circular 12-ring apertures. Zeolite 13X contains more cations and has low Si/Al ratio as compared to zeolite Y. The adsorptive properties of these properties are influenced by the electric field around the cation (inside the pores) as well as the available pore volume. Zeolite13x is generally synthesised using sodium aluminosilicate gels precursors via hydrothermal synthesis route. Silica and alumina can be obtained from wide range of sources such as fly ash.

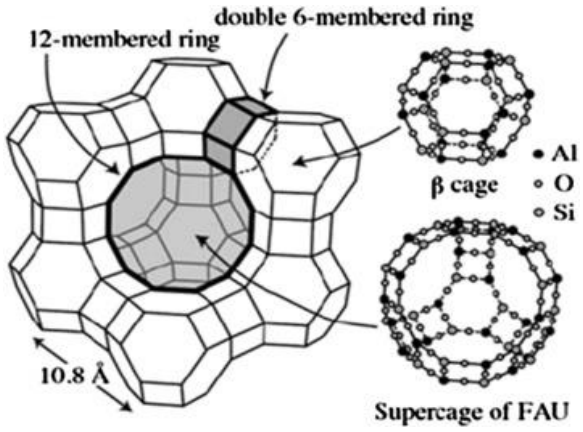

Figure 2.2: Schematic illustration of FAU framework and typical cation sites in low-silica X (LSX) zeolite.[19]

2.3 Zeolite templated carbons

Zeolite-templated carbons (ZTCs) are microporous, amorphous carbon materials with a very high surface area and homogeneous pores that complement the structure of the zeolite utilised in the template carbonisation synthesis.[36] Zeolites are suitable for replication processes because the size of their pores and channels are quite similar to the geometry of organic molecules used in replication. If carbon is deposited in the cages of the zeolite, and then detemplated from the zeolite framework, carbons whose structure is similar to the pores of the zeolite can be expected. The size of the pores of the zeolite determines the rigidity of the porous carbon, if the pores are too small carbon deposition becomes difficult. The unfilled pores lead to collapsing of the regular structure after zeolite washing with the acid. Even though all channels can be filled, the structure of the porous carbon can still collapse.[37]

Thus, ZTCs can be classified into three groups as follows:
Type I: ZTCs that have completely 3-dimensional ordered framework replicated by the zeolite template. The ZTCs have high surface area with no graphene stacking.
Type II: Similar to type I but with extra deposited carbonaceous components outside the channels of the hard template.
Type III: These materials show no mimicking of the parent zeolite, they are very disordered materials.[38]

The first ZTC with structure regularity was reported by Kyotani *et al.* [37] using the montmorillonite layered clay in 1988 which was recently visited by Mayers *et al.* [39] using the commercialised montmorillonite-layered clay. During zeolite templated synthesis, zeolites such as zeolite Y, mordenite, zeolite beta or zeolite L are impregnated with substrate or precursor materials such as acrylonitrile, poly-(acrylonitrile) , poly(furfuryl alcohol) or phenol formaldehyde polymers,[40-42] so that the obtained carbons, retain the structural ordering of the zeolite. Two types of synthetic routes (one- or two-step processes) have been investigated. The one-step process involves impregnation of organic precursor, either using a polymeric solution or gaseous feedstock. The two-step process involves the use of both polymeric solution and gaseous feedstock. Carbon loading is then followed by carbonisation at 700-900 °C and detemplation of the zeolite via acid etching. Fig 2.3 shows a general representation of ZTC synthesis.

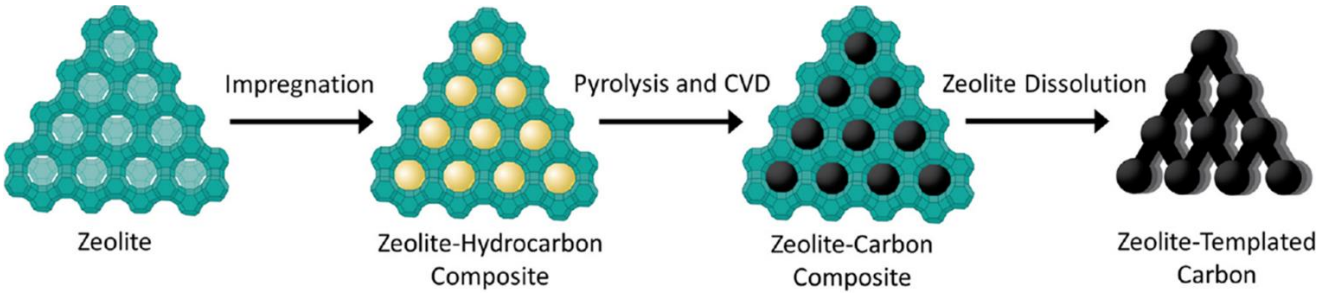

Figure 2.3: A general representation of ZTC synthesis.[43]

Ma *et al.* [41] used zeolite Y as a hard template to achieve highly ordered pore structure. Kyotani and co-workers [37] tested the use of zeolites beta, ZSM-5, mordenite and zeolite L as templates synthesis of porous carbons and concluded that the zeolite beta had better structural regularity followed by zeolite L, modernite and ZSM-5. They further explained that carbons obtained from zeolite Y have a better structural regularity than zeolite beta. The size and shape of the channels plays a major role on structural regularity of the prepared carbons. Higher structural regurlarity is often achieved when templates have pore channel that are 3-dimensional and have sizes large than 0.6 nm as long as chemical vapour deposition (CVD) is employed as a carbon filling method.[37] Kyotani and co-workers [37] further attributed the poor structural regularity obtained for zeolite L as due to the external deposition of ethylene on the surface of the zeolite. Zeolites which are normally used as acid catalyst are frequently poisoned by the formation of coke on the acidic sites. In ZTC synthesis, coke formation is advantageous as it favours carbon loading inside the nanopores of zeolite. ZTCs synthesis is favoured by low Si/Al ratio (high Al content) of the zeolite. Furthermore, the use of H-type zeolite (i.e., zeolite containing H^+ as the exchangeable cation) is prohibited for the synthesis of ZTCs. When ploymeric carbon precursor such as furfuryl alcohol attaches to H-type zeolite it polymerises and pore blockage occurs, resulting in inadequate loading of the zeolite with FA.[26]

Masika *et al.* [44] used zeolite 13X as hard template and ethylene as carbon source to synthesise ZTCs with great structural similarity as shown by the XRD patterns with a peak at $2\theta = 6.3°$ which is similar to that of zeolite 13X. Pore size distribution measured by N_2 isotherms, corresponded to those previously reported for ZTCs. Balahmar *et al.*[45] obtained a surface area of 1927 $m^2.g^{-1}$ using zeolite 13X as a hard template. Rambau *et al.* [46] reported ZTCs with large specific surface area of 3341 $m^2.g^{-1}$, and high microporosity and hydrogen uptake. Mokaya and Pacula[47] reported hydrogen uptake of 2.3 wt.% at 1 bar on ZTCs, utilising zeolite β as a hard template. Nitrogen-doped ZTCs were prepared and tested for hydrogen uptake by Xia *et al.*[48] and uptake of 6.0 wt.% at 20 bar was reported. Potassium hydroxide (KOH) chemical activation of ZTCs

enhanced the textural characteristics of these carbons, hence enhancing hydrogen uptake. Surface area increased from 1400-1650 m^2/g to between 1850 and 3100 m^2/g, whereas the pore volume rose from 0.8-1.1 cm^3/g to 1.5-1.75 cm^3/g resulting in increased hydrogen uptake capacity (at -196 °C and 20 bar) of between 60 and 96% from 2.4-3.5 wt % for ZTCs to between 4.3 and 6.1 wt %.[49]

The high cost of production (as a result of expensive zeolites, carbon precursors and the process) of zeolites inhibit the scale up production of zeolite templated carbons. Holler and Wirsching [50] were the first to synthesise coal fly ash derived zeolites, after realising that coal fly ash has similar composition as some volcanic material precursor of natural zeolites. Musyoka *et al.*[51] used Zeolite X, made from coal fly ash, as a cost-efficient and competitive method of making templated carbons. This method does not only present cost-effective way of producing zeolites but also plays a huge role on reducing environmental pollution. More alternative cheaper and environmentally friendly methods need to be developed. In this study, simulated biogas and methane are used as carbon precursors which will afford a cheap alternative approach for ZTC synthesis.

2.3.1 Synthesis techniques for zeolite templated carbons

With the flexible deposition process known as chemical vapor deposition (CVD), gaseous substrates are broken down into reactive species that then build films or particles.[52] The versatility of CVD is demonstrated by various substrates and precursors that can be used to deposit a given thin film.[53] The controlled production of nanomaterials in porous templates, particularly zeolite nanopores, has become a new focus of CVD techniques.[40, 54-57] In CVD, substrate temperature affects the rate of film growth while vapor super saturation affects the nucleation rate of the film. These factors influence epitaxy, grain size, grain shape and texture. Growth of a single crystal film is supported by low gas supersaturation and high substrate temperatures, whereas polycrystalline, nanocrystalline and amorphous films are influenced by high gas super saturation and low substrate temperatures. There are various types of CVD processes and reactors, each process is influenced by the type of precursor, deposition conditions and the forms of energy introduced to the process to establish a chemical reaction. The following are well established processes: (1) Metal-organic CVD - used when the precursor is a metal-organic substance (e.g., triethylaluminum, trimethylgallium); (2) Plasma-enhanced CVD - When microwave-based plasmas are used to initiate or promote chemical reactions; (3) Low-pressure CVD - it works under low gas pressure; (4) Laser-assisted CVD - laser is used to

promote chemical reactions; (5) Aerosol-assisted CVD - to make evaporation easier, liquid precursors are introduced into the reactor as a form of aerosol.[58] The advantages of CVD technologies include the capacity to consistently deposit thin films of materials, even on irregular shapes, and to controllably generate films with widely varied stoichiometry.

Wet impregnation is frequently used in the synthesis of amine-containing adsorbents. Amine compounds are typically dissolved in methanol or other solvents. After that, porous substances are added to the solution. Solvents are evaporated to produce the adsorbents.[59]

Ma *et al.* [41] synthesised a three-dimensional nanoporous structure using zeolite Y template, by heating zeolite/polyfurfuryl alcohol (PFA) composite to 700 °C in inert atmosphere. At 700 °C, propylene was introduced to complete CVD process. After the CVD, the material was further carbonised at 900 °C under inert conditions. Zeolite was detemplated by acid treatment. Musyoka *et al.* [35] recently prepared templated carbons using clay and clay derivatives where furfuryl alcohol (FA) was impregnated into the clay samples followed by polymerisation at 80°C for 24h and 150°C for 8h under the flow of argon gas. The temperature of the furnace was increased to 700°C at a heating rate of 5°C/min and maintained there for 3h to carbonise the material.

2.3.2 Modification of ZTCs

I. Porosity enhancement

Disordered pore (type III) can be achieved by heat treating the zeolite/carbon composite above the zeolite stability temperature. The disordered zeolite framework will still act as template which will easily provide highly porous carbons where S_{BET} can be as high as 3683 m^2g^{-1} .[38]

II. Chemical modification

The functions of ZTCs can be enhanced by addition of heteroatoms such as nitrogen, boron, sulphur and oxygen. N-Doping is effective to improve hydrophilicity, B-doping enhanced hydrogen storage and Enhanced heat of adsorption for H_2 and CO_2 was seen in S-doped ZTCs.[60] Additionally activation of type II and III ZTCs can result in high porosity. Activation by CO_2, KOH and H_3PO_4 have led to the highest S_{BET} of 3064 m^2 g^{-1} although not as high as for type I ZTCs.[49]

III. Shaping of ZTCs

High surface area materials typically have low packing densities, which has an impact on the volumetric uptake of gases. Densification or compaction can be used to enhance density thus improving volumetric uptake. Pores of most porous materials collapse even at the slightest compaction, however due to the high mechanical stability of ZTCs moderate compaction pressure can densify the material with moderate loss of pore structure.[45] Zeolites are known for their great mechanical stability, which inspired Balahmar *et al.*[45] to investigate the impact of fabricating ZTCs from compressed zeolite pellets. The compaction increased the density of the zeolite by 50%, due to the reduced inter-particle voids. The structural properties of the zeolite remained unchanged as confirmed by N_2 adsorption isotherms and X-ray diffraction (XRD).

To increase the volumetric gas absorption of ZTCs, Kyotani and co-workers [61] employed a hot-pressing technique at 300 °C and 147 MPa without the use of a binder and attained packing densities of between 0.7 and 0.9 g/cm^3. This method affords pore size control by varying the hot-pressing pressure.

A high voltage source is used in the versatile, readily scaled-up process of electrospinning, which draws fibers from a polymer solution via a needle and onto a metal collector plate. Annamalai *et al*.[62] studied extremely porous ZTC encased in electrospun fibers, and the resultant composites were tested for hydrogen storage. The obtained composite had retained 76% H_2 uptake as compared to the powdered ZTCs sample.

Molefe *et al.*[63], used a polymer with intrinsic microporosity to provide a straightforward monolith shaping method for ZTCs and their MOFs composite (PIM-1). The ZTC and PIM-1 composite had improved thermal stability, although the thermal stability of the composite made up of the three filler components (PIM-1, UiO-66(Zr), and ZTC) was lower, it was still within the desirable ranges for most porous materials. The surface area of the composite was determined to be between 1054 and 2433 $m^2.g^{-1}$.

2.4 Metal-organic framework derived carbons

In this research iron-based metal-organic frameworks (MOFs) derived from acid mine drainage waters (AMD) are carbonised to produce porous carbons. AMD is produced when sulphide bearing rocks are exposed to water and oxygen.[64] Although this process occurs naturally, mining can accelerate it by exposing sulphide bearing rocks to oxygen and water. Due to their elevated amounts of metals like iron, aluminum, manganese, and other heavy metals, AMD

constitutes a risk to the environment.[65] Metals can be recovered as hydroxides by precipitating with alkaline solutions. This method affords easy control of the pH, it is economically viable and can be applied to large operating units.[66] Iron extracted from AMD can be used for the synthesis of Matérial Institut Lavoisier (MIL-88B and MIL-101) MOFs, shown in Fig. 2.4 below.

MOFs are made of metal ions/metal clusters connected to organic molecules through coordination bonds. MOFs are special for their high porosity, thermal stability, large internal surface area, very low densities, ease of synthesis, among others. Their properties make them suitable for applications in drug deliveries, chemical sensors, gas storage and separation. They are suitable for catalysis because of the easily accessible uniform metal centres.[67] MIL-101 and MIL-88B consist of iron(III) octahedral clusters interconnected by 1,4-benzenedicarboxylate anions.

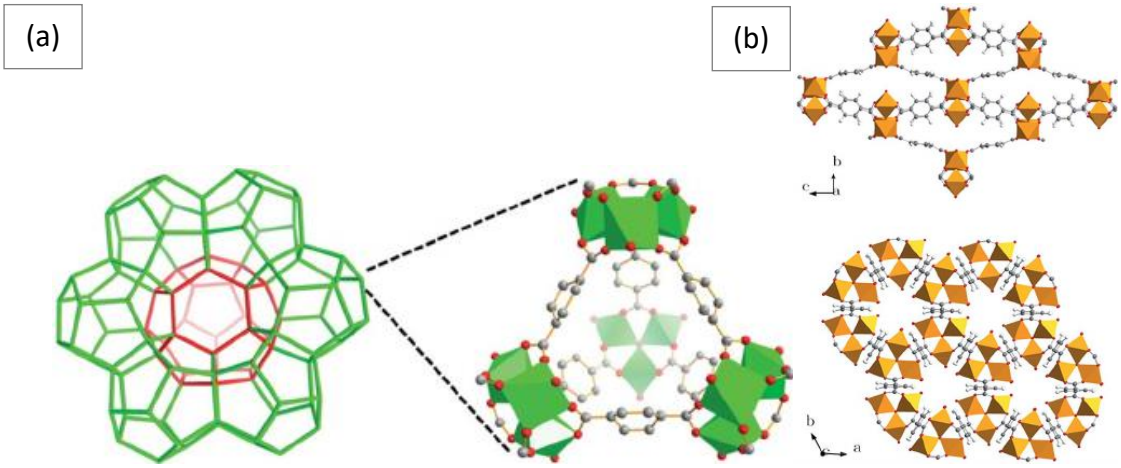

Figure 2.4: (a) left: zeotype crystalline structure of MIL-101.[68] (b) MIL-88B structure viewed along a axis (top) and c axis (bottom).[67]

Similarly, to MOFs, nanoporous carbons have gained interests as adsorbents due to the high porosity, large surface areas, high thermal stability, low density and inexpensiveness. MOFs can be turned into porous carbonaceous materials via direct carbonisation and/or pyrolysis, by physical or chemical activation of organic precursors, carbonisation of polymeric aerogels, chemical vapor deposition (CVD) and template synthetic procedures.[69-71] MOFs can be carbonised to make MOF derived carbons (MDCs) which can later be tested for adsorption perfomances. The fabrication of MDCs can be achieved via two routes: Direct carbonisation and template impregnation followed by carbonisation. In direct carbonisation, thermal treatment of MOFs can be used to change their structures into nanocomposites made of metal/metal oxides and carbon material. Calcination of MOFs must be conducted under inert atmosphere (i.e., nitrogen or argon).[72] Some of the metals vaporise at the working

temperatures and the remainder can be removed chemically.[73] For the template impregnation method, MOFs are impregnated with carbon containing liquid, which acts as a carbon precursor, and then the impregnated MOF is carbonised. Liu *et al.* [71] impregnated MOF-5 with furfuryl alcohol and carbonised it at 1000 °C for 8 h under inert atmosphere. ZnO was reduced and Zn metal vaporised (boiling point: 908 °C) with argon. The prepared carbons had hydrogen adsorption of 2.6 wt% at 1 bar. Van Tran *et al.* [73-74] utilised MIL-88B for generation of MDCs, the MOF was prepared by combining Fe cluster and 1,4-benzendicarboxylic acid (H_2BDC). The prepared MDCs had a decreased surface area (202 m^2/g) at temperatures above 600 °C. Lee *et al.* [75] prepared MIL-88B MDCs which exhibited surface area increase (170 – 265 m^2/g) with an increase in temperature (600 – 800 °C). Tran *et al.* [74] prepared amino-functionalised MIL-88B MDCs for adsorption of ciprofloxacin from aquatic solutions. MIL-101 has also been carbonised and used as sorbents for stir bar sorptive-dispersive microextraction of sulfonamides by Qin *et al*.[76] The obtained surface area for the MDCs was at 129.5 m^2/g at 900 °C. In this study, MDCs will be tested for H_2 adsorption and investigated for their catalytic ability for the synthesis of carbon nanotubes.

2.5 Carbon nanotubes

Since the unearthing of carbon nanotubes (CNTs) by Iijima[77] in 1991, CNTs have been used for various applications such as gas storage, as electrode materials for electrochemical double layer capacitors, as electron field emitters, catalyst supports, biomedical applications, biosensors for toxic gases and as material for probe tip for atomic force microscopy. The distinct structural, electrical, mechanical, electromechanical, and chemical properties of CNTs determine the uses for them.[78] The synthesis of CNTs can be achieved using the arc-discharge method which requires the use of high temperatures (>1700 °C). Another technique for making CNTs is laser ablation, but it too has problems with high temperatures.[79-81] Catalytic chemical vapour deposition (CCVD) has been used to prepare single and multi-walled carbon nanotubes (SWCNTs and MWCNTs) by catalytic breaking down of various hydrocarbons. The use of a catalyst has helped in lowering the high temperatures to below 1000 °C. When certain parameters are controlled, long SWCNTs or MWCNTs can be produced with low defects, less impurities and high yields.[78] This method affords scale up production of CNTs.

2.5.1 Types of CNTs

Single-walled carbon nanotubes (SWCNTs) and multi-walled carbon nanotubes are the two main types of carbon nanotubes (MWCNTs) see Fig. 2.5. SWCNTs are cylindrical materials that

are made up of rolled up single layer of carbon atoms called graphene. When another layer of graphene rolls on top of the other, there results a double walled carbon nanotube. Additional layers of graphene sheets result in the formation of MWCNTs. The name "nanotubes" comes from the nanometer (10^{-9} m) sized diameters, and they are usually few micrometers long. These cylindrical carbon molecules have special qualities that could be advantageous for the aforementioned uses in nanotechnology. CNTs have a black soot physical appearance and are chemically stable at room temperature and pressure.

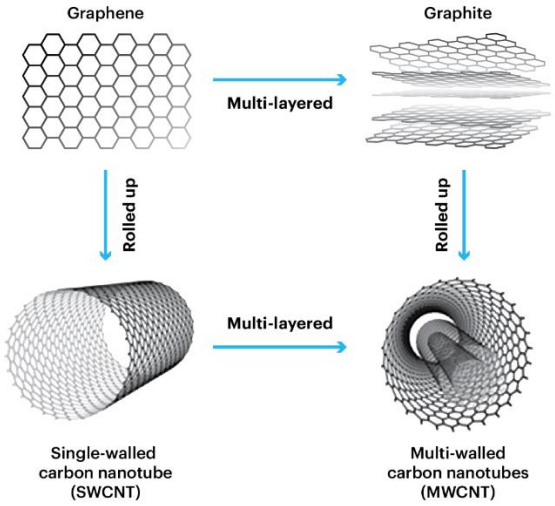

Figure 2.5: Types of CNTs defined by the rolling graphene sheets.[82]

2.5.2 Properties of CNTs and applications

I. Mechanical properties

CNTs exhibit extraordinary mechanical properties; Slavetat *et al.*[83], Treacy *et al.* [84], Pipes *et al.* [85] reported a Young's modulus of approximately 1 Tera Pascal and 100 times tensile strength as compared to most steels. Young's modulus is affected by the disorder in the CNTs structures, the high the amount of the disorders the lower the Young's modulus. Additionally, CNTs are very flexible as they can be bent few times at a right angle without any structural damage.

II. Electrical and thermal conductivity

Depending on helicity, CNTs can be classified as conductive or semiconductive materials which will lead to nanoscale wires and electrical components. The symmetry, unique electronic and tubular porous structure, specific surface area, pore size distribution and surface characteristic of graphene, ensure that CNTs have high current carrying capacity.[86] These properties of CNTs favour fast ion and electron transportation.[87] The unique structures and small size of CNTs enhances their Thermal properties. Diamond is held together by sp^3 bonds and has high

thermal conductivity, since CNTs are made of sp^2 bonds they are expected to have even higher thermal conductivity.[88] Hone[89] recorded thermal conductivity of over 150 W/m K at room temperature for bulk samples of SWCNTs, while individual MWCNTs had a conductivity of over 3000 W/m K. In order to evaluate the thermal conductivity of CNTs and how it varies with temperature, Berber *et al.* [88] coupled equilibrium and nonequilibrium molecular dynamics simulations with precise carbon potentials. They obtained 6600 W/m K for an isolated CNT at room temperature and this figure is comparable to that of diamond.

2.5.3 Growth mechanism

CNT growth mechanism is still a widely debatable process. Nevertheless, a general mechanism can be explained as follows: A hydrocarbon breaks down into carbon atoms and hydrogen, with the carrier gas transporting the hydrogen. Carbon is absorbed and dissociates on the catalyst metal surface, as-dissolved carbon precipitates then forms solid cylindrical networks with no dangling bonds. The process is maintained by the exothermic nature of the hydrocarbon decomposition, where the heat is transferred into the metal surface and the endothermic reaction of the carbon crystallisation (solid cylindrical networks), where the heat is absorbed from the metal surface.[90-92]

The above process can take place in two ways, i.e, tip growth and root/base growth models, see Fig. 2.6. The tip growth mechanism transpire due to the feeble interaction of the catalyst and the support. Hydrocarbon decomposes on top of the metal catalyst then carbon diffuses into the bottom of the metal, CNT precipitates thus dislodging the metal from the support. The growth gets terminated when the metal catalyst in covered with carbon (catalysts gets deactivated). Root/base growth occurs when when there is a substantial interaction between the metal and the support. In this case, hydrocarbon decomposes at the bottom of the metal and then carbon is forced to precipitate on top of the metal since the metal cannot be dislodged from the support. CNT then grows with the metal lodged on its root/base. The process is terminated once the metal is covered with carbon. [93-96]

3.

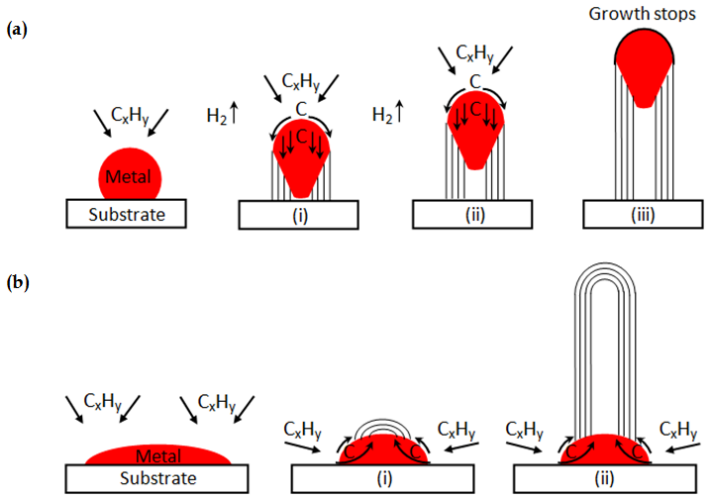

Figure 2.6: Proposed growth mechanisms for CNTs: (a) tip-growth model, (b) basegrowth model.[93]

2.5.4 CNT synthesis methods

Many researchers have targeted the preparation of high quality and high yield of CNTs. Arc discharge, laser ablation, and chemical vapour deposition are the three most popular processes for making CNT. There are other methods which are not popular and still being developed such as autoclave synthesis and metal-free catalytic CVD.

I. Arc-discharge method

CNTs were first synthesised using the arc-discharge methods by Iijima in 1991.[77] This technique produces CNTs by evaporating carbon under direct current (dc) arc discharge in the presence of an inert gas (He or Ar) at low pressure (500-700 mbar). Typically, a 100 A current is fed through two carbon rods or electrodes that are put end to end and spaced apart by about 1 mm, forming a plasma between them. Carbon on the anode is vaporised and deposited on the cathode when the plasma's generated temperature hits 4000 K. As the carbon is deposited on the cathode, the distance between the two electrodes is decreased. To keep the distance constant, the anode must continuously be moved. The anode's diameter is kept smaller than the cathodes, and both electrodes are cooled by water. It is important to maintain a constant current flow as to avoid fluctuating arc which will result in unstable plasma and affect quality of the CNTs.[97-99] Lots of researchers have used and published many reviews about the arc discharge method. In 2006, Ando and Zhao [100] mass produced SWCNTs and MWCNTs with high crystallinity using the arc discharge method. Harris *et al.*[101] investigated the solid state growth mechanism for CNTs and discovered that heating rate also plays important role in

promoting CNT growth. Tessonnier and Su ,[102] Prasek *et al.*,[103] Journet *et al.* [104]and many other researchers have looked at the synthesis of CNTs using the arc discharge method.

II. Laser Ablation

In this method, a pulse or continuous laser strikes and vaporises a mixture of graphite and metal catalyst (Ni, Co) target, in the presence of an inert gas such as helium or argon at a pressure of 500 Torr (67 kPa) in a 1473 K furnace. Gou *et al.* [105] discovered this method when they were studying the effect of laser impingement on metals. As the target is vapourised, there is a formation of C_3, C_2, C and catalyst vapour clouds. As the vapours cool, the smaller carbon species combine to form large carbon molecules and adhere to slowly condensing metal catalysts which prevents the formation of cage structures. The process is terminated when the conditions have cooled or by large catalyst clusters.[106-107]

III. Catalytic chemical vapour deposition

Catalytic chemical vapour deposition (CCVD), in addition to arc-discharge and laser ablation, is a particularly effective technique for making SWCNTs and MWCNTs. In the CCVD synthesis process, hydrocarbons break down in the presence of a catalyst between 500 and 1000 °C. Different types of CVD have been employed, such as fixed bed, fluidised beds, aerosol, floating catalysts, and plasma-enhanced CVD. Various metal catalysts such as iron, cobalt, nickel, molybdenum on supports like MgO, SiO_2, Al_2O_3, CaO and ZrO_2 prepared by impregnation, co-precipitation, or sol–gel processes, have been used for the production of CNTs.[78, 108] Unsupported catalysts such as metallo-organic (ferrocene, iron pentacarbonyl) compounds can be used. The use of a catalyst has helped in lowering the high temperatures to below 1200 °C. This method affords scale up production of CNTs. When certain parameters are controlled, long SWCNTs or MWCNTs can be produced with low defects, less impurities and high yields.[78]

The fixed bed method was first employed by Yacaman *et al.* [109] in 1993, they decomposed ethylene at 700 °C over graphite supported iron particles. The decomposed carbon piled on the metal surface and grew into tubular structures. In this process a boat carrying the catalyst is placed inside the tube furnace and a hydrocarbon is passed through the heated furnace, this process can take place over minutes or hours. This method has limitations in the amount of catalyst used, the larger amounts of catalysts with respect to the surface area of the boat increases the depth of the catalyst, thus making it difficult for hydrocarbons to decompose on the metals at the bottom of the boat. This was further supported by Kathyayini *et al.* [110] when they observed that the same amount of CNTs is formed when 1 g or 0.5 g of the catalyst was

used. Zeng *et al.* [111] proved that CNT yield improved by more than 3 times when the catalyst is shared amongst two boats as compared to filling one boat. The larger the contact area the better the yield.

Since CCVD is the most suitable method for scale up synthesis of CNTs, research on new effective catalysts is essential. Pérez-Cabero *et al.* [112] suggested that, because the interaction between produced carbon and metal particles is thought to be less structure-sensitive with Fe than with other CNT growth catalysts, the development of CNTs over Fe catalysts occurs more readily. Surface area and porosity of support material controls the dispersion of the transition metal particles which then influences CNTs production.[78]

2.5.5 Purification of CNTs

The prepared CNTs normally contain carbonaceous impurities and metal catalyst particles. Amorphous carbon, fullerenes, and carbon nanoparticles are the most occuring carbonaceous impurities. Laser ablation and arc discharge methods make use of graphite rods as source of carbon, the un-vapourised graphitic partciles normally exist as impurities.[113] CNTs can be purified using three methods, namely chemical, physical and combination of both. The chemical method is based on selective oxidation of carbonaceous impurities and dissolution of metal catalyst impurities. The physical method separates impurities according to their sizes, aspect ratio, gravity and magnetic properties. The third method, uses the combination of selective oxidation and physical properties.

i. Chemical oxidation

Selective oxidiation purification method can be achieved in both wet and dry conditions. Wet conditions involves the use of concentrated acids or strong oxidants (HNO_3, HCl, H_2SO_4). Dry conditions mainly refer to the use of air, oxygen or other gases at controlled temperatures. This method is based on the fact that amorphous carbons and carbon nanoparticles (CNPs) can be eliminated easily due to their high oxidations rates. As a result of dangling bonds and other structural features that are easily oxidised, amorphous carbons oxidize at a faster pace. The large carbon curvature and pentagonal rings on the CNPs ensures that they have high oxidative activity. [113-115] This method results in opened tubes, damaged surface structures and introduces oxygenated functional groups on the CNTs.

The wet condition method has gained great attention due to its high efficiency and easy to implement conditions. In this method, CNTs are refluxed in a concentrated acid to dissolve

carbon impurities and metal particles. Dong *et al.* [116] sonicated CNTs in concentrated nitric acid and sulfuric acid and they observed that the acid mixture attacked the C-C bonds and introduced defects and oxidised the CNTs at the defects sites leading to shorter CNTs. However, this method was successful in removing the metal particles and amorphous carbons. Mohanapriya and Lakshminarayanan [117] and Delpeux *et al*.[118] refluxed CNTs in nitric acid for short period of ~30 min and they realised that tubes are opened and metal particles are removed with minimal structural damages. Today, reaserchers have estabilished several acid refluxing methods over a wide average duration, acid concentration and temperature to minimise structural damage to the CNTs.

Apart from the wet conditions, dry gas purification can be used. In this method, CNTs are purified under an oxidising atmosphere at a temperature range of 200 – 750 °C. Air, steam, mixture of Cl_2, H_2O and HCl, a mixture of O_2, SF_6 and $C_2H_2F_4$, are the commonly used oxidants.[113] The oxidants react with the CNPs and amorphous carbons far greater than the walls of the CNTs, thus effectively removing the impurities. Ajayan *et al.* [119] oxidised the CNTs in air for 30 minutes at 750 °C, but they only got a small sample of pure CNTs (1-2 wt%). This was attributable to the unequal CNT exposure to the oxidant and the low CNT-to-impurity selectivity during oxidation. The purified yield of CNTs was enhanced to about 35 wt% by Park *et al.* [120] utilising a spinning quartz tube to equally expose the CNTs and impurities to the oxidant at 760 °C for 30 min.

ii. Physical based purification

Chemical purification has a problem of destroying the structure of CNTs or change surface properties. To preserve the structural and surface properties of CNTs, physical purification method can be used. Impurities have different sizes, aspect ratio, gravity and magnetic properties which enable physical separation. Various physical methods such as filtration, centrifugation, chromatography, electrophoresis, and high temperature annealing have been used.

Filtration is mainly based on physical properties such as size, aspect ratio, and solubility of carbons. Different filtration membranes have been developed to separate CNTs from impurities and to separate CNTs of different sizes. Particles of smaller size and those that are soluble in organic solvents (toluene, CS_2) can be filtered out. Bonard *et al.* [121] and Shelimov *et al.* [122] used the combination of filtration and sonication to purify MWCNTs. The CNTs were immersed in a mixture of water and sodium dodecyl sulphate and a stabilised colloid suspension was formed.

Successive filitrations were carried out to achieve the highest purity. Abetemarco *et al.* [123] arranged filtration membranes in the order from large pores to small pores, all large particles were retained by the large pore sized membranes, while the small CNTs were retained by the small pore sized membranes. The large particles normally block the pores thus making the filtration slow and inefficient. This method preserve the structure of CNTs.

Centrifuge separates particles based on their response towards gravity. Different masses of particles will gravitationally sink in a tube at various rates. Amorphous carbons can be separated from CNTs using a low speed centrifugation. CNPs are separated from CNTs using a high speed centrifugation. The short fall of this process is that CNTs need chemical oxidation with nitric acid, which introduces fuctional groups to their surfaces.[124-126]

iii. Multi-step Purification

A multi step purification is necessary when single step purification can not effectively remove impurities present in CNTs. Combination of chemical and physical purification in multi-step purification can be used to effectively remove amorphous carbons, CNPs, and metal particles. Montoro *et al.* [127] implemented a multi-step purification which was made of four procedures. Fullerene and other soluble impurities were removed through the Sohxlet extraction, amorphous carbons were effectively removed by liquid oxidation using H_2O_2. Metal particles were removed in the presence of nitric acid, hydrofluoric acid and sodium dodecylsulphate (SDS). The product was filtered and dispersed in SDS to remove the graphitic and protected metal particles.

2.6 Chapter summary

This chapter is subdivided into four subsections reviewing zeolites, ZTC, MDCs and CNTs. The first subsections explain characteristics of zeolites and give examples of natural found (i.e., Clinoptilolite, Chabazite, Mordenite, Erionite, Ferrierite, Analcime and Phoilipsite) zeolites and their uses. Synthetic and natural zeolites have been tested for gas storage such as H_2. Several studies have shown that zeolites can store small amounts of H_2 (<1 wt.%) at room temperature. However, better adsorption (>1 wt.%) can be achieved under cryogenic temperatures.

Second subsections explain ZTCs and their characteristics. ZTCs are synthesised via CVD, wet impregnation or combination of CVD and wet impregnation. The amorphous microporous carbons have a promising H_2 storage capacity due to their large surface area as compared to their templates (Zeolites). Certain modification can be done on ZTCs to enhance gas adsorption. Modifications such as doping with heteroatoms (Nitrogen, Boron, sulphur) or activation by CO_2,

KOH and H_3PO_4. Densification or compaction can be used to enhance density thus improving volumetric uptake of gases.

Third subsections focus on MDCs derived from Fe-MIL88B and Fe-MIL101. The iron MOFs are derived from AMD. Iron metals are recovered from AMD as hydroxides by precipitating with alkaline solutions. The as-synthesised MOFs are then carbonised with the aim to increase surface area, H_2 adsorption, thermal and chemical stability.

The last subsections explain synthesis of CNTs utilising MDCs as catalysts. Various synthetic methods are reviewed, and CVD is the most suitable method for CNTs. Amorphous carbons, fullerenes, and carbon nanoparticles are common carbonaceous contaminants found in freshly manufactured CNTs, along with metal catalyst particles. There are three ways to purify CNTs: chemically, physically, or by combining the two.

Carbon based materials and their applications dates back to more than five decades when they were discovered from incomplete combustion of wood. Since then, various types of carbon homologues were discovered, including graphene, carbon fibers, graphite, carbon foam, fullerene, activated carbon, carbon nanotubes. Certain carbon materials are synthesised through the use of carbon precursor. Glucose, sucrose, ethylene, propylene, acetronitrile and vinyl cyanide are commonly used carbon precursors in the synthesis of porous carbons, however, this carbon precursors tend to be very expensive. Methane possibly from biogas can provide cheaper alternative synthesis of porous carbons such as ZTCs, MDCs and CNTs. Due to their unique properties, ZTCs, MDCs and CNTs can be used as hydrogen storage materials.

Chapter 3

3. Experimental

3.1 Introduction

This chapter discusses the chemicals and materials used for the experiments, experimental set-up and the synthesis conditions, as well as the characterisation techniques utilised. The first part discusses the synthetic routes of zeolite templated carbons (ZTCs) using ethylene, simulated biogas, and methane. The section discusses the synthesis of ZTCs, which can be achieved either by one- or two-step synthesis routes. The second part discusses the synthesis of MOFs which are in turn carbonised to form MDCs. In the third part, MDCs are utilised for the synthesis of CNTs**.** Finally, the characterisation techniques employed are presented.

3.2 Zeolite templated carbons synthesis using ethylene, simulated biogas, and methane as carbon precursors

Zeolite 13X was adopted as the sacrificial template to generate highly porous templated carbons. Zeolite 13X was selected due to its large pore size which is in the range of 0.6-0.7 nm. The pore structures of zeolite 13X are 3D and connected by circular 12-ring apertures which makes it easier to generate carbon materials consisting of similar structural ordering.

3.2.1 Chemicals

Commercial zeolite 13X was obtained from Sigma-Aldrich with average particle size of 2 µm and was used without further purification. Furfural alcohol (FA) was obtained from Sigma-Aldrich. Ethanol (CH_2CH_2OH, 99.5 %) was obtained from Merck. Hydrochloric acid (HCl, 37 %) and hydrofluoric acid (HF, 40 %) were both supplied by Associated Chemical Enterprise. The synthesised materials were denoted as follows:

The one-step synthesised ZTCs from ethylene/methane were denoted as ZTCet/mt

The two-step synthesised ZTCs from ethylene/methane and furfural alcohol were denoted as FAZTCet/mt

3.2.2 Zeolite templated carbons using a one-step method

3.2.2.1 Templating with ethylene

The dried zeolite 13X (5g) was transferred into the tube furnace and temperature was increased to 700 °C under inert conditions (Argon). At 700 °C ethylene was introduced into the furnace to have a gas mixture of ethylene and argon (1 argon: 4 ethylene) for 3 h. Gas flow was then switched to argon only and temperature increased to 900 °C were carbonisation of the deposited ethylene took place for 3 h. Finally, temperature was cooled to room temperature to signify the completion of the CVD process. See Fig. 3.1. below which shows synthesis parameters and heating profile conditions.

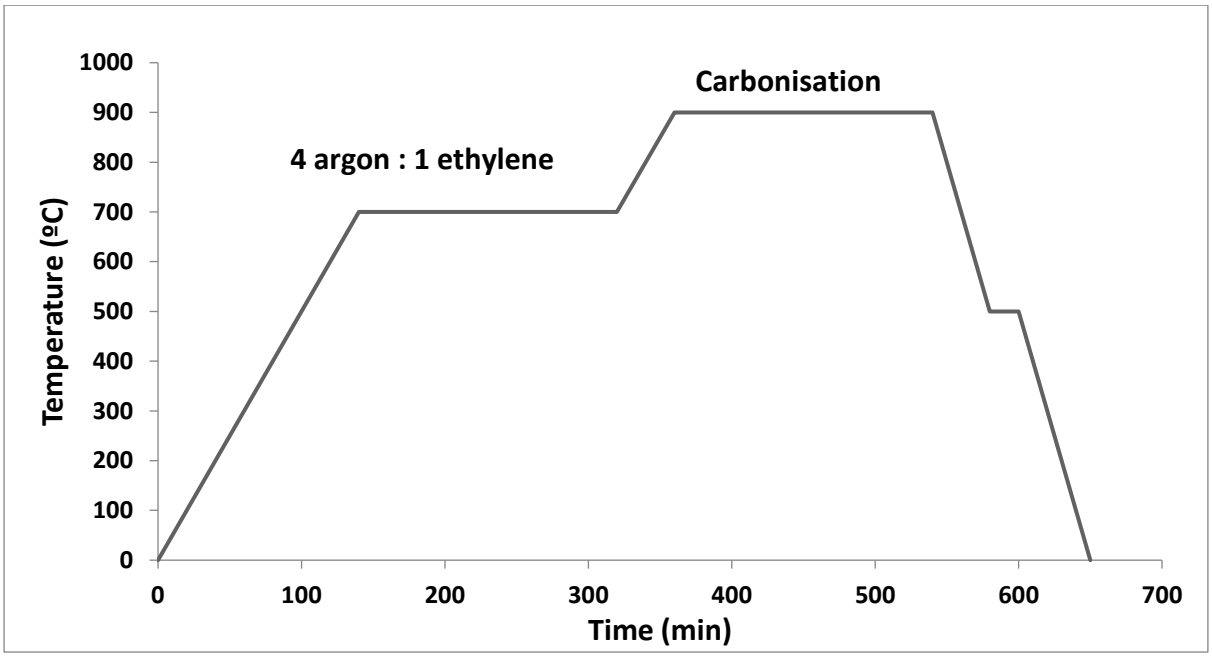

Figure 3.1: The 1 step CVD synthesis parameters and conditions.

To remove the zeolite from the carbons, sample was washed with 20% hydrofluoric acid (40 ml) for 3 h and thereafter the sample was filtered and washed with deionised water (1000 mL). The sample was further washed via reflux in 20% hydrochloric acid at 70 °C for 24 h. ZTC powder was filtered and washed with deionised water (1000 mL) and dried in a conventional oven at 90 °C. The one-step synthesised ZTCs from ethylene were denoted as ZTCet.

3.2.2.2 Templating with simulated biogas

The commercial zeolite 13X (2.5 g) was dried under vacuum at 200 °C for 12 h to remove any trapped or absorbed water molecules from the zeolite cavities. The temperature was increased to 900 °C for 1 h and thereafter, a mixture of argon, carbon dioxide and methane (1: 2: 3) gas was passed through the tube furnace where CVD and carbonisation of CH_4 took place for 3 h.

Then the temperature cooled down to signify the end of the CVD process. See Fig. 3.2 below. Methane deposition into the pores of the zeolite failed/ did not occur (No carbon product was formed).

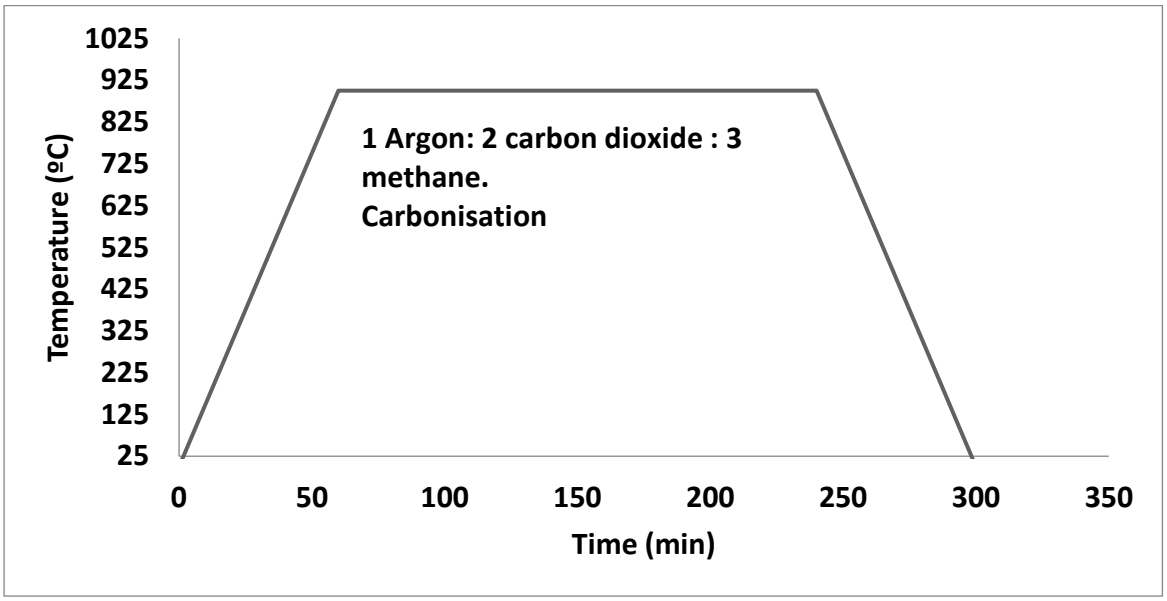

Figure 3.2: The one-step CVD synthesis parameters and conditions of simulated biogas.

3.2.2.3 Templating with methane

The commercial 13X (5 g) was dried under vacuum at 200 °C for 12 h to remove any trapped or absorbed water molecules from the zeolite cavities. The temperature was increased to 900 °C for 3 h and thereafter, a mixture of argon and methane (1:1) gas was passed through the tube furnace where CVD and carbonisation of methane took place for 3 h. Then the temperature cooled down to signify the end of the CVD process. See Fig. 3.3 for synthesis conditions and parameters. The sample then underwent the detemplation process following similar procedure as reported earlier. The one-step synthesised ZTCs from methane were denoted as ZTCmt.

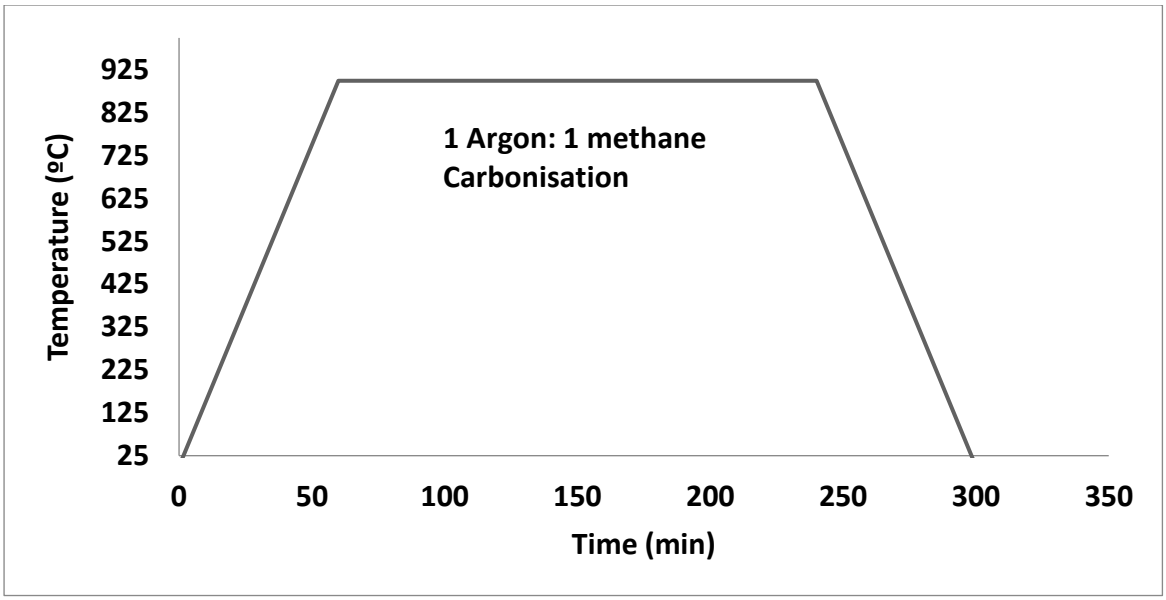

Figure 3.3: The one-step CVD synthesis parameters and conditions for methane.

3.2.3 Zeolite templated carbons using a two-step method

To stop the zeolites from reabsorbing air moisture, zeolite 13X (5 g) was dried at 200 °C for 12 h in a tube furnace with the flow of argon. Furfural alcohol (17 mL) was impregnated into 5 g of dried zeolite for 24 h. The composite sample was filtered, then air dried at ambient temperature for 3 h after being rinsed with ethanol (1 mL). The sample was then dispersed in quart boat before being put into the tube furnace for the chemical vapour deposition (CVD) procedure. Excess air was then removed using argon gas. The sample was first polymerised at 80 °C for 24 h under argon gas, then again at 150 °C for 8 h. The temperature program shown in Fig. 3.4 is used during the CVD process.

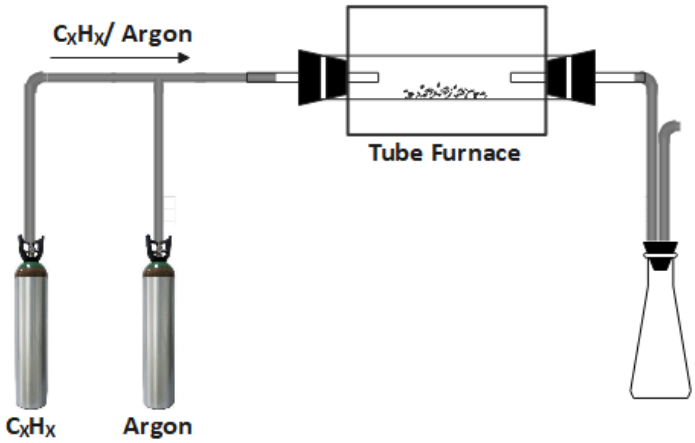

Figure 3.4: CVD setup of synthesis of ZTCs.

3.2.3.1 Templating using ethylene

Polymerisation was followed by templating using ethylene. In this case, after polymerisation, the temperature was increased up to 700 °C for stabilisation of the impregnated zeolite 13X for 3 h still under argon gas. At 700 °C ethylene was introduced into the furnace to have a gas mixture of ethylene and argon (1 argon: 4 ethylene) for 3 h. Gas flow was then switched to argon only and temperature increased to 900 °C were carbonisation of furfural alcohol deposited ethylene took place for 3 h. Finally, temperature was cooled to room temperature to signify the completion of the CVD process. Fig. 3.5 shows the synthesis conditions and parameters. The sample then underwent the detemplation process following similar procedure as reported earlier. The two-step synthesised ZTCs from ethylene and furfural alcohol were denoted as FA-ZTCet.

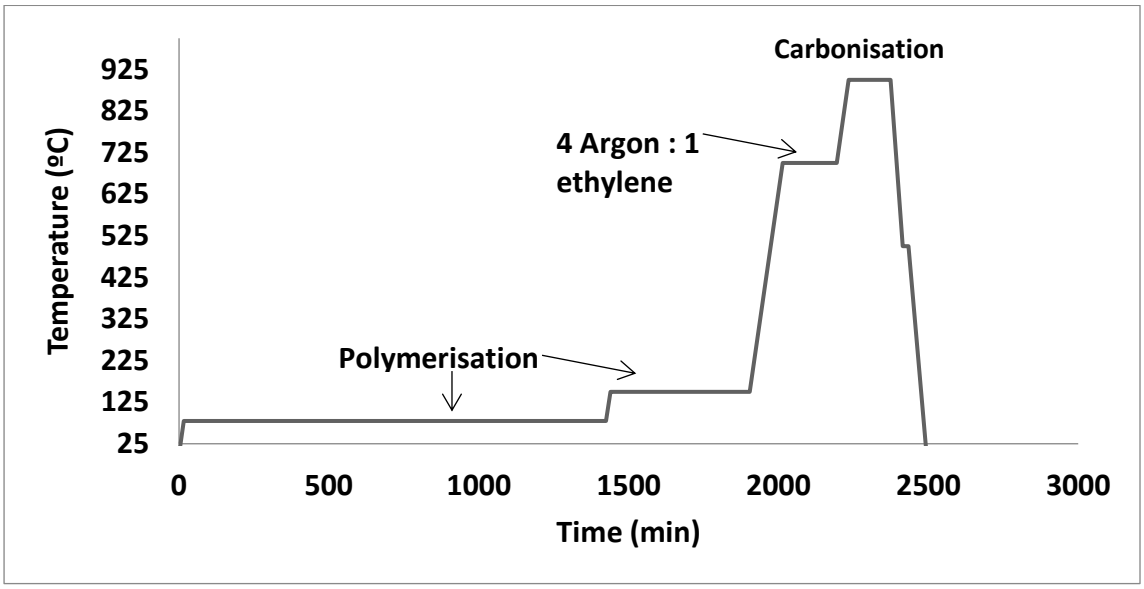

Figure 3.5: The two-step CVD synthesis parameters and conditions for ethylene.

3.2.3.2 Templating with methane

Here also, polymerisation was followed by templating using methane. In this case, after polymerisation at 150 °C, the temperature was then increased up to 900 °C for 3 h followed by addition of methane into the tube to make a gas ratio of 1 argon: 1 methane and allowed to flow for 3 h. After 3 h, the temperature was allowed to cool down to signify the end of experiment. See Fig. 3.6 below for synthesis conditions and parameters. The detamplation process described above (3.2.2.1) was followed. The two-step synthesised ZTCs from methane and furfural alcohol were denoted as FA-ZTCmt

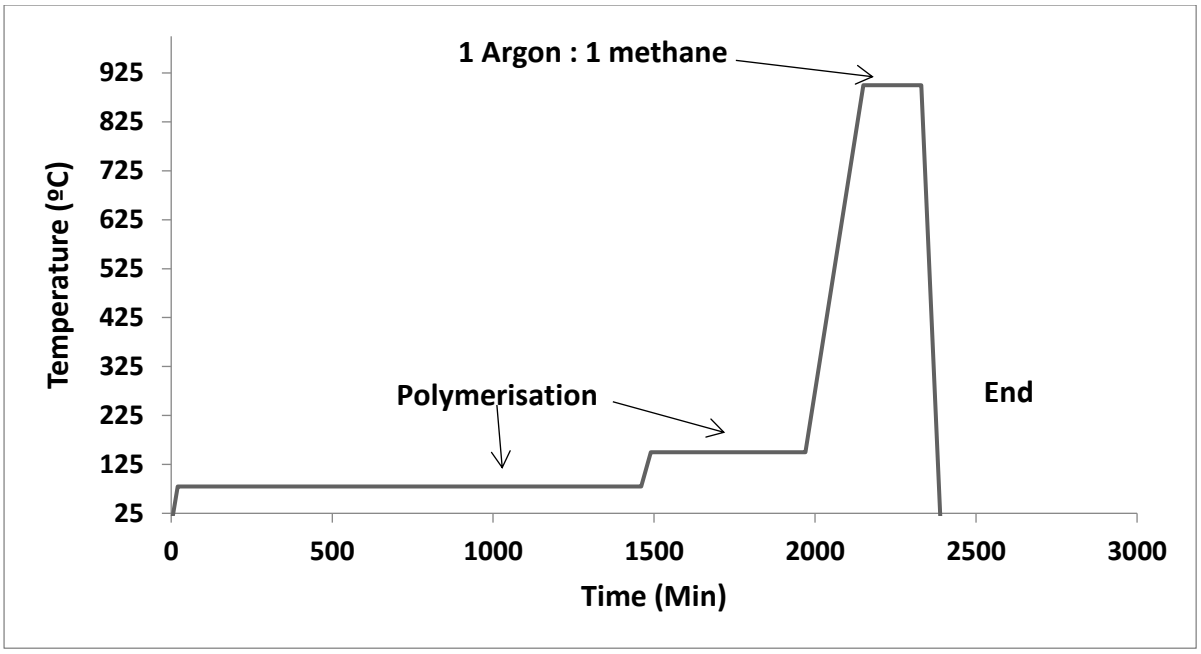

Figure 3.6: The two-step CVD synthesis parameters and conditions for methane.

3.3 Synthesis of metal-organic frameworks (MOFs) and MOF-derived carbons (MDCs)

3.3.1 Chemicals and Materials

Ditopic terephthalic acid (H_2BDC, 98 %) was obtained from Sigma Aldrich, iron hydroxide ($Fe(OH)_3$) extracted from AMD obtained from a coal mine in Gauteng South Africa, hydrogen peroxide (H_2O_2, 30 %), dimethylformide (DMF, 99.5 %), sodium hydroxide (NaOH, 1 M), nitric acid (HNO_3, 55 %), glacial acetic acid (CH_3COOH, 98.5 %) were all obtained from Associated Chemical Enterprises. All chemicals were used without further purification.

3.3.2 Synthesis of metal-organic frameworks (MOFs)

Fe-based MOFs (MIL-88B and MIL-101) were used as precursors for MDCs. Synthesis of the MOFs is as described below.

Extraction of iron: 30 % H_2O_2 (30 mL) was added to AMD (1000 mL) and the solution was left to stir for 1.5 h at ambient temperature. 4 M NaOH solution was added into the solution and left to stir for 15 min. The precipitate was filtered and washed with H_2O (1000 mL). The resulting powder ($Fe(OH)_3$) was dried at 80 °C.

MIL-88B: $Fe(OH)_3$ (0.6634 g) was dissolved in HNO_3 (2.5 mL) by heating at 50 °C. H_2BDC (1.05 g) was dissolved in DMF (40 mL) by sonication. $Fe(OH)_3$ solution was added into H_2BDC solution and stirred at room temperature followed by the addition of glacial acetic acid (1.2 mL). The

solution was transferred into the Teflon cup and heated at 150 °C for 15 h. The resulting residue was centrifuged and washed three times with DMF (50 mL ×3).

MIL-101: $Fe(OH)_3$ (0.2619 g) was dissolved in HNO_3 (0.6 mL) by heating at 50 °C. H_2BDC (1.05 g) was dissolved in DMF (40 mL) by sonication. $Fe(OH)_3$ solution was added into H_2BDC solution and stirred at room temperature then transferred into a Teflon cup. The Teflon cup was placed in a vacuum oven and heated at 110 °C for 20 h. The resulting residue was centrifuged and washed three times with hot DMF (50 mL × 3).

3.3.3 Synthesis of MOF derived carbons (MDCs)

For the MDCs preparation, in a tube furnace, 5 g of MOFs were heated for two hours at 800 °C under argon flow before being cooled to ambient temperature. The resulting black powder was refluxed using 10 % HCl at 70 °C overnight. The resulting material was then thoroughly washed with deionised water, dried in a conventional oven at 90 °C and collected for characterisation. MDCs derived from MIL-88B were denoted as MDC-88B while MDCs from MIL-101 were denoted MDC-101.

3.4 Synthesis of MDC-grown-Carbon nanotubes

0.5 g of MOF was placed in a ceramic boat and transfered into the tube furnace. After purging the tube furnace with argon for 15 min, the temperature was increased to 700 °C (5 °C/min) under argon. At 700 °C, hydrogen was added into the tube to have a gas ratio of 1 H_2: 5 Ar for 1 h. The temperature was then increased up to 900 °C under argon only. At 900 °C methane was introduced to make a gas mixture of 1 CH_4 : 2 Ar for 1 h. CNTs from MIL-88B are denoted as CNT-88B and from MIL-101 as CNT-101. The experimental set-up for the chemical vapour deposition (CVD) utilising methane gas is shown in Fig.3.3.

3.5 Characterisation techniques

The carbon materials and precursor materials were analysed using various techniques which will be discussed below. The conditions at which the materials were analysed are also presented.

3.5.1 X-ray diffraction (XRD)

Perhaps the most popular x-ray diffraction method for characterising materials is powder XRD. The sample often takes the form of fine grains of a crystalline substance that are powdery in texture. Additionally, polycrystalline solids or particles in liquid suspensions can be studied using this technique. Crystals are homogenous solid substances made of regular arrays of atoms

in three-dimension space to form symmetrically arranged planes. Each material has a unique d-spacing(d) between different planes.[128]

The XRD instrument consists of an X-ray source (monochromatic in nature) which irradiates the sample then measures the intensity and scattering angles of the X-rays that are diffracted from the material. The technique employs the Bragg's law:

$$n\lambda = 2d \sin\theta \quad (1)$$

Where d is the spacing between diffracting planes in the atom lattice

θ is the incident angle, also called Bragg's angle

n is any integer number

λ is the incident beam wavelength

Powder materials are typically distributed in a random manner; however, by scanning this material via a variety of 2θ angles, all potential lattice diffraction directions could be identified.[128-129]

Figure 3.7 XRD instrumentation

Rigaku Ultima IV diffractometer using Ni-filtered Cu-Kα radiation (0.154 nm) in the range of 2θ = 1–90° at a scanning rate of 0.1°s^{-1} was used for structural comparison between ZTCs and zeolite 13X.

3.5.2 Thermogravimetric analysis (TGA)

TGA is a method used to measure the mass loss of a sample as a function of temperature in a controlled atmosphere.[130] The sample is placed in an alumina pan that is supported on a balance. This pan is then transferred in which the mass of the material is determined per change in temperature.

Figure 3.8: Thermogravimetric analysis instrumentation

TGA was carried out in this study utilising a Mettler, Toledo, TGA/SDTA 851e. Alumina crucible containing 10 mg of the sample was loaded, and it was heated to 900 °C at a rate of 10 °C/min with an air flow of 10 mL/min. By analysing the sample mass as a function of temperature, TGA examines a sample's thermal stability. At the precision balance scale, the sample is put in an aluminum crucible. In order to regulate the sample's environment, an inert or nonreactive gas is utilised.

3.5.3 Scanning electron microscope (SEM)

SEM is one of the most adaptable tools used on analysis of materials to determine their morphology and chemical composition. SEM utilises a concentrated beam of high energy electrons to produce signals from the surface of the analysed sample. [131] The gathered information provides details on the sample, such as its exterior shape, chemical makeup, crystalline structure, and the orientation of the materials that went into its construction. Secondary electrons, back-scattered electrons photons and visible light can also be obtained using SEM.[132] Images of the samples are obtained when secondary electrons are detected by secondary electron detector. A 2-dimensional image is typically created by collecting information from the chosen portion of the material and displaying the spatial changes in these properties.[133] By using SEM, it is possible to determine the materials elemental composition. This procedure can be carried out when the backscattered electrons create images that display the compositional contrast from number elements and their distribution.[134]

Figure 3.9: Scanning electron microscopy instrumentation

The morphological properties of the MOF (both before and after carbonisation), zeolite 13X, and templated carbon samples were examined using a JEOL-JSM 7500F scanning electron microscope. To prevent charging during analysis, the samples were mounted on a copper stub that had been coated with carbon and threaded with conductive sticky carbon tape.

3.5.4 Transmission electron microscope (TEM)

TEM is a very useful instrument for material science. TEM and light microscope operate under the same principle. The difference being, TEM uses electrons instead of photons. High resolution can be obtained using TEM due to the shorter wavelength of the electrons. Chemical analysis is performed by transmitting an intensely energetic electron beam through a very thin sample and observing the interaction of the beams with the sample's atoms. Condenser lens is used to focus the beam of electrons into a small thin coherent beam. The beam then radiates the sample and some of the beams are transmitted pending on the size and electron nature of the sample. The transmitted electrons are focused using the objective lens onto a charged couple device. Objective lens blocks out high-angle diffracted electrons thus enhancing the contrast of the image.[135-138]

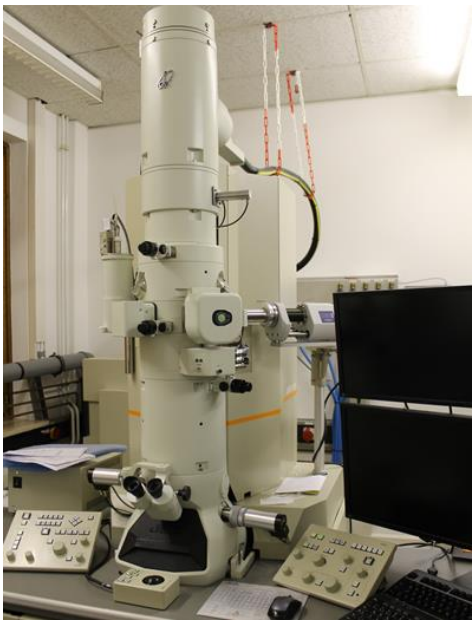

Figure 3.10: Transmission electron microscopy instrumentation

Micrographs were taken using a JEOL-Jem 2100 model transmission electron microscopy with a LaB6 filament working at 200kV. After being ultrasonically mixed with ethanol, the solid powders were cast in small drops onto holey carbon sheets fixed on copper grids. TEM is a method that transmits electrons to produce images of the specimen's chemical makeup.

3.5.5 Raman spectroscopy

Raman spectroscopy is a useful technique to understand the graphitic nature of the obtained carbon materials, it has potential to distinguish between ordered and disordered carbons. It is recognised as one of the most sensitive methods to study the structural properties of carbonaceous materials. Every bond in the molecule has a specific vibrational frequency which corresponds to the band in a Raman spectrum.[139] Raman spectroscopy utilises the Raman effect which occurs when a photon interacts with gas or liquid or solid molecules resulting in scattered electrons.[140] The scattered photon (~ 1 photon in 10 million), scatters at a frequency higher than the incident photon. In principle, Raman operates by observing molecular bond polarisation that occurs during light interaction with a molecule inducing distortion of the electron cloud.[139] The change in polarisability occurs at specific energy transitions of molecular bonds, which in turn give rise to Raman active modes.[141] These are represented by the Raman spectrum, which consists of Raman scattering light intensity and wavelength position.

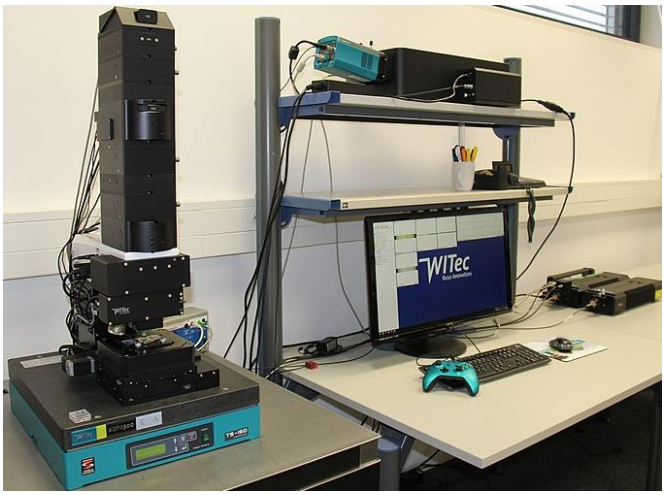

Figure 3.11: Raman spectroscopy instrumentation

Analysis was done on WITec alpha 300 RAS + Confocal micro-Raman microscope (Focus Innovations, Germany), Operated at 5mW laser power and wavelength of 532nm in 120 s spectral acquisition time.

3.5.6 Adsorption studies and textural properties

By measuring the N_2 adsorption isotherm at 77K, the Brunauer-Emmet-Teller (BET) theory is used to calculate the surface area and pore size of various materials. BET extends on the Langmuir theory which assumes multilayer adsorption occurs on the surface of the material.[142-143] The isotherms are recorded following the adsorbed N_2 amount per gram of solid with an increase in relative pressure as well as the reverse process.

Figure 3.12: N_2 adsorption instrumentation

BET surface area measurements were conducted using Micromeritics(R) ASAP 2020 HD at liquid N_2 temperature (77K) and relative pressure (P/P_0) ranging from 0 to 1. N_2 adsorption-

desorption isotherms were obtained after outgassing at 200 °C under vacuum overnight. The linear region of the N_2 isotherms provided the BET surface areas. Using the Horvath-Kawazoe (HK) model, pore size distribution plots and pore volumes were generated. The Micromeritics(R) ASAP 2020 HD equipment was also used to measure the H_2 adsorption isotherms at 77 K and up to 1 bar.

3.6 Chapter summary

This chapter is subdivided into three subsections discussing the experimental set-up and the synthesis parameters, as well as a fourth subsection on characterisation techniques. The first subsection discusses the templation process of ZTCs using ethylene, biogas, and methane as carbon precursors. The synthesis procedure was done following two routes: the one-step and the two-step approaches. The one-step route involves the use of one carbon precursor while the two-step involves impregnation of the zeolite using FA and an introduction of a carbonaceous gas during the carbonisation step. The second subsection discusses the extraction of iron from AMD, hydrothermal synthesis of MOFs, and direct carbonisation to obtain MDCs. In the third subsection, CNTs are synthesised from MDCs by CVD. The obtained carbonaceous materials were characterised using techniques using a variety of techniques including powder XRD, TGA, SEM, TEM, Raman spectroscopy, BET analysis and H_2 adsorption.

Chapter 4

4 Results and discussions: Zeolite templated carbons

This chapter discusses the results obtained for ZTCs obtained from ethylene and methane using the one-step and two-step processes. Structural similarities and textual properties of the ZTCs are discussed.

Utilisation of biogas as carbonaceous feedstock for preparation of high surface area zeolite templated carbons

Keaoleboga Mosupi[1,2], Henrietta W. Langmi[2], Xoliswa Dyosiba[1], Nicholas M. Musyoka[1*]

[1]Centre for Nanostructures and Advanced Materials (CeNAM), Chemicals cluster, Council for Scientific and Industrial Research (CSIR), Meiring Naude Road, Brummeria, Pretoria, 0001, South Africa, kmosupi@csir.co.sa

[2]Department of Chemistry, University of Pretoria, Private Bag X20, Hatfield, 0028, South Africa.

[*]Corresponding author: Nmusyoka@csir.co.sa

Abstract

Biogas, a product of anaerobic digestion, is an attractive renewable energy source due to its continuous production and use cycle. Recently there has been great interests on value addition of biogas, concerning the utilisation of the main component methane (CH_4). In this work we focused on utilisation of simulated biogas (CH_4 and CO_2 mixture) and pure CH_4 for synthesis of zeolite templated carbons (ZTC). ZTCs are known to have attractive properties such as large surface area, uniform pores and high pore volumes, and have found applications in gas storage and gas separation. When methane was utilised on both one-step and two-step process, the obtained ZTCs had higher surface area and hydrogen (H_2) adsorption as compared to the simulated biogas feedstock. The high surface area obtained was 2974 m^2/g while the best H_2 storage capacity was at 1 bar was 2.77 %wt. Structural (XRD) and morphological (SEM and TEM) characterisation were found to be almost similar to the samples obtained when ethylene was used as a carbon source. The study has proven that sustainable source of feedstock in ZTCs production can be utilised to create value added products.

Keywords: Biogas, methane, Zeolite 13X, zeolite templated carbons, hydrogen adsorption, chemical vapour deposition.

4.1 Introduction

Raw biogas is the product of anaerobic species that decompose organic matter under controlled temperature, acidity, and moisture conditions. Various types of feedstock can be used as organic matter for the production of biogas, e.g., municipal solid waste, animal manure, algae, kitchen waste, crops straws and leaves, among others.[1] The constituents of biogas are CH_4, CO_2, H_2S, H_2, N_2, volatile organic compounds (VOCs), siloxanes, CO, NH_3 and traces of water vapour. Biogas can be used as a fuel for gas turbines, to produce heat for domestic and industrial environments, and even as a raw material in the chemical industry.

The use of biogas is mainly dependent on the high presence of CH_4, which has high calorific value as compared to other constituents. The higher the content of CO_2 and N_2 the lower the calorific value of biogas. Removal of unwanted compounds such as VOCs, siloxanes, CO, NH_3, which is regarded as "biogas cleaning" is the first step to biogas treatment. It is then followed by biogas upgrading which mainly focuses on the removal of CO_2. The recovered CO_2 can be used as a precursor for production of chemicals such as methanol, dimethyl carbonate, methane, etc. The product of upgraded biogas, biomethane, is then used as a source of fuel and as a carbonaceous feedstock to produce solid carbons. Amongst many existing templated carbons, ZTCs are an attractive group of porous sorbents.[144] ZTCs are produced using zeolite as nanocasting template utilising a gaseous or liquid carbonaceous feedstock. Ethylene has been preferred as an ideal gaseous feedstock and furfural alcohol as preferred liquid feedstock for impregnating zeolite template.

ZTCs are known to be utilised in many applications such as hydrogen storage, carbon capture, methane storage, gas separation, amongst others. There are two approaches that can be followed for the synthesis of ZTCs, i.e., one-step process which involves impregnation of zeolite template with gaseous carbon source and a two-step process which involves impregnation of the template with liquid carbon feedstock followed by gaseous feedstock.[145]

To the best of our knowledge, there are no studies that have reported on the use of biogas as carbon source for synthesis of ZTCs. Even on the case of utilising pure methane which is the largest constituent of biogas. In this work we report on the use of simulated biogas, i.e., mixture of CO_2 and CH_4 based on their average composition in biogas. We further compare the obtained ZTCs from simulated biogas to that obtained using pure methane (supposed to be obtained from upgraded biogas).

The study demonstrated that utilisation of biogas in its raw form does not lead to production of ZTCs due to competition of CO_2 during its chemical vapour deposition (CVD) process. However, when pure methane is utilised, the ZTCs obtained are almost of equivalent quality as compared to those obtained when using commercial ethylene gas feedstock. The study contributes to circular economy through the use of sustainable feedstock (biomethane), rather than the reliance on fossil derived gas feedstocks.

4.2 Materials and experimental procedure

Zeolite X, was purchased from Sigma Aldrich, whereas ethylene, methane and argon were purchased from air products. The chemicals and reagents used in this study were used without further purification.

Synthesis of ZTCs using simulated biogas: The commercial 13X (5g) was dried under vacuum at 200 °C for 12 h to remove any trapped or absorbed water molecules from the zeolite cavities. The temperature was increased to 900 °C for 3 h and thereafter, a mixture of carbon dioxide and methane (ratios 2:3, 4:1, 2.3:1) gas was passed through the tube furnace for 3 h.

Synthesis of ZTC using methane: The dried zeolite was packed in a sample boat and placed in a tube furnace. The temperature was increased to 900 °C for 3 h and thereafter, a mixture of argon and methane (ratio 1:1) gas was passed through the tube furnace where CVD and carbonisation of CH_4 took place for 3 h. To remove the zeolite from the carbons, sample was washed with 20% hydrofluoric acid (40 ml) for 3 h and thereafter the sample was filtered and washed with deionised water (1000 mL). The sample was further washed via reflux in 20% hydrochloric acid at 70 °C for 24 h. Thereafter the recovered ZTC was filtered and washed with deionised water (1 L) and dried in a conventional oven at 90 °C for 12 h.

The procedure for the synthesis of ZTC following the two-step approach is as follows: To stop the zeolites from reabsorbing air moisture, zeolite 13X (5 g) was dried at 200 °C for 12 h in a tube furnace with the flow of argon. Furfural alcohol (17 mL) was impregnated into 5 g of dried zeolite for 24 h. The composite sample was filtered, then air dried at ambient temperature for 3 h after being rinsed with ethanol (1 mL). The sample was then dispersed in quart boat before being put into the tube furnace for the chemical vapour deposition (CVD) procedure. Excess air was then removed using argon gas. The sample was first polymerised at 80 °C for 24 h under argon gas, then again at 150 °C for 8 h. Temperature was then increased to 900 °C, once at 900 °C, methane was introduced into the tube furnace for 3 h. The sample then underwent the detemplation process following similar procedure as reported earlier. For comparison purposes

the experimental procedure was repeated using ethylene as a carbon source. The samples obtained from methane were called ZTCmt and FAZTCmt and the samples obtained from ethylene were called ZTCet and FAZTCet.

4.3 Characterisation

Phase identification of the prepared samples was conducted using Rigaku Ultima IV diffractometer using Ni-filtered Cu-Kα radiation (0.154 nm) in the range of 2θ = 1–90° at a scanning rate of 0.1°s^{-1}. The obtained ZTCs' morphology was examined under a JEOL-JSM 7500F scanning electron microscope. ZTC pictures were captured using a JEOL-Jem 2100 model transmission electron microscope (TEM). Using the Micromeritics(R) ASAP 2020 HD, BET surface area measurements were made at liquid N_2 temperature (77K) and relative pressures (P/P_0) ranging from 0 to 1. After outgassing at 200 °C under vacuum for the whole night, N_2 adsorption-desorption isotherms were obtained. The linear portion of the N_2 isotherms yielded the BET surface areas. Using the Horvath–Kawazoe (HK) model, pore size distribution plots and pore volumes were derived. H_2 adsorption isotherms at 77 K and up to 1 bar, were also measured on the Micromeritics(R) ASAP 2020 HD instrument. All gas sorption isotherms were obtained using ultra-high purity grade (99.999 %) gas. Thermal stability of the prepared samples was determined using TGA instrument (TA instruments, Q500 model) alumina crucibles under air at a temperature rate of 10 °C/min at a temperature range of 0 °C to 1000 °C.

4.4 Results and discussions

Structural analysis

The comparative XRD patterns of commercial zeolite 13X and samples obtained when using ethylene and pure methane as carbonaceous feedstock are represented in Fig. 4.1. All the carbon samples, whether synthesised using the one or two-step method, displayed a dominant sharp peak at 2θ= 6.3° which originated from the (111) structural regularity of FAU zeolite, which was also observed by Musyoka et al [146]. This peak denotes the maintenance of the zeolite's structural regularity over a wide area on the carbon. Two large peaks at 2θ = 23°and 2θ =42°, were also visible in the manufactured porous carbons, indicating the existence of graphitic carbons, such as graphene layers, nano-graphene networks, or graphene stacking. These two peaks could be indexed as the 002 and 101 planes of the graphitic carbons in compared to disordered carbon structures. The methane that was externally deposited on the template's pores caused the graphitic substance. High CVD temperatures (900 °C) are to blame for the exterior deposition, which occurred.[147-148] The absence of the strong peaks seen on the zeolite 13X XRD pattern provided evidence of the ZTC's amorphous nature.

Unfortunately, ZTCs were not obtained when simulated biogas was used as carbon source due to zeolite having greater affinity towards CO_2 than CH_4 because of the large quadrupole moment of CO_2. The quadrupole moment has a strong attraction towards the electrostatic field of the cationic sites thus greater selectivity and higher adsorption capacity.[149] Pour *et al* [150] studied clinoptilolite and zeolite 13X ability to separate CO_2 from CH_4, and concluded that both materials have high affinity towards CO_2 due to the quadrupole moment of CO_2 molecules with the surface of adsorbents. CH_4 is a non-polar molecule with no dipole and quadrupole moment, which results in weak interaction with zeolites. The attraction of CO_2 towards zeolite 13X is supported by many other researchers, i.e., Silva *et al* [151] , Kareem *et al* [152] and Mulgundmath *et al* [153] It can then be concluded that, the use of biogas as a carbon feedstock in synthesis of zeolite templated carbons is not possible since zeolite 13X has preferential adsorption of CO_2 over CH_4 and CO_2 is thermally stable to be carbonised in the pores of the zeolite.

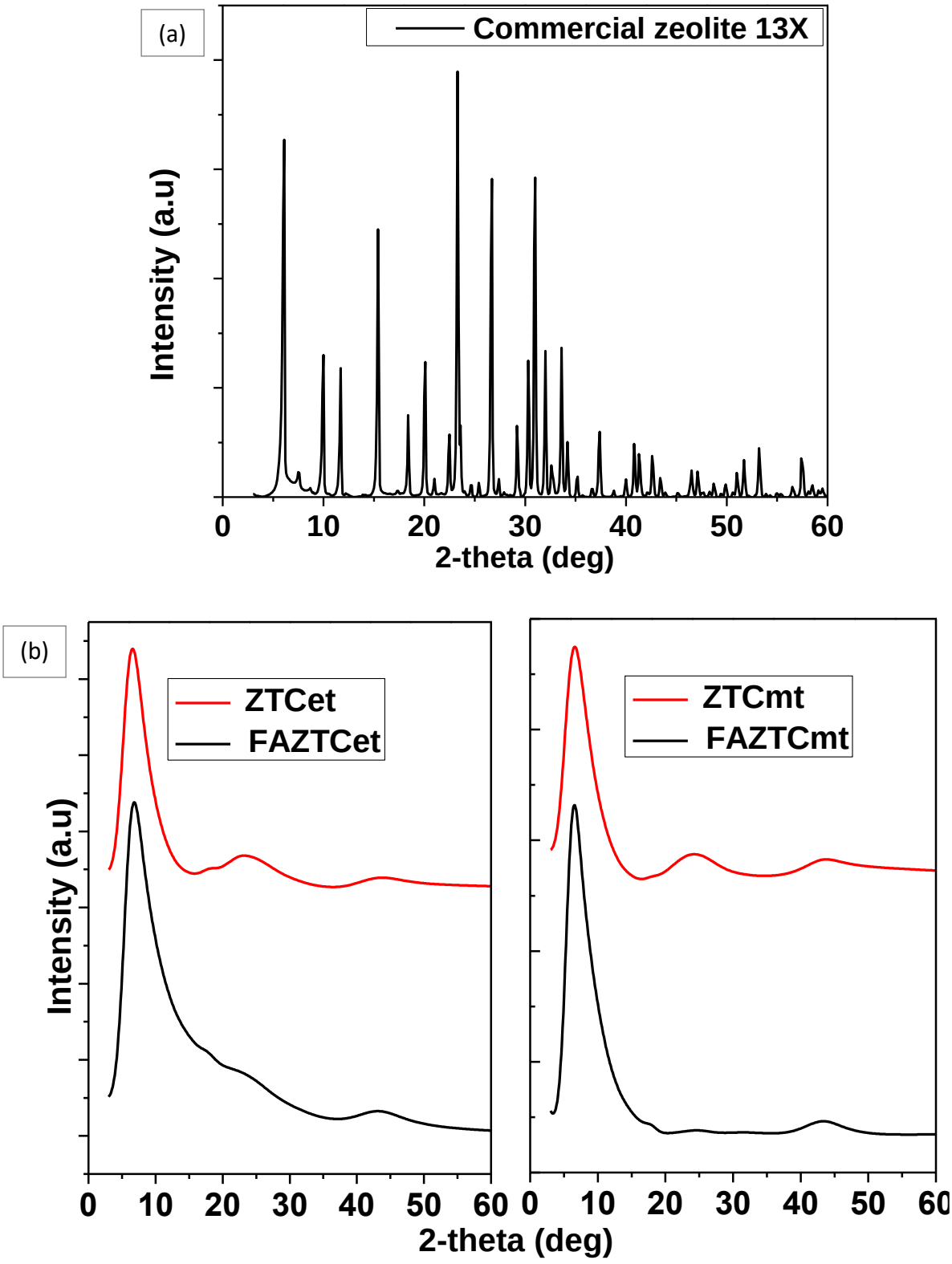

Figure 4.1: X-ray diffraction pattern for (a) Commercial zeolite 13X (b)ZTCet, FAZTCet, ZTCmt and FAZTCmt.

Morphological Analysis – Scanning Electron Microscopy (SEM)

SEM images presented in Fig. 4.2, confirmed morphological similarity between the zeolite and the carbon replicas. The octahedral pyramidal shape which is associated with zeolite 13X was observed on the templated carbons. The templated carbons (Fig. 4.2b, c, d, e) have a smooth surface which resembles that of the parent zeolite (Fig. 4.2a) and the results are in line with those reported by Kyotani *et al* [40] using zeolite Y.

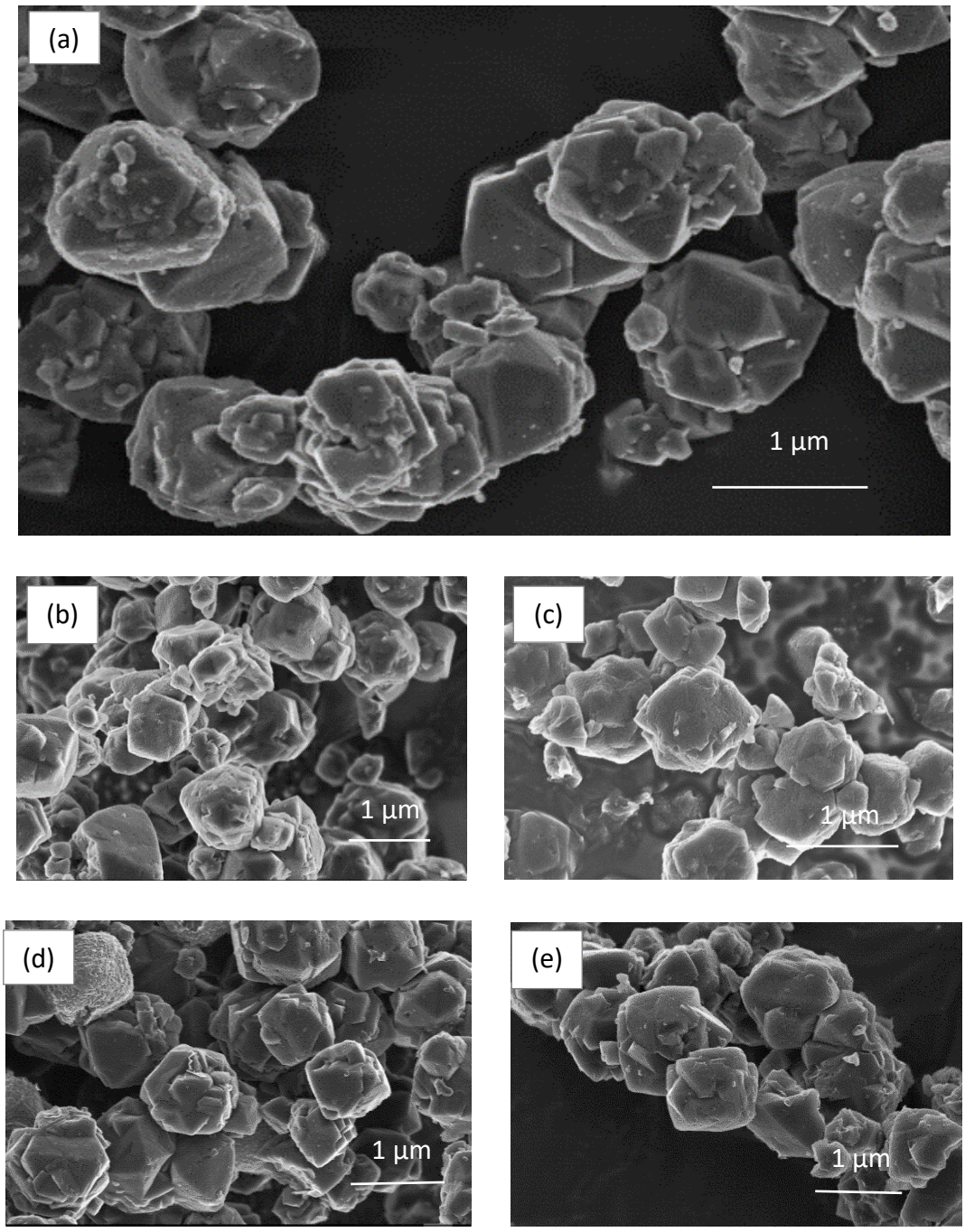

Figure 4.2: SEM images of (a) Commercial Zeolite 13X (b) ZTCet (c) ZTCmt (d) FAZTCmt (e) FAZTCet

Transmission electron microscope

Representative transmission electron micrographs obtained for samples ZTCmt and FAZTCmt are presented in Fig. 4.3. It is noteworthy that the particles are free of any appreciable exterior layer, which eliminates the possibility of graphitisation caused by carbon deposited on the outside of the zeolite particle. The selected area diffraction pattern (SAED), which denotes scattering from an amorphous material, significantly contributed to the understanding of the ZTCs' amorphous nature.

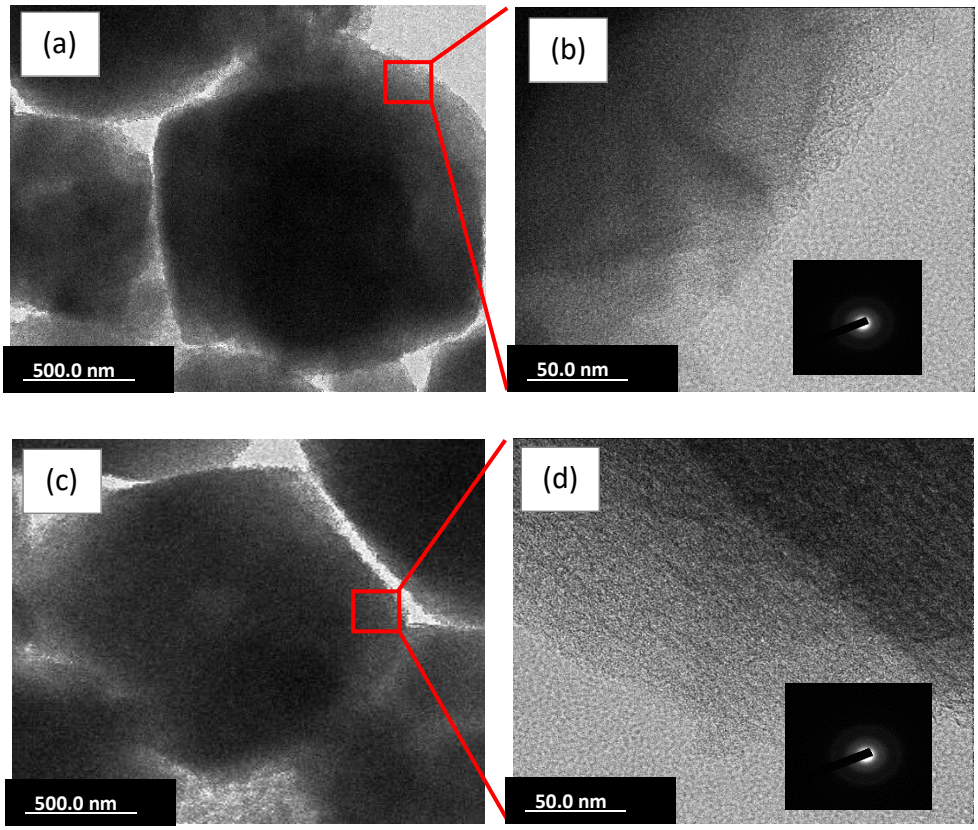

Figure 4.3: TEM images of templated carbons (a) low resolution ZTCmt (b) high resolution ZTCmt (c) Low resolution FAZTCmt (d) High resolution FAZTCmt

Thermogravimetric analysis

Determination of the temperature at which materials decompose is of great importance for application purposes. Therefore, TGA was done on the ZTCs and the results presented in Fig. 4.4. Around 0 and 80 °C there is weight loss of ~ 5% due to the evaporation of water molecules trapped within the ZTCs pores. ZTCs are thermally stable up to 500 °C, after which there is a noticeable weight loss between 600 and 700 °C, as shown by TGA. This drastic weight loss can be attributed to carbon burn off. The complete loss of weight of the material indicates that the detemplation processes was successful (no traces of the zeolite 13X).

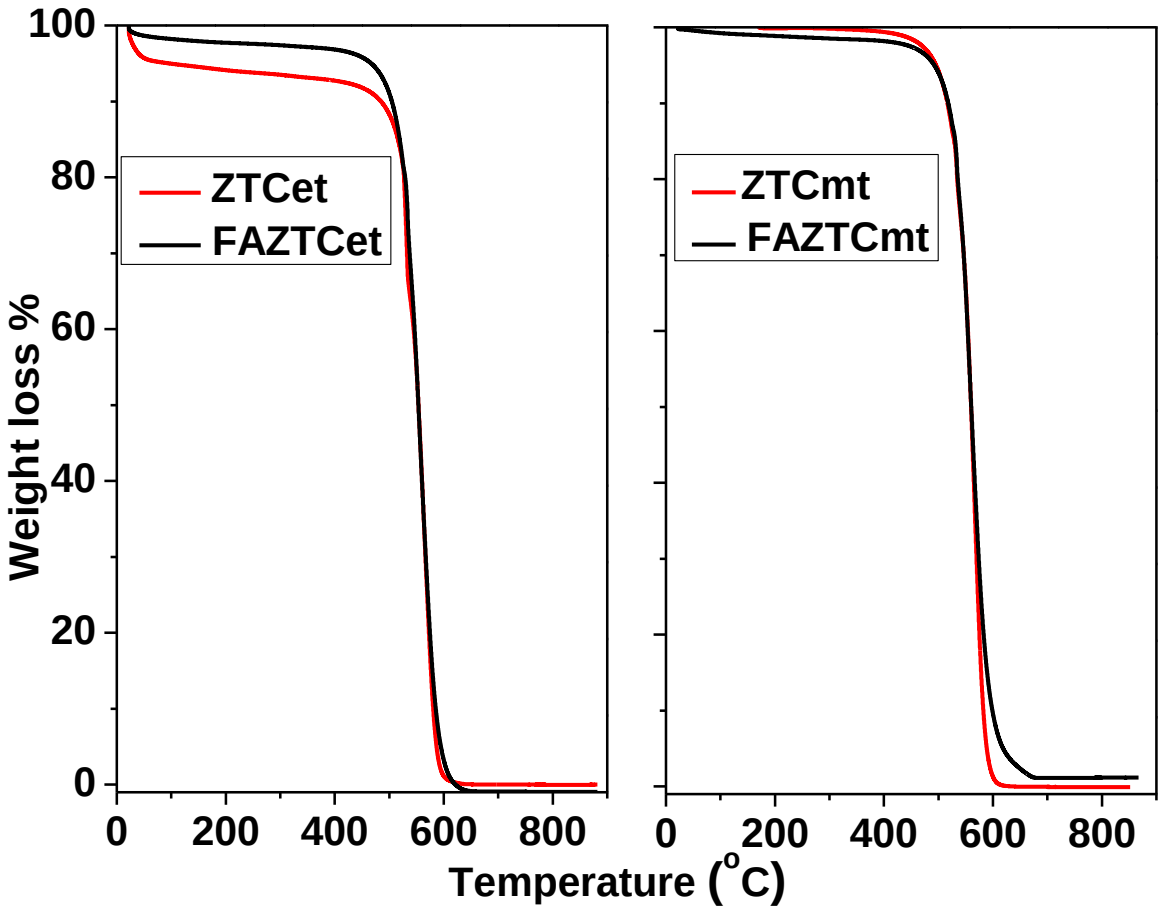

Figure 4.4: Thermogravimetric analysis for ZTCet, FAZTCet, ZTCmt and FAZTCmt.

Raman spectroscopy

Raman spectroscopy is an important technique to understand the graphitic nature of the carbon material, it has potential to differentiate between ordered and disordered carbons.[154] Fig. 4.5, shows the Raman spectrum of ZTC synthesised using one- and two-step processes. The spectrum shows the D-band which represents the disordered carbons and G-band shows the ideal graphitic lattice vibration mode.[148] As expected for sp^2-carbons, the spectrum of the one-step process showed the D band of ZTCet and ZTCmt at 1361 cm^{-1} and 1337 cm^{-1} while the G band is located at 1603 cm^{-1} and 1595 cm^{-1} respectively. The two-step process shows the D band of FAZTCet and FAZTCmt at 1349 cm^{-1} and 1341 cm^{-1} while the G band is located at 1603 cm^{-1} and 1599 cm^{-1} respectively. In contrast to graphites, ZTCs appear to be largely composed of a single layer of nanometer-sized graphene sheets, as evidenced by the G bands' location, which is somewhat higher than that of graphene, and the strong intensity of the D bands relative to that of the G bands. [155] The broad bands observed between 2300 and 3300 cm^{-1} which are attributed to the second order Raman scattering as a result of two-phonon process, are also in agreement with this interpretation.[156] The higher intensity ratio (I_D/I_G) of methane products as observed in Table 4.1, proves that the high temperature affected the amorphous

carbon by forming more defects. The intensity of D band is almost equal to G band on methane derived ZTCs as compared to the ethylene derived ZTCs, this suggests that methane derived ZTCs are dominated by defects. The defects may be as a result of the sp^3-carbons, dangling bonds, presences of defective pores (diameter greater than 2.2 nm)[157] and other types of defects.

Table 4.1: Raman analysis data of ZTCet, ZTCmt, FAZTCet and FAZTCmt

Sample name	D Band	G Band	I_D/I_G
ZTCet	1361	1603	0.86
ZTCmt	1337	1595	0.95
FAZTCet	1349	1603	0.89
FAZTCmt	1341	1599	0.96

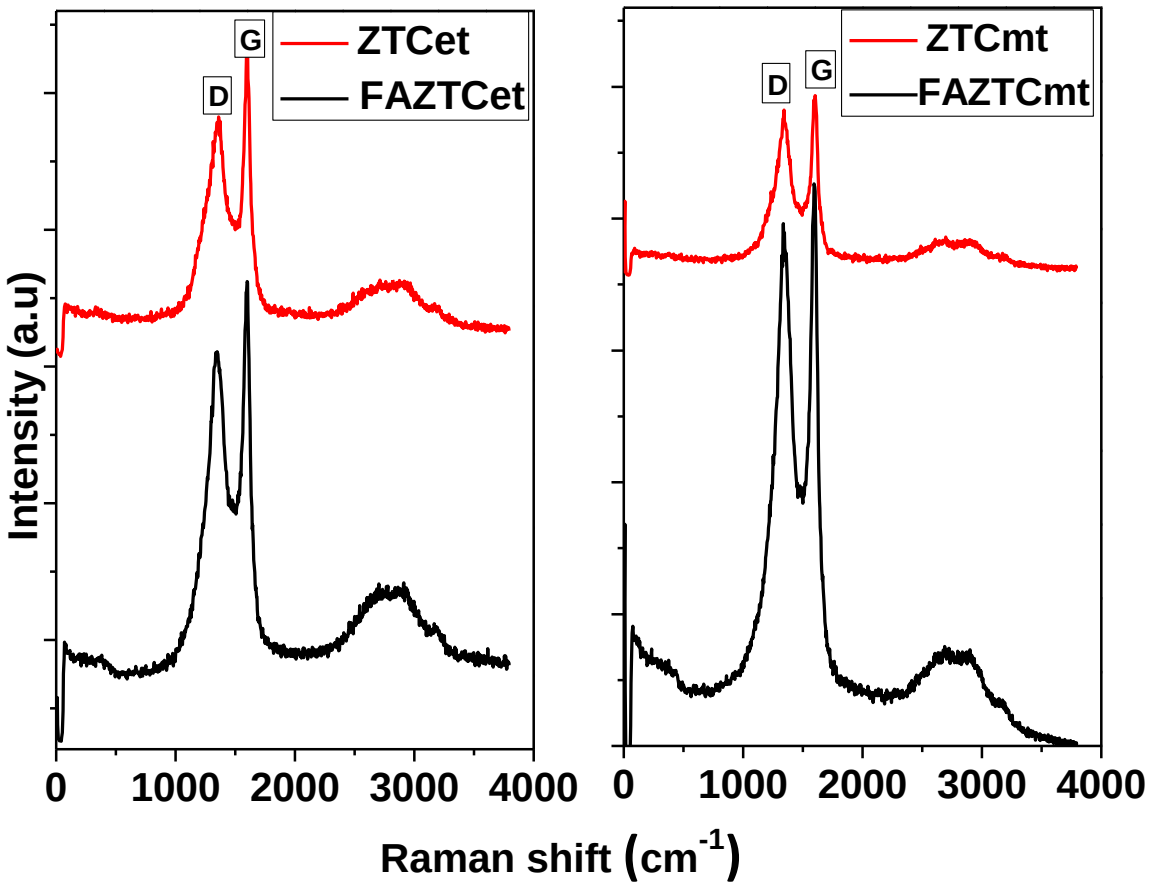

Figure 4.5: Raman analysis for ZTCet, FAZTCet , ZTCmt and FAZTCmt.

Adsorption studies and physical properties

N_2 sorption isotherm

N_2 sorption isotherm at 77 K of both one- and two-step synthesis routes for ethylene and methane derived ZTCs are presented in Fig. 6. Type IV isotherms were represented in the synthesised materials. The presence of micropores is suggested by the sharp rise in N_2 adsorption at the lower relative pressure ($p/p_0 < 0.1$). The replication of the zeolite structural ordering has been accomplished if there are micropores present. The hysteresis loop, which is caused by capillary condensation and indicates the presence of mesopores, occurs at approximately $p/p_0 > 0.2$.[158] Mesoporosity, which may be caused by spaces between particles or by insufficient carbon filling of zeolite micropores.[159]The isotherms are consistent with results from carbons made from zeolite templates that exhibit high degrees of structural organisation. [35, 44-45, 160]

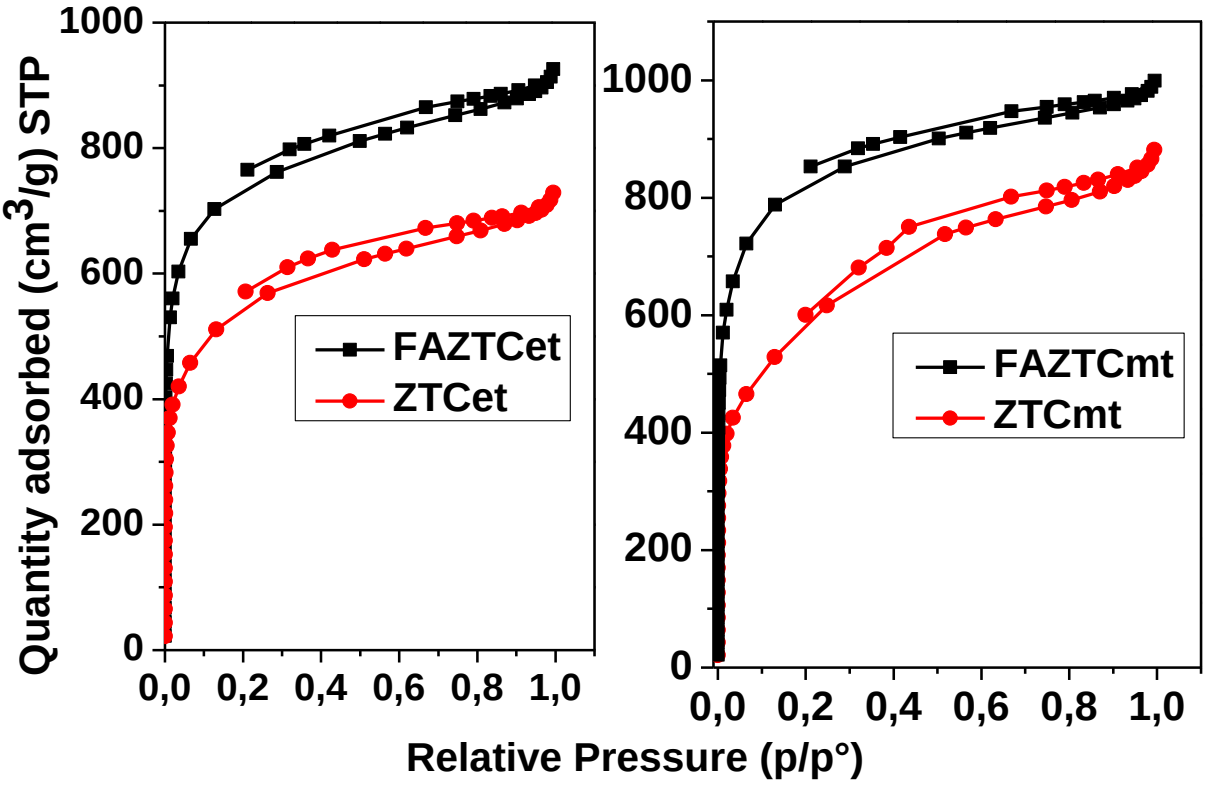

Figure 4.6: N_2 sorption isotherms at 77K, 1 bar plot for ZTCet, FAZTCet , ZTCmt and FAZTCmt.

Pore size distribution

Fig. 4.7 represent the pore size distribution plots (PSD) generated using the Horvath-Kawazoe (H-K) method. The PSD of the carbons appeared to be dominated by the pores at around 1.2 nm (the maximum values are recorded in Table 4.2) which is consistent with previous studies reported by Masika and Mokaya [44]. These finding agree with higher zeolite structural ordering which does not possess pore sizes large than 1.5nm. The carbons obtained using methane had a narrow sharp PSD which shows that the carbons are highly porous. The pore splitting at the range 0.8 – 1.22 nm for two-step synthesis may be as a result of ultramicropore filling of the zeolite pores during polymerisation and CVD process. The one-step synthesis method did not show this pore splitting which may be due to the inability of molecules to access ultramicropores.

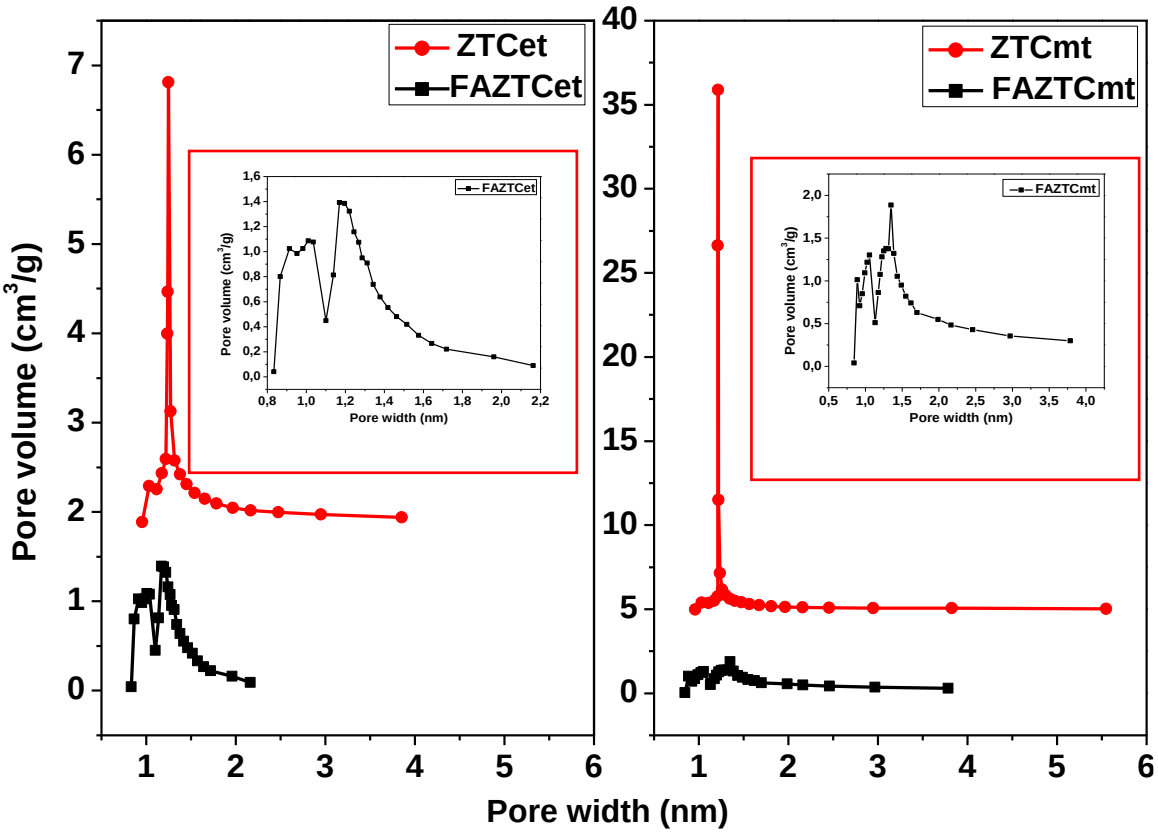

Figure 4.7: Pore size distribution plot for ZTCet, FAZTCEt , ZTCmt and FAZTCmt.

Table 4.2: Textual properties and H_2 uptake capacities of ZTCmt, ZTCet, FAZTCmt, and FAZTCet

Sample name	**BET Specific surface area(m^2/g)**	**Average Pore size (nm)**	**Average Pore volume (cm^3/g)**	**H_2 uptake (wt. %)**
ZTCmt	2015	1.21	0.95	1.91
ZTCet	1850	1.24	0.79	1.88
FAZTCmt	2974	1.28	1.21	2.77
FAZTCet	2674	1.22	1.08	2.50

Hydrogen sorption studies

The H_2 sorption isotherms of zeolite templated carbons, at 77K and 1 bar, are presented in Fig. 4.8. The absence of the hysteresis loop suggests the complete reversibility of hydrogen adsorption. It is evident that, ZTCs can adsorb hydrogen at relatively high pressures since there is no saturation at 1 bar. Specific surface area, pore volume, and micropores of a material are influential on adsorption of hydrogen. FAZTCmt (2.77%) which has higher surface area and pore volume, has high hydrogen storage capacity of as compared to FAZTCet (2.50%). Post synthetic modification to improve textual properties which will in turn increase hydrogen uptake could be expected. This observation where also observed by many other researchers.[35, 46, 49, 146-147]

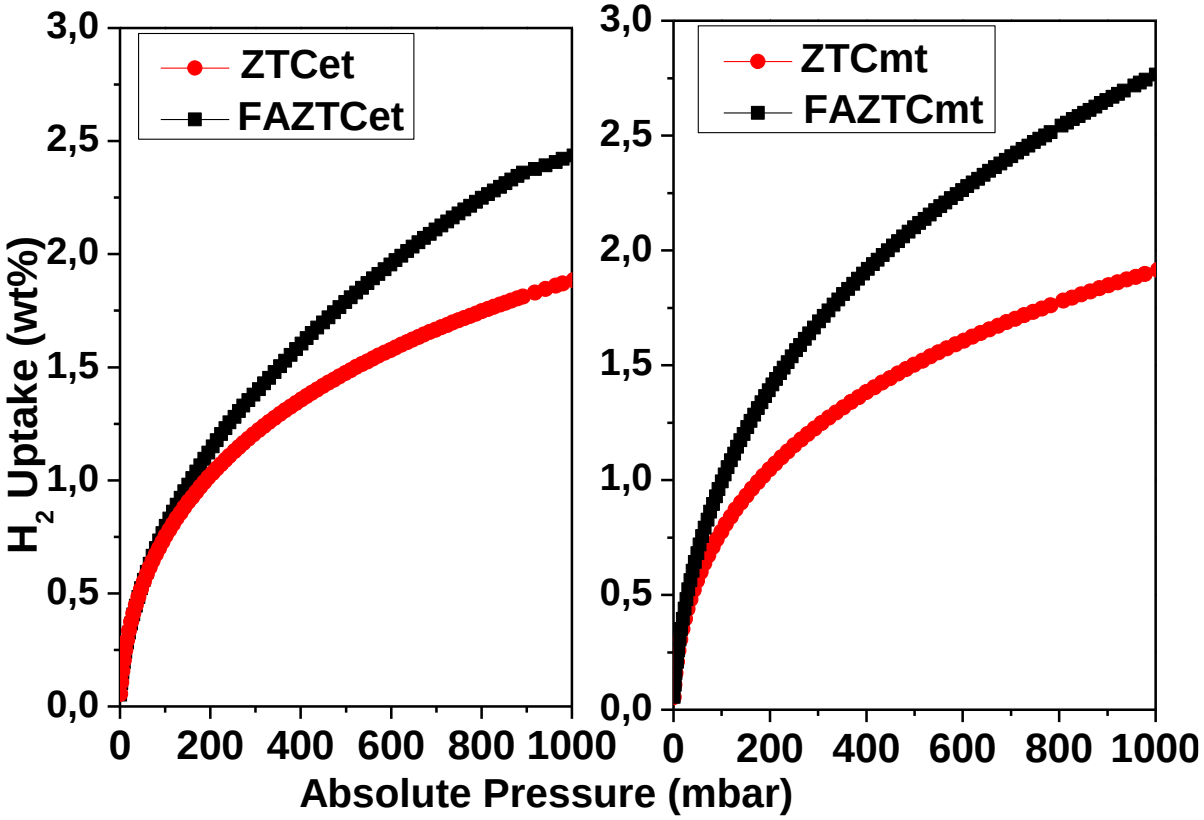

Figure 4.8: H_2 uptake for ZTCet, FAZTCet, ZTCmt and FAZTCmt.

4.5 Conclusions

The study has demonstrated that utilisation of biogas in its raw form does not lead to production of ZTCs due to competition of CO_2 during the CVD process. However, when pure methane was utilised, the ZTCs obtained were almost of similar quality as compared to those obtained using commercial ethylene gas feedstock. When one-step process was followed (using CH_4 only), the surface area of the obtained ZTCs (2015 m^2/g) is lower than the surface area of the two-step process (2974 m^2/g) that utilised prior impregnation of furfural alcohol followed by CH_4. The morphology of all the obtained ZTCs was a close replica of the parent zeolite. We demonstrated that complete template removal through TGA (i.e., weight loss of ~99% at 900 °C). Noteworthy, the study has demonstrated the potential for value-addition of biogas through development of a new product streams (ZTC) which has not been reported before.

Acknowledgements

The authors of this paper would like to acknowledge the financial support from Future Leaders – African Independent Research (FLAIR) Fellowship for N M Musyoka, the Council for Scientific and Industrial Research (CSIR) and University of Pretoria (UP) for providing facilities. Any opinions, findings and/or recommendations expressed here are those of the authors and not of the funding bodies.

4.6 Chapter summary

This chapter discusses the results of the obtained ZTCs that were synthesised using the one-step and two-step processes with either ethylene or methane as carbon sources. The study indicated successful replication of the zeolite on the ZTCs. SEM and XRD were used to confirm the results. The methane ZTCs (2974 m^2/g) obtained using the two-step process had higher surface area as compared to those obtained using ethylene (2674 m^2/g). Comparison on carbon sources was also studied and it was observed that methane synthesised ZTCs had higher surface area when either one-step or two-step processes are employed. The ZTCs with the highest surface area had higher H_2 adsorption (2.77%) at 1 bar and 77K.

Chapter 5

5 Results and discussions: MOF derived carbons and carbon nanotubes

This chapter comprises of the discussions of the obtained results of the MOFs, MDCs and CNTs. MOFs were successfully obtained from AMD and were further carbonised to synthesis MDC. The obtained MDCs were used as catalysts for the synthesis of CNTs. H_2 uptake was tested on MOFs and MDCs.

Synthesis of solid carbons using iron-based metal organic frameworks (MIL-88B & MIL-101)

Keaoleboga Mosupi[1,2], Ashton Swartbooi[1], Nqobile Mthembu[1,2], Henrietta W. Langmi[2], Nicholas M. Musyoka[1*]

[1]Centre for Nanostructures and Advanced Materials (CeNAM), Chemicals cluster, Council for Scientific and Industrial Research (CSIR), Meiring Naude Road, Brummeria, Pretoria, 0001, South Africa, kmosupi@csir.co.sa

[2]Department of Chemistry, University of Pretoria, Private Bag X20, Hatfield, 0028, South Africa.

[*]Corresponding author: NMusyoka@csir.co.sa

Abstract

Metal organic frameworks (MOF) have great properties as porous materials; however, most types are known to have very low thermal stability which can be shortcoming for various applications. Carbonisation strategy can be employed to enhance thermal stability of this porous materials. Two MOF types (MIL-88B & MIL-101) derived from acid mine drainage waters (AMD) were carbonised to generate carbons which were then tested for hydrogen adsorption and further used to grow carbon nanotubes (CNTs). For the growth of CNTs, CH_4 was used as carbon precursor. The obtained results shown that the MOF structures were completely carbonised and multiwalled carbon nanotubes (MWCNTs) were prepared. Surface area of MOF-derived carbons (MDC-88B and -101) was found to be 267 and 272 m^2/g with hydrogen adsorption of 0.58 wt% and 0.54 wt% respectively. The MWCNTs had a reasonable degree of graphitisation ($I_G/I_D = 1$). This study confirms that AMD derived MOFs can be used as catalyst for synthesis of CNTs and their derived carbons can be used for H_2 adsorption.

Keywords: Carbon nanotubes, metal organic framework, materials institute Lavoisier (MIL), Growth mechanism, MOF derived carbons.

5.1 Introduction

Metal organic frameworks (MOFs) have gained increasing interests as adsorption materials because of their large surface area and pore volume.[161-162] However, for the same reasons as MOFs, nanoporous carbons have also become popular as adsorbents. Several techniques can be used to create porous carbonaceous materials, such as chemical vapor deposition (CVD), template synthesis processes, direct carbonisation of MOFs, pyrolysis followed by physical or chemical activation of organic precursors, carbonisation of polymeric aerogels, and others. [69-71] MOFs can be carbonised to make MOF derived carbons which can later be tested for adsorption perfomances. The procedure for fabrication of MDCs can be achieved via two routes: Direct carbonisation and template impregnation. On direct carbonisation, thermal treatment of MOFs can be used to change their structures into nanocomposites made of metal/metal oxides and carbon material. Calcination of MOFs must be conducted under inert atmosphere (i.e., nitrogen or argon).[72] Some of the metals vaporise at the working temperatures and the remainder can be removed chemically, through acid washing.[73] For template impregnation method, MOFs are impregnated with carbon containing liquid which acts as a carbon precursor. Liu *et al* [71] impregnated MOF-5 with furfuryl alcohol and carbonised it at 1000 °C for 8 h under inert atmosphere. ZnO was reduced and Zn metal vaporised (boiling point: 908 °C) with argon. The prepared carbons had hydrogen adsorption of 2.6 wt% at 1 bar. Van Tran *et al* [73-74] utilised Fe-MIL-88B for generation of MDCs, the MOF was prepared by combining Fe cluster and 1,4-benzendicarboxylic acid (H_2BDC). The prepared MDCs had a decreased surface area (202 m^2/g) at temperatures above 600 °C. Lee *et al* [75] prepared Fe-MIL-88B which exhibited surface area increase (170 – 265 m^2/g) with an increase in temperature (600 – 800 °C). Tran *et al* [74] prepared amino-functionalised Fe-MIL-88B MDCs for adsorption of ciprofloxacin from aquatic solutions. Fe-MIL-101 has also been carbonised and used as sorbents for stir bar sorptive-dispersive microextraction of sulfonamides by Qin *et al*.[76] The obtained surface area for the MDCs was at 129.5 m^2/g at 900 °C. In this study, the prepared MDCs will be tested for H_2 adsorption and used as catalysts for the synthesis of carbon nanotubes.

Since the unearthing of carbon nanotubes (CNTs) by Iijima[77] in 1991, CNTs have been used for various applications such as gas storage, as electrode materials for electrochemical double layer capacitors, as electron field emitters, catalyst supports, biomedical applications, biosensors for toxic gases and as material for probe tip for atomic force microscopy. The applications of CNTs are governed by their unique structural, electromechanical, mechanical, electronic and chemical properties.[78] Iijima first synthesised CNTs using arc-discharge method which requires the use of high temperatures (>1700 °C). Laser ablation is another method used for the synthesis of CNTs, however, it also faces challenges

of high temperatures.[79-81] Catalytic chemical vapour deposition (CCVD) has been used to prepare single and multi-walled carbon nanotubes (SWCNT & MWCNT) by catalytic decomposition of various hydrocarbons. The use of a catalyst has helped in lowering the high temperatures to below 1000 °C. When certain parameters are controlled, long SWCNT or MWCNT can be produced with low defects, less impurities and high yields.[78] This method affords scale up production of CNTs.

Since CCVD is the most suitable method for scale up synthesis of CNTs, research on new effective catalysts is crucial. Various metal catalysts such as Fe, Co, Ni, Mo on supports like MgO, SiO_2, Al_2O_3, CaO and ZrO_2 prepared via impregnation, co-precipitation, or sol–gel processes have been used for the production of CNTs [78, 108]. Pérez-Cabero *et al* [112] suggested that, Synthesis of CNTs over iron metal catalysts, takes place much easier because interaction between formed CNTs and iron metal leans more towards structure in-sensitivity as compared to other metal catalyst.

In this research iron-based metal organic frameworks (MOFs) derived from acid mine drainage waters (AMD) are used as catalyst in the production of CNTs. AMD is produced when sulphide bearing rocks interact with water and oxygen.[64] Although this process occurs naturally, mining can accelerate it by exposing sulphide bearing rocks to oxygen and water. AMD poses an environmental risk due to the fact that it is made of high concentration levels of metals such as iron, aluminium, manganese and other heavy metals.[65] Metals can be recovered from AMD as hydroxides by precipitating with alkaline solutions. This method affords easy control of the pH, it is economically viable and can be applied to large operating units.[66] Iron extracted from AMD can be used for the synthesis of Matérial Institut Lavoisier (MIL-88B and MIL-101) MOFs.

When hydrocarbons and organic linkers of the MOF are decomposed on the surface of MIL-88B & -101, they interact with the iron metal clusters to form CNTs that have the same inner diameter as the diameter of the iron cluster. This method avoids the need of catalyst supports, additionally if the morphology of the MOFs is reserved then CNTs surface area will be improved.

5.2 Materials and experimental procedure

Ditopic terephthalic acid (H_2BDC, 98 %) was obtained from Sigma Aldrich, iron hydroxide ($Fe(OH)_3$) extracted from AMD obtained from a coal mine in Gauteng South Africa, hydrogen peroxide (H_2O_2, 30 %), dimethylformide (DMF, 99.5 %), sodium hydroxide (NaOH, 1 M), nitric acid (HNO_3, 55 %), glacial acetic acid (CH_3COOH, 98.5 %) were all obtained from Associated Chemical Enterprises. Methane gas was obtained from Air products. All chemicals were used without further purification.

Synthesis of metal organic frameworks

Extraction of iron: 30 % H_2O_2 (30 ml) was added to AMD (1000 ml) and the solution was left to stir for 1.5 h at room temperature. 1M NaOH solution was added into the solution and left to stir for additional 15 min. The precipitate was filtered and washed with H_2O (1000 ml). The resulting powder was dried at 80 °C for 12 h.

Fe-MIL-88B: AMD-derived iron salt (0.6634 g) was dissolved in HNO_3 (2.5 ml) by heating at 50 °C. The organic linker solution was prepared by ultrasonic assisted dissolution of H_2BDC (1.05 g) was dimethylyformide (DMF) (40 ml). AMD-derived iron salt solution was added into H_2BDC solution and stirred at room temperature followed by the addition of glacial acetic acid (1.2 ml). The solution was transferred into the Teflon cup and heated at 150 °C for 15 h. The resulting residues was centrifuged and washed 3 times with DMF (50 ml ×3). The product was denoted as MIL-88B.

Fe-MIL-101: AMD-derived iron salt (0.2619 g) was dissolved in HNO_3 (0.6 ml) by heating at 50 °C. H_2BDC (1.05 g) disolution in dimethylyformide (DMF) (40 ml) was assisted by ultrasonication. The precipitated iron salts solution was combined with the H_2BDC solution and stirred at room temperature. The combined solution was then transferred into a Teflon cup. The solution was then heated at 110 °C for 20 h. The resulting residues was centrifuged and washed 3 times with hot DMF (50 ml ×3). The product was denoted as MIL-101.

Synthesis of MDCs: The acquired MOFs were put in a tube furnace for the synthesis of MOF-derived carbons (MDCs), which involved heating them at 800 °C for 2 h while under argon flow and then allowing them to cool to ambient temperature. 10% HCl was used to reflux the resulting black powder for 12 h at 70 °C. The resultant material was washed with deionised water before being collected for characterisation. Carbons from MIL-88B were denoted as MDC-88B and the carbons from MIL-101 were denoted as MDC-101.

Synthesis of MDC-grown-CNTs: The 0.5 g of MOF was placed in a quartz boat and transfered into the tube furnace. After purging the tube furnace with argon for 15 min, temperature was increased to 700 °C (5 °C/min) under argon. At 700 °C, hydrogen was allowed to flow through the tube to have gas ratio of 1 H_2 : 5 Ar for 60 min. Temperature was then increased up to 900 °C under argon only. At 900 °C CH_4 was introduced to make gas mixture of 1 CH_4 : 2 Ar for 60 min. CNTs from MIL-88B are denoted as CNT-88B whereas those obtained from MIL-101 are denoted as CNT-101. The experimental set-up for the chemical vapour deposition (CVD) utilising methane gas is shown in Fig. 5.1.

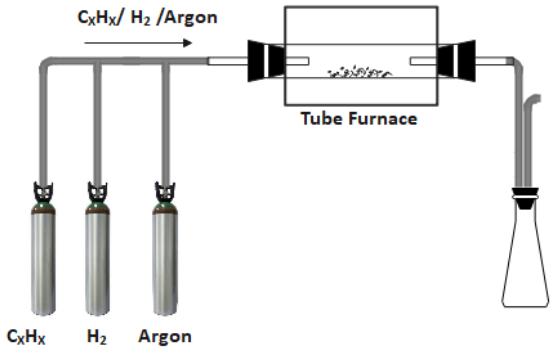

Figure 5.1. CVD set-up for synthesis of MDC-grown-CNTs

5.3 Characterisation

Phase identification of the prepared samples was conducted using Rigaku Ultima IV diffractometer using Ni-filtered Cu-Kα radiation (0.154 nm) in the range of 2θ = 1–90° at a scanning rate of 0.1°s^{-1}. The obtained MOFs, MDCs' and CNTs' morphology was examined under a JEOL-JSM 7500F scanning electron microscope. MOFs, MDCs' and CNTs' pictures were captured using a JEOL-Jem 2100 model transmission electron microscope (TEM). Using the Micromeritics(R) ASAP 2020 HD, BET surface area measurements were made at liquid N_2 temperature (77K) and relative pressures (P/P_0) ranging from 0 to 1. After outgassing at 200 °C under vacuum for the whole night, N_2 adsorption-desorption isotherms were obtained. The linear portion of the N_2 isotherms yielded the BET surface areas. Using the Horvath–Kawazoe (HK) model, pore size distribution plots and pore volumes were derived. H_2 adsorption isotherms at 77 K and up to 1 bar, were also measured on the Micromeritics(R) ASAP 2020 HD instrument. All gas sorption isotherms were obtained using ultra-high purity grade (99.999 %) gas. Thermal stability of the prepared samples was determined using TGA instrument (TA instruments, Q500 model) alumina crucibles under air at a temperature rate of 10 °C/min at a temperature range of 0 °C to 1000 °C.

5.4 Results and discussions

Structural analysis

X-ray powder diffraction (XRD)

Many researchers have indicated that, the characteristics of the X-ray diffraction pattern of CNTs are closely related to those of graphite. Peaks that appear at 2θ = 26, 2θ =43° and 43.48° indicate the presence of 002, 100 and 101 graphene layers, nano-graphene networks, or graphene stacking. The remaining peaks in the spectrum, however, are attributed to various crystal planes of Fe catalytic particles 2θ = 35.8°, 37.8°, 44.9°, 57° and 62°, see Fig. 5.2 a and b. These peaks are related to 220,

311, 400, 511 and 440 reflections of Fe_3C (cementite) and α-Fe (ferrite). These results are consistent with those obtained previously by Jedrzejewska *et al* [163], Siddheswaran *et al* [164] and Yang *et al* [165].

For MDCs there is noticeable absence of peaks associated with the parent MOFs (Fig. 5.2c). This indicates direct carbonisation of the MOFs at elevated temperatures. The Fe metal species are converted into iron oxides which are soluble in HCl and are washed out during washing step. The peaks at 2θ = 26° and 2θ =43° which represent the 002 and 101 planes of graphitic nature of carbons.

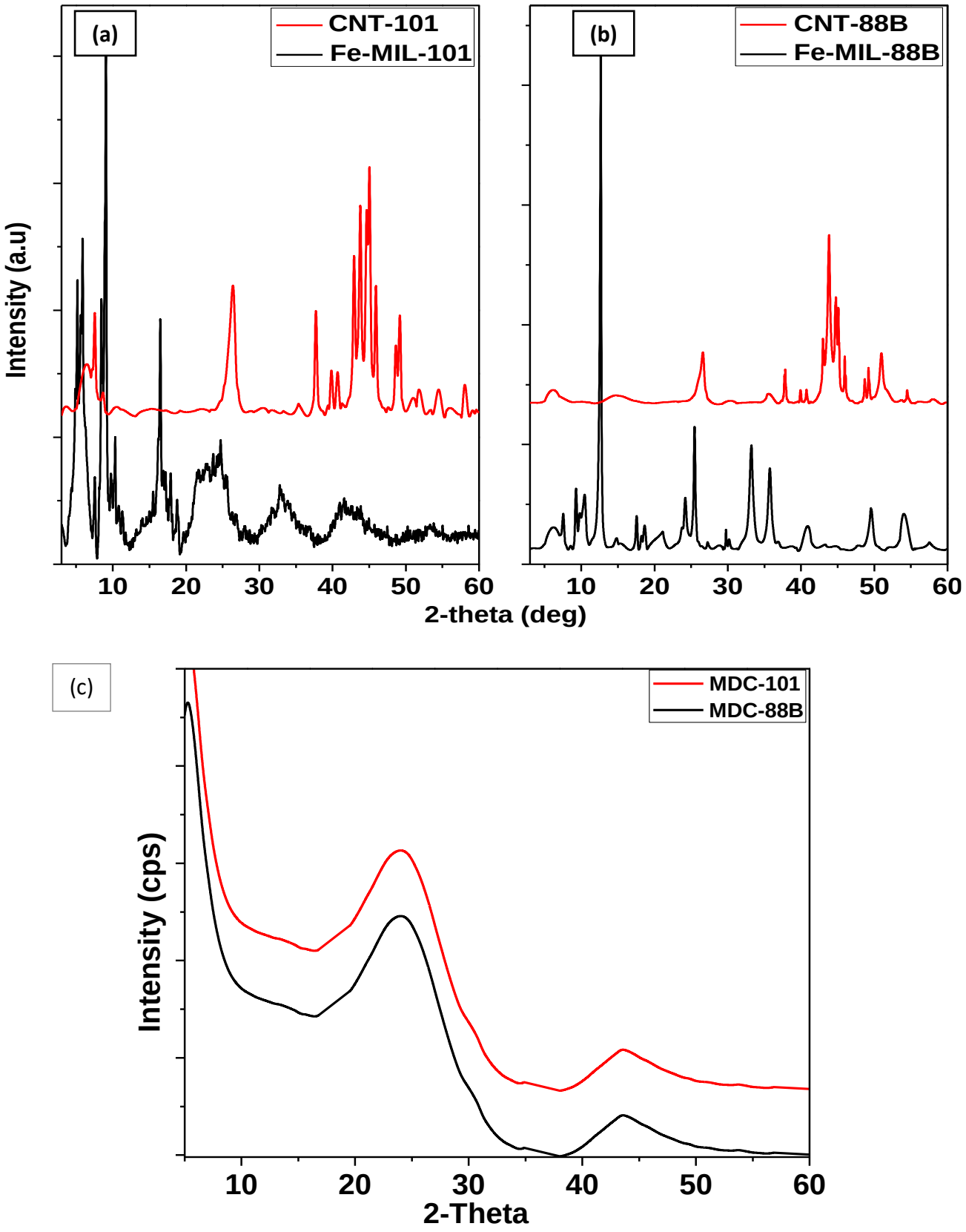

Figure 5.2: XRD analysis of (a) CNTs derived from Fe-MIL-101 and (b) CNTs derived from Fe-MIL88B () MDCs made from direct carbonisation of Fe-MIL-101 and Fe-MIL-88B

Raman analysis

Raman spectroscopy is a useful technique for characterisation of graphene and MWCNT as it can give information about structural defects and electronic data.[166] Fig. 5.3 presents the Raman spectra of the as-prepared MDC and CNT samples. The spectrums have three main bands: for MDC and CNT-88B. The graphitisation degree of the MOF derived carbons was determined using Raman spectroscopy. Both carbons display two prominent peaks corresponding to typical D-band and G-band of carbon materials (Fig. 5.3a). The D band for MDC-88B is located at 1336 and G band at 1587 cm^{-1} respectively while for MDC-101 the D band is at 1341 and G band at 1591 cm^{-1}. The ratio of D and G bands intensity (I_D/I_G) can be used as the measure of structural ordering, where the higher ratio signifies more defects. The intensity ratio (I_D/I_G) (Table 5.1) of MDC-88B (0.75) is slightly different from that of MDC-101 (0.91) although they are very comparable. There's high presence of structural defects that might be due to the acid watching.

For CNT-88B (Fig. 3b), D band is located at 1352 cm^{-1}, G band located at 1581 cm^{-1} and 2D located at 2690 cm^{-1}. For CNT-101 (Fig. 3b), D band is located at 1360 cm^{-1}, G band at 1593 cm^{-1} and 2D band at 2704 cm^{-1} respectively. D bands are due to the structural disorder or defects, G band is attributed to the ordered graphite in the CNTs and 2D is attributed to the second order Raman scattering because of two-phonon process.[167-168]. Serrano-Lotina and Dasa [169] postulated that, ratio that is closer to zero signifies CNTs with less defects, while close to one estimates CNTs with abundant structural defects. The intensity ratios of CNT-88B and CNT-101 are 1 and 1.03 respectively (See Table 5.1). The intensity of the D band is much higher than intensity of G band for both samples (CNT-88B and CNT-101), which was also observed by Ismagilov *et al* [170] and it further supports evidence of great presence of defects. The 2D intensity is inversely proportional to the number of walls of the CNTs.[171] This suggest that the MIL-88B CNTs (Fig. 5.3b) have few number of walls as compared to the MIL-101 CNTs (Fig. 5.3b).

Table 5.1: Raman analysis data

Sample name	D Band	G Band	I_D/I_G
MDC-88B	1336	1587	0.75
MDC-101	1341	1591	0.91
CNT-88B	1352	1581	1.00
CNT-101	1360	1593	1.03

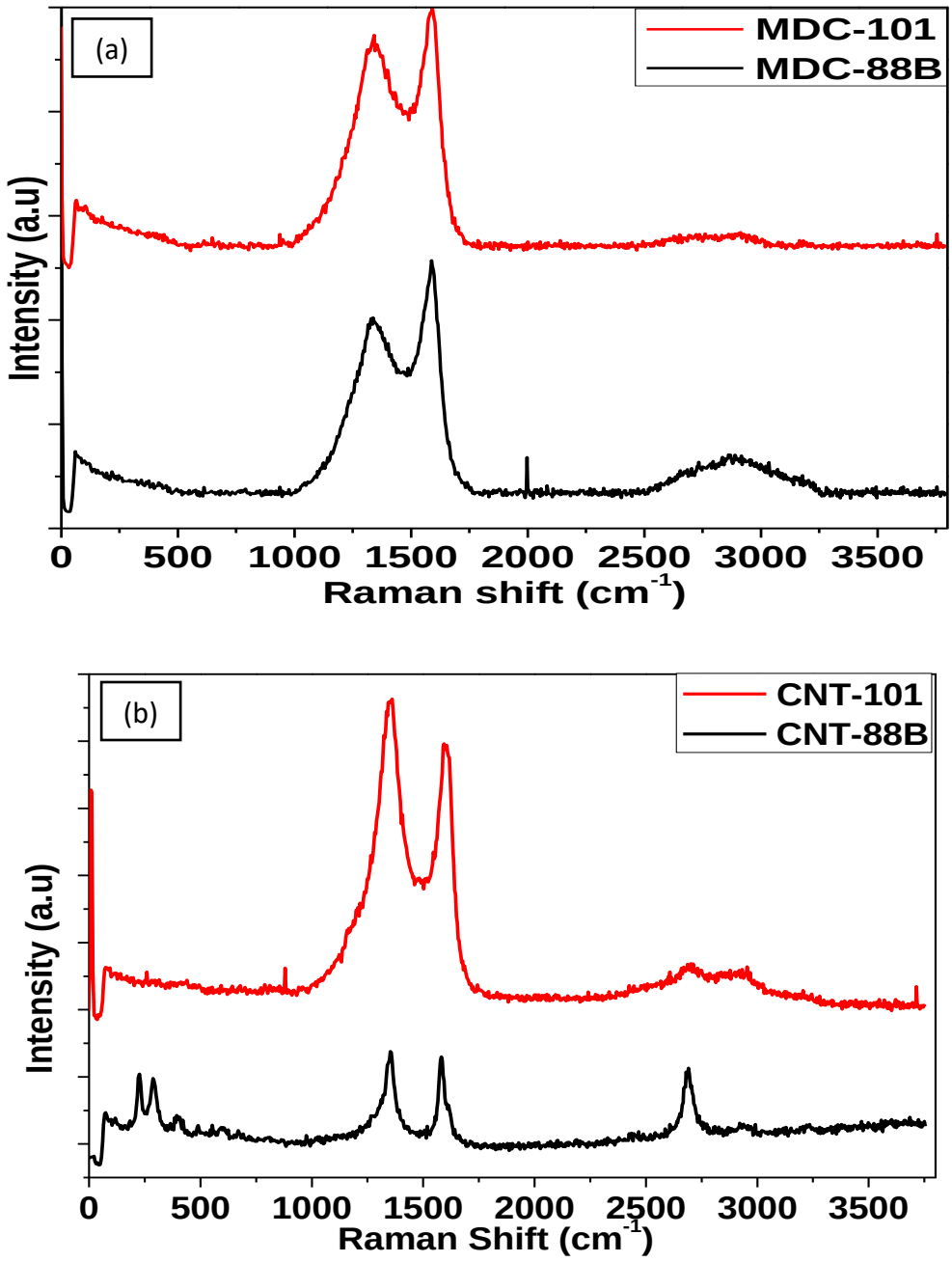

Figure. 5.3: Raman analysis of (a) MDC-88B and -101 (b) CNT-88B and -101

Morphological analysis

Scanning electron microscopy (SEM)

Synthesis of pure and high quality MIL-88B crystals is often challenging, there is often chances of getting a mixture of MIL-101 and MIL-53 crystals.[172-173] Fig. 5.4a shows the as-prepared elongated hexagonal bipyramidal morphology and a mixture of MIL-101. Fig. 5.4b, shows the octahedron shaped crystals with smooth facets and well-faceted small crystals of MIL-101 which is reported by other researchers as the shape for this MOF type.[174-175]

Fig. 5.4c and d shows the derived carbons, SEM was used to gain insight on the effect of pyrolysis temperature on morphology of the materials. The obtained carbons are highly amorphous and the structures of the MOFs was not retained. The thermal stability of MIL-88B and and MIL-101 are normally below 500 °C hence these materials are completely decomposed at 800 °C to form new structures. Van Tran *et al*,[73-74] Farisabadi *et al* [176] and Qin *et al* [76] obtained similar results.

Fig. 5.4e and f shows the carbon nanotubes synthesised from MIL-88B and MIL-101 using methane as a carbon precursor. The grown CNTs consists of tubular/cylindrical structures with different diameters and they are distributed randomly forming a clustered and cob-web like structures.

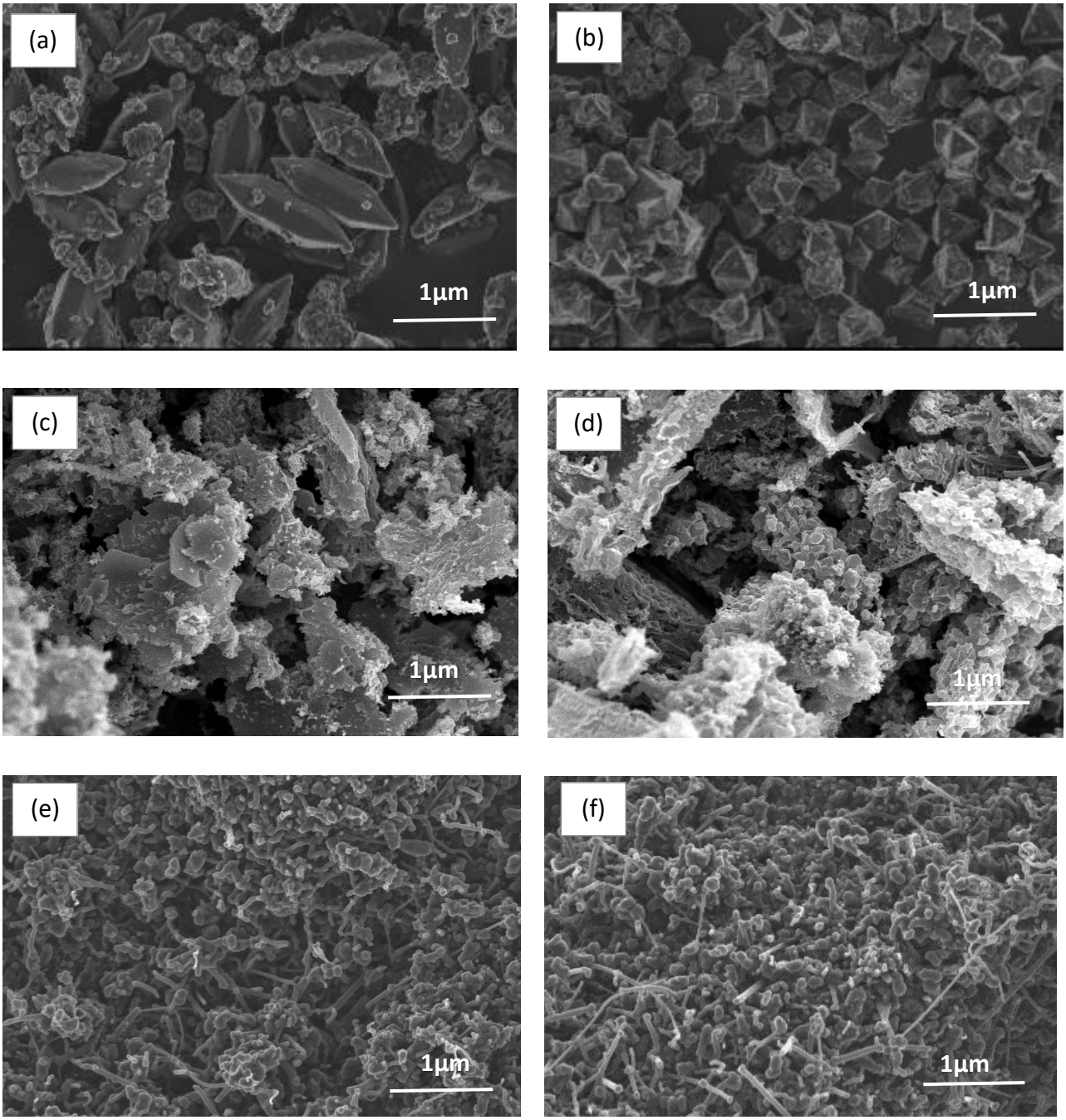

Figure. 5.4: SEM images of (a) Fe-MIL-88B, (b) Fe-MIL-101 , (c) MDC-88B , (d) MDC-101 , (e) CNT-88B, (f) CNT-101.

Transmission electron microscope (TEM)

HRTEM analysis was used to determine whether the as-synthesised structures were MWCNT, SWCNT, herringbone type, stacked cup, concentric, nested, or strolled sheets. It is further used to determine the growth mechanism of CNTs, i.e., whether it is by tip or base growth. Additionally, the inner diameter and outer diameters of the tubes can be determined. Fig. 5.5a presents HRTEM images of the CNTs grown on Fe-MIL-88b while Fig. 5.5b shows images of CNTs grown on MIL-101. It is evident from the images that MWCNTs (see, inset) were synthesised as shown by graphitic layers/sheets. CNTs were grown via a tip growth mechanism as shown by metal particle at the tip of the tubes.

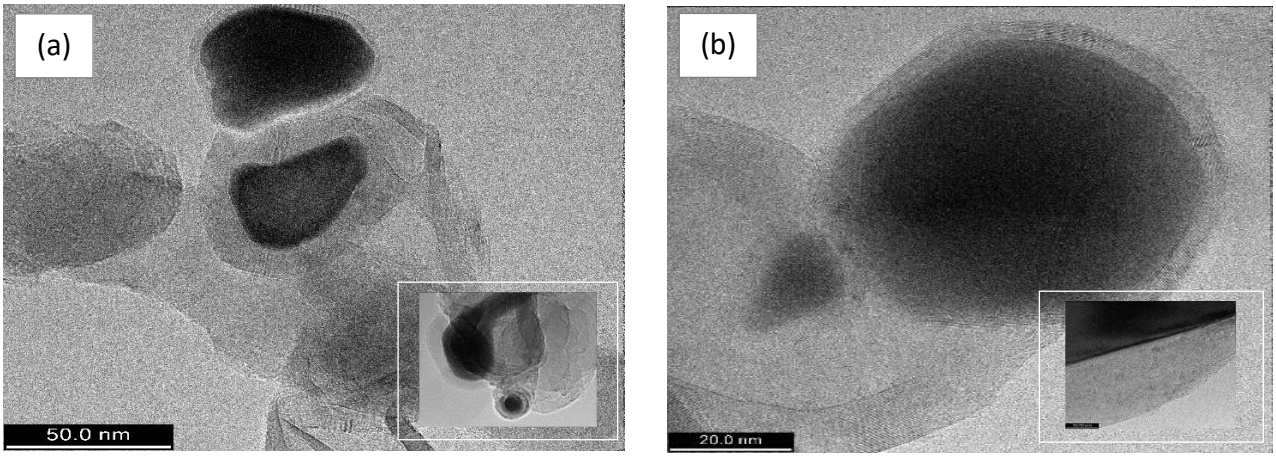

Figure. 5.5: TEM images of CNTs dominated by carbon spheres

Thermal analysis

Thermogravimetric analysis (TGA)

The TGA plots for MOFs, MDCs and CNTs are shown in Fig. 5.6. Initial weight loss of 18% and 22% can be attributed to the loss of guest molecules within the structure of MIL-88B and MIL-101 respectively. Approximately, 30 % and 42% weight loss at 350 °C is related to the decomposition of MIL-88B and MIL-101 respectively (Fig. 5.6a).

In Fig. 5.6b, TGA presents a weight loss of less than 5 wt% at initial temperatures (30-100 °C) which can be attributed to loss of water trapped within the pores of the MDCs. The carbonaceous material was noted to be thermally stable up to 480 °C. The materials completely decomposed which shows that it was purely carbonaceous, and the iron metals has been successfully washed out.

Fig. 5.6c shows TGA curves of the obtained CNTs. TGA can be used to examine the activity of each MOF-based catalyst in terms of carbon yield, by analysing the weight loss of deposited carbon in

thermal oxidation. The noticeable weight gain between 200 °C and 400 °C is due to the oxidation of the Fe metal.[177-178] About 43% and 45% of weight loss is observed in temperatures between 500 and 700 °C which is attributed to graphitic combustion. The remaining residue after combustion was attributed to the iron particles of the MOF catalysts. The residue amounted to 57% for CNT-88B and 55% for CNT-101.

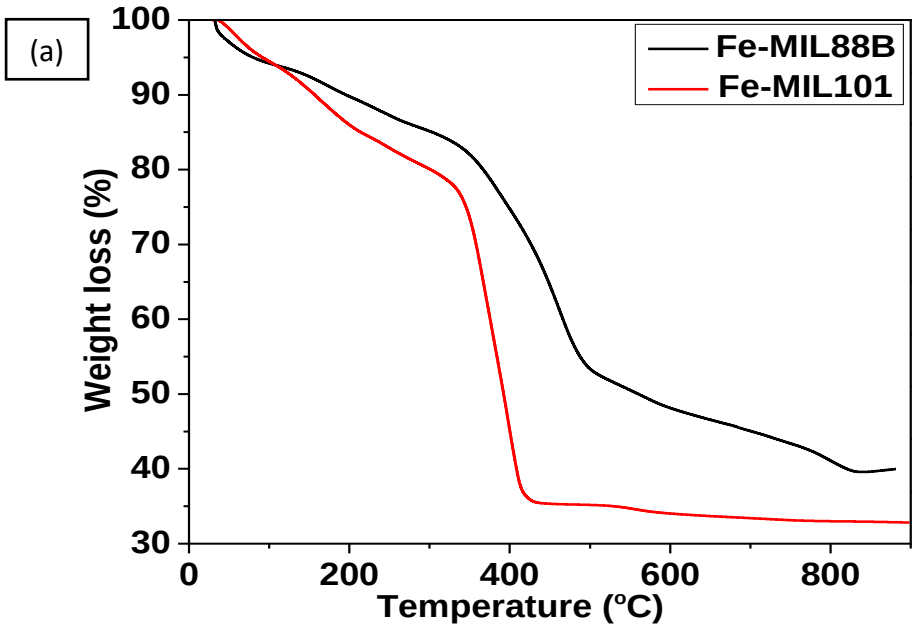

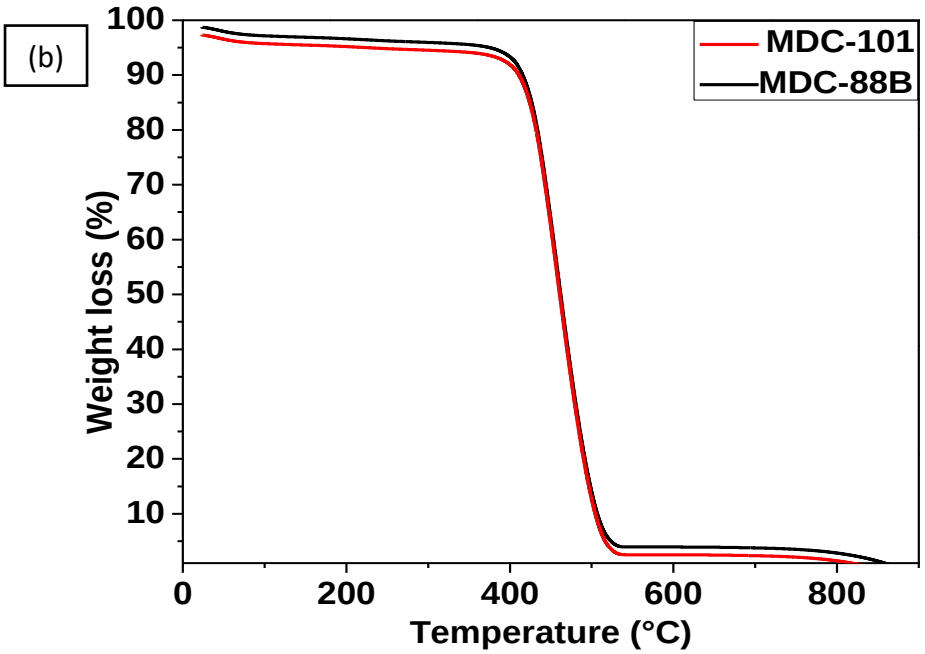

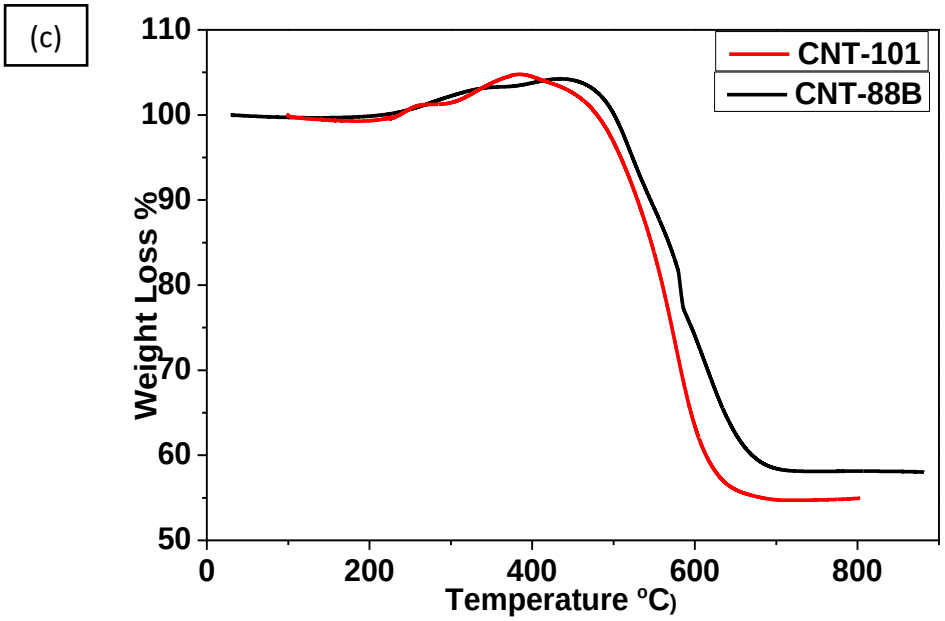

Figure. 5.6: TGA plots of (a) MIL-88B and MIL-101 (b) MDC-88B and -101 (c) CNT-88b and -101

Adsorption studies and physical properties

N_2 sorption isotherm and Pore size distribution

Surface area and porosity of the as-prepared MOFs and MDCs was determine using N_2 sorption studies. There is presence of hysteresis loop in Fe-MIL-88B and -101, Fig. 5.7a and MDC-88B and -101, Fig. 5.7b, which is consistent with type IV isotherms as per IUPAC classification.[179] The hysteresis loop on MDCs samples at $p/p_0 > 0.1$, shows the presence of mesopores. The steep N_2 adsorption at the lower partial pressure ($p/p_0 < 0.1$) suggest presence of micropores. Surface area of the materials is shown in Table 5.2.

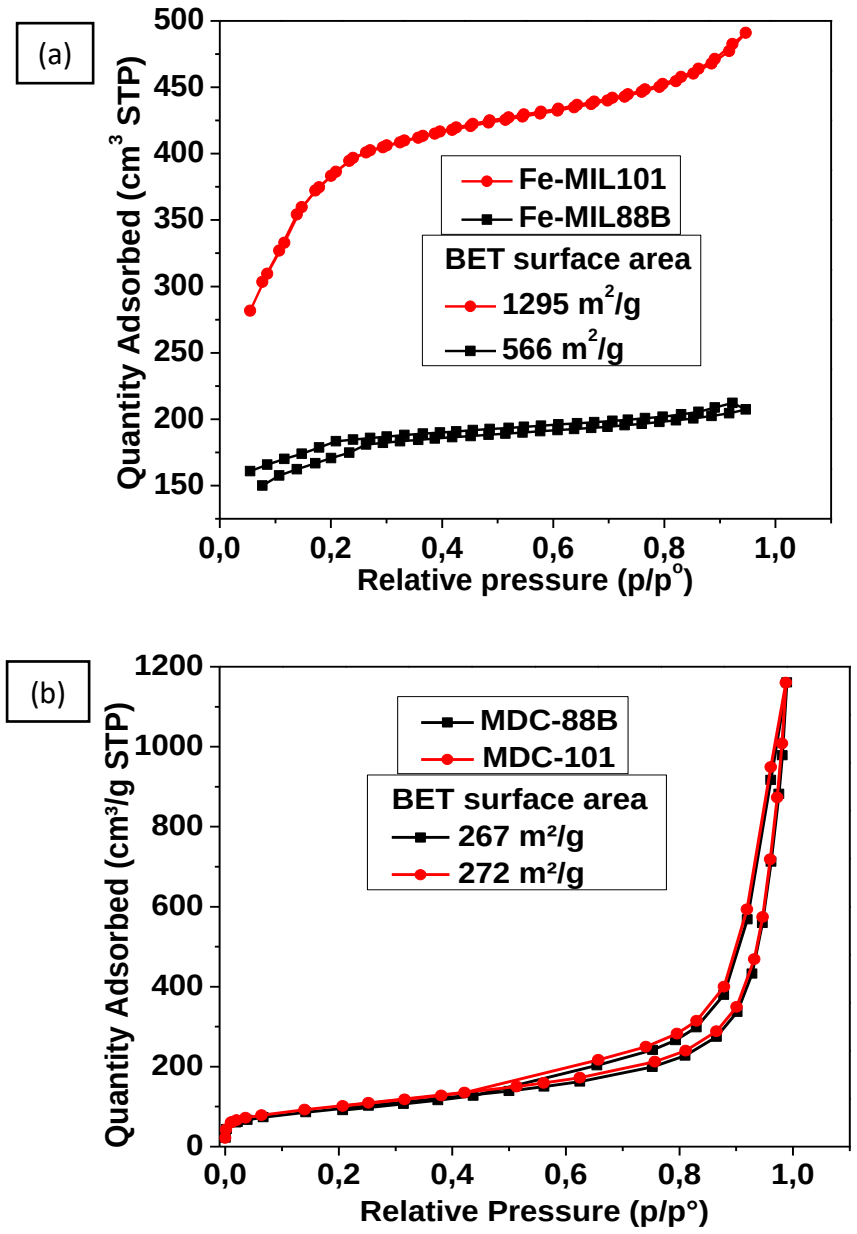

Figure. 5.7: N_2 sorption isotherm of (a) MOFs and (b) MDCs

Fig. 5.8a presents the pore size distribution (PSD) of Fe-MIL-101 and Fe-MIL-88B. The PSD of the MOFs appeared to be dominated by the pores at around <2 nm (micropores) and pores > 2nm (mesopores). The maximum values are recorded in Table. 5.2.

Fig. 5.8b, shows the pore size distribution plots of the prepared carbons. The pore sizes of MDCs vary from micropores (<2nm), mesopores (2 -50 nm) and macropores (>50 nm). Average pore size of MDCs is shown in Table. 5.2. This wide range shows the disintegration of the MOF structure which is dominated by micropores.

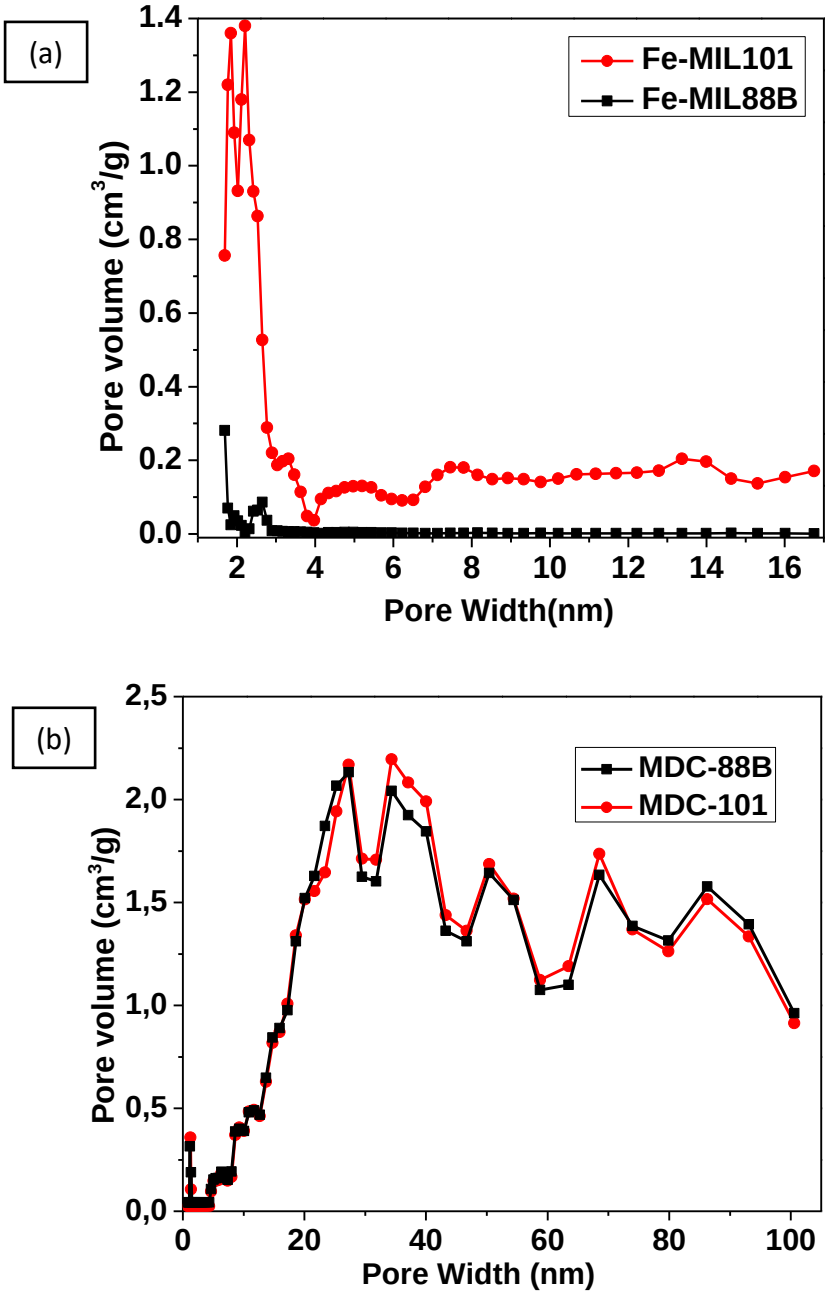

Figure 5.8: Pore size distribution of (c) MOFs and (d) MDC

Table 5.2: Textual properties and H_2 uptake capacities of Fe-MIL-88B, -101, MDC-88B and -101

Sample name	**BET Specific surface area(m^2/g)**	**Pore size (nm)**	**Pore volume (cm^3/g)**	**H_2 uptake (wt. %)**
Fe-MIL-88B	566	1.61	0.33	0.91
Fe-MIL-101	1295	1.61	0.76	1.07
MDC-88B	267	2.31	0.14	0.54
MDC-101	272	2.11	0.15	0.58

Hydrogen sorption studies

The hydrogen adsorption isotherms measured for Fe-MIL-88B, Fe-MIL-101 are presented in Fig. 5.9a and for MDC-101 and MDC-88B in Fig. 5.9b at 1 bar and 77K. The H_2 showed no saturation at 1 bar, which is indicative that, at higher pressures, the as-synthesised materials will be able to adsorb higher H_2 quantity. Fe-MIL-101 (1.07 %) had higher H_2 adsorption as compared to Fe-MIL-88B (0.91%). High adsorption of H_2 is directly related to high surface area obtained for Fe-MIL-101. MDC-101(0.58%) had a comparable hydrogen adsorption as MDC-88B (0.54%). The low hydrogen adsorption is as a result of the collapsed microporosity, low pore volume and specific surface area. Efforts to maintain the structural properties of MOFs will increase hydrogen adsorption.

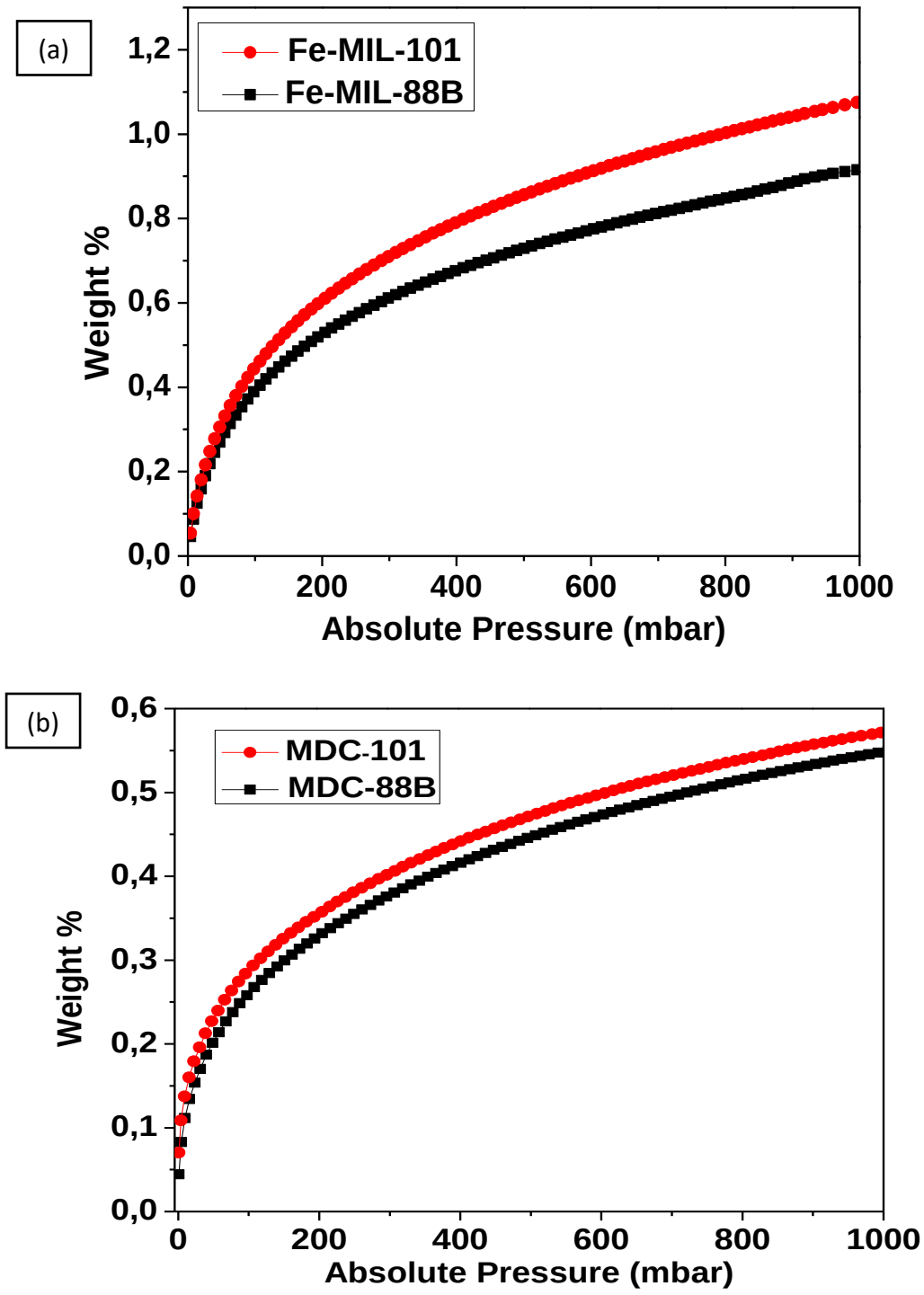

Figure 5.9: Hydrogen adsorption on (a) MOFs and (b) MDCs

5.5 Conclusions

When compared to the parent Fe-MOFs, the carbonised Fe-MOF samples shown a decrease in surface area and hydrogen uptake capabilities. The MOF structure directly collapsing is the cause of this deterioration. It is challenging to accurately control the morphology of MOF-derived carbons because metal nanoparticles aggregate irreversibly and because there is inadequate induction force during structural change at elevated temperature. The as-synthesised carbons have wide range of pore sizes which can be used in other applications. The synthesis of MWCNTs from decomposition of

methane using iron-based MOFs derived from acid mine drainage water via CVD has been demonstrated. The high CVD temperatures decompose organic linkers (H_2BDC) which leaves the metal clusters unsupported, and this resulted in tip growth mechanisms of the CNTs. Raman spectroscopy results suggested high degree of defects for the obtained CNTs. In summary, it can be concluded that Fe-MIL-88B and Fe-MIL-101 can be used as catalyst for the synthesis of MWCNTs.

Acknowledgements

The authors of this paper would like to acknowledge the financial support from Future Leaders – African Independent Research (FLAIR) Fellowship – awarded to N M Musyoka. The Council for Scientific and Industrial Research (CSIR) and University of Pretoria (UP) are also appreciated for providing facilities and support to make the study possible. Any opinions, findings and/or recommendations expressed here are those of the authors and not of the funding bodies.

5.6 Chapter summary

This chapter discusses the obtained results of MOFs, MDCs and CNTs. Synthesis of MOFs from AMD was successful. Fe-MIL-101(1295 m^2/g) had a higher surface area as compared to Fe-MIL-88 (566 m^2/g). Direct carbonisation was applied to MOF for porosity, and surface area enhancement by conversion to carbon material or MOF derived carbons (MDCs). This process is a common way of obtaining hierarchical porous carbons possessing high surface area, large pore volume with good thermal and chemical stability. The carbonised Fe-MOFs samples showed a decrease in surface area which might be due to collapsed MOF structure. The derived carbons were used as catalysts for synthesis of MWCNTs.

Chapter 6

6. Conclusions and future work

6.1 Introduction

The study on preparation of high surface area porous carbons using methane as the carbonaceous feedstock was successfully conducted with promising H_2 uptake.

6.2 Zeolite templated carbons using methane as carbon precursor

The firsts subobjective of the study was to synthesise ZTCs using methane as carbon source and compare the properties with those obtained using ethylene as carbon precursor. One- and two-step process were used for ZTCs synthesis and compared to each other. SEM and XRD confirmed the successful replication of the zeolite for both methane and ethylene. ZTCs from the two-step process had higher N_2 adsorption as compared to the one-step process at lower relative pressures. The two-step methane process sample (FAZTCmt (2974 m^2/g)) had higher surface area and pore volume (1.21 cm^3) as compared to the ethylene sample (FAZTCet (2674 m^2/g and 1.08 cm^3)). The obtained results confirmed that methane is a better carbon precursor alternative as compared to ethylene. The one-step process had lower surface areas which shows that wet impregnation step is crucial on the synthesis of ZTCs. The obtained ZTCs were dominated by pores at 1.2 nm which signifies the successful replication of the parent zeolite. The two-step process had pore splitting at the pore range of 1 -1.6 nm which confirms the presence of small and large micropores. FAZTCmt sample had higher H_2 uptake which further confirms the direct correlation of textual properties to gas adsorption.

6.3 Solid carbons from MIL-88B and MIL-101

The MOFs prepared from AMD went under direct carbonisation to obtained MDCs. MDCs obtained from direct carbonisation of MIL-88B had a surface area of 267 m^2/g and MDCs from MIL-101 was 272 m^2/g. The MOFs and their respective carbons were tested for H_2 uptake. MIL-101 (1.07 wt%) had higher H_2 uptake as a result of higher surface area, as compared to MIL-88B (0.91 wt%). The collapsed structure of the MDCs resulted in lower surface areas thus lower H_2 uptake. The as-synthesised carbons have wide range of pore sizes which can be used in other applications. The synthesis of MWCNTs from decomposition of methane using iron-based MOFs derived from acid mine drainage water via CVD has been demonstrated. The high CVD temperatures decompose organic linkers (H_2BDC) which leaves the metal clusters unsupported, and this resulted in tip growth mechanisms of the CNTs.

6.4 Future work

Future studies will investigate the use of biogas as to produce zeolite templated carbons or other carbon materials. Ionic species (Na^+) must be exchanged with ions that have strong affinity towards methane over carbon dioxide. To increase H_2 uptake doping of ZTCs with atoms such as nitrogen, sulphur, and boron must be investigated. Further understanding on the use of MOF as catalyst on the synthesis of CNTs is needed. Fine tuning of the catalyst to produce longer CNTS.

References

1. Okonkwo, U. C.; Onokpite, E.; Onokwai, A. O., Comparative study of the optimal ratio of biogas production from various organic wastes and weeds for digester/restarted digester. *Journal of King Saud University-Engineering Sciences* **2018,** *30* (2), 123-129.
2. Andriani, D.; Wresta, A.; Atmaja, T. D.; Saepudin, A., A review on optimisation production and upgrading biogas through CO2 removal using various techniques. *Applied biochemistry and biotechnology* **2014,** *172* (4), 1909-1928.
3. Harasimowicz, M.; Orluk, P.; Sakrzewska-Trznadel, G.; Chmielewski, A., Application of polyimide membranes for biogas purification and enrichment. *Journal of Hasardous Materials* **2007,** *144* (3), 698-702.
4. Ramaraj, R.; Dussadee, N., Biological purification processes for biogas using algae cultures: a review. *International Journal of Sustainable and Green Energy* **2015,** *4* (1), 20-32.
5. Davis, M. E., Ordered porous materials for emerging applications. *Nature* **2002,** *417* (6891), 813-821.
6. Farrusseng, D.; Aguado, S.; Pinel, C., Metal–organic frameworks: opportunities for catalysis. *Angewandte Chemie International Edition* **2009,** *48* (41), 7502-7513.
7. Nasir, S.; Hussein, M. Z.; Sainal, Z.; Yusof, N. A., Carbon-based nanomaterials/allotropes: A glimpse of their synthesis, properties and some applications. *Materials* **2018,** *11* (2), 295.
8. Beenakker, J.; Borman, V.; Krylov, S. Y., Molecular transport in subnanometer pores: zero-point energy, reduced dimensionality and quantum sieving. *Chemical Physics Letters* **1995,** *232* (4), 379-382.
9. Fan, S.; Chapline, M. G.; Franklin, N. R.; Tombler, T. W.; Cassell, A. M.; Dai, H., Self-oriented regular arrays of carbon nanotubes and their field emission properties. *Science* **1999,** *283* (5401), 512-514.
10. Ryoo, R.; Joo, S. H.; Kruk, M.; Jaroniec, M., Ordered mesoporous carbons. *Advanced Materials* **2001,** *13* (9), 677-681.
11. Subramoney, S., Novel nanocarbons—structure, properties, and potential applications. *Advanced Materials* **1998,** *10* (15), 1157-1171.
12. Zhang, W.; Li, G.; Yin, H.; Zhao, K.; Zhao, H.; An, T., Adsorption and desorption mechanism of aromatic VOCs onto porous carbon adsorbents for emission control and resource recovery: Recent progress and challenges. *Environmental Science: Nano* **2021**.
13. Gupta, V. K.; Saleh, T. A., Sorption of pollutants by porous carbon, carbon nanotubes and fullerene-an overview. *Environmental science and pollution research* **2013,** *20* (5), 2828-2843.
14. Bhadra, B. N.; Jhung, S. H., A remarkable adsorbent for removal of contaminants of emerging concern from water: porous carbon derived from metal azolate framework-6. *Journal of hasardous materials* **2017,** *340*, 179-188.
15. Ray, P. Z.; Shipley, H. J., Inorganic nano-adsorbents for the removal of heavy metals and arsenic: a review. *RSC Advances* **2015,** *5* (38), 29885-29907.
16. Wang, H.; Gao, Q.; Hu, J., High hydrogen storage capacity of porous carbons prepared by using activated carbon. *Journal of the American Chemical Society* **2009,** *131* (20), 7016-7022.
17. Yamasaki, A., An overview of CO2 mitigation options for global warming—emphasizing CO2 sequestration options. *Journal of chemical engineering of Japan* **2003,** *36* (4), 361-375.
18. Cundy, C. S.; Cox, P. A., The hydrothermal synthesis of zeolites: history and development from the earliest days to the present time. *Chemical reviews* **2003,** *103* (3), 663-702.
19. Johnson, E.; Arshad, S. E., Hydrothermally synthesised zeolites based on kaolinite: a review. *Applied Clay Science* **2014,** *97*, 215-221.
20. Król, M., Natural vs. synthetic zeolites. Multidisciplinary Digital Publishing Institute: 2020.
21. Mumpton, F. A., Using zeolites in agriculture. *Innovative biological technologies for lesser developed countries* **1985**, 127-158.
22. Liu, Y.; Kravtsov, V. C.; Eddaoudi, M., Template-Directed Assembly of Zeolite-like Metal–Organic Frameworks (ZMOFs): A usf-ZMOF with an Unprecedented Zeolite Topology. *Angewandte Chemie* **2008,** *120* (44), 8574-8577.

23. Weckhuysen, B. M.; Yu, J., Recent advances in zeolite chemistry and catalysis. *Chemical Society Reviews* **2015,** *44* (20), 7022-7024.
24. Le Van Mao, R.; Vu, N. T.; Xiao, S.; Ramsaran, A., Modified zeolites for the removal of calcium and magnesium from hard water. *Journal of Materials Chemistry* **1994,** *4* (7), 1143-1147.
25. Nguyen, M.; Tanner, C., Ammonium removal from wastewaters using natural New Zealand zeolites. *New Zealand Journal of Agricultural Research* **1998,** *41* (3), 427-446.
26. Zheng, Y.; Li, X.; Dutta, P. K., Exploitation of unique properties of zeolites in the development of gas sensors. *Sensors* **2012,** *12* (4), 5170-5194.
27. Siriwardane, R. V.; Shen, M.-S.; Fisher, E. P., Adsorption of CO2, N2, and O2 on natural zeolites. *Energy & fuels* **2003,** *17* (3), 571-576.
28. Harlick, P. J.; Tezel, F. H., An experimental adsorbent screening study for CO2 removal from N2. *Microporous and Mesoporous Materials* **2004,** *76* (1-3), 71-79.
29. Cavenati, S.; Grande, C. A.; Rodrigues, A. E., Adsorption equilibrium of methane, carbon dioxide, and nitrogen on zeolite 13X at high pressures. *Journal of Chemical & Engineering Data* **2004,** *49* (4), 1095-1101.
30. Weitkamp, J.; Fritz, M.; Ernst, S. In *Zeolites as media for hydrogen storage*, Proceedings from the ninth international zeolite conference, Elsevier: 1993; pp 11-19.
31. Amankwah, K.; Noh, J.; Schwarz, J., Hydrogen storage on superactivated carbon at refrigeration temperatures. *International journal of hydrogen energy* **1989,** *14* (7), 437-447.
32. Darkrim, F.; Aoufi, A.; Malbrunot, P.; Levesque, D., Hydrogen adsorption in the NaA zeolite: a comparison between numerical simulations and experiments. *The Journal of Chemical Physics* **2000,** *112* (13), 5991-5999.
33. Langmi, H.; Walton, A.; Al-Mamouri, M.; Johnson, S.; Book, D.; Speight, J.; Edwards, P.; Gameson, I.; Anderson, P.; Harris, I., Hydrogen adsorption in zeolites A, X, Y and RHO. *Journal of Alloys and Compounds* **2003,** *356*, 710-715.
34. Streb, A.; Mazzotti, M., Adsorption for efficient low carbon hydrogen production: part 1—adsorption equilibrium and breakthrough studies for H2/CO2/CH4 on zeolite 13X. *Adsorption* **2021,** *27* (4), 541-558.
35. Musyoka, N. M.; Ren, J.; Langmi, H. W.; Rogers, D.; North, B. C.; Mathe, M.; Bessarabov, D., Synthesis of templated carbons starting from clay and clay-derived zeolites for hydrogen storage applications. *International journal of energy research* **2015,** *39* (4), 494-503.
36. Haul, R., J. Kärger, D. M. Ruthven: Diffusion in Zeolites and other Microporous Solids, J. Wiley & Sons INC, New York 1992. ISBN 0-471-50907-8. 605 Seiten, Preis: £ 117. *Berichte der Bunsengesellschaft für physikalische Chemie* **1993,** *97* (1), 146-147.
37. Kyotani, T.; Ma, Z.; Tomita, A., Template synthesis of novel porous carbons using various types of zeolites. *Carbon* **2003,** *41* (7), 1451-1459.
38. Miao, J.; Lang, Z.; Xue, T.; Li, Y.; Li, Y.; Cheng, J.; Zhang, H.; Tang, Z., Revival of Zeolite-Templated Nanocarbon Materials: Recent Advances in Energy Storage and Conversion. *Advanced Science* **2020,** *7* (20), 2001335.
39. Moss, S. J.; Ledwith, A., *Chemistry of the Semiconductor Industry*. Springer Science & Business Media: 1989.
40. Kyotani, T.; Nagai, T.; Inoue, S.; Tomita, A., Formation of new type of porous carbon by carbonisation in zeolite nanochannels. *Chemistry of materials* **1997,** *9* (2), 609-615.
41. Ma, Z.; Kyotani, T.; Liu, Z.; Terasaki, O.; Tomita, A., Very high surface area microporous carbon with a three-dimensional nano-array structure: synthesis and its molecular structure. *Chemistry of materials* **2001,** *13* (12), 4413-4415.
42. Wada, Y.; Okubo, T.; Ryo, M.; Nakasawa, T.; Hasegawa, Y.; Yanagida, S., High efficiency near-IR emission of Nd (III) based on low-vibrational environment in cages of nanosized zeolites. *Journal of the American Chemical Society* **2000,** *122* (35), 8583-8584.
43. Taylor, E. E.; Garman, K.; Stadie, N. P., Atomistic structures of zeolite-templated carbon. *Chemistry of Materials* **2020,** *32* (7), 2742-2752.
44. Masika, E.; Mokaya, R., Preparation of ultrahigh surface area porous carbons templated using zeolite 13X for enhanced hydrogen storage. *Progress in Natural Science: Materials International* **2013,** *23* (3), 308-316.

45. Balahmar, N.; Lowbridge, A. M.; Mokaya, R., Templating of carbon in zeolites under pressure: synthesis of pelletized zeolite templated carbons with improved porosity and packing density for superior gas (CO 2 and H 2) uptake properties. *Journal of Materials Chemistry A* **2016,** *4* (37), 14254-14266.
46. Musyoka, N. M.; Rambau, K. M.; Manyala, N.; Ren, J.; Langmi, H. W.; Mathe, M. K., Utilisation of waste tyres pyrolysis oil vapour in the synthesis of Zeolite Templated Carbons (ZTCs) for hydrogen storage application. *Journal of Environmental Science and Health, Part A* **2018,** *53* (11), 1022-1028.
47. Pacuła, A.; Mokaya, R., Synthesis and high hydrogen storage capacity of zeolite-like carbons nanocast using as-synthesised zeolite templates. *The Journal of Physical Chemistry C* **2008,** *112* (7), 2764-2769.
48. Xia, Y.; Mokaya, R.; Grant, D. M.; Walker, G. S., A simplified synthesis of N-doped zeolite-templated carbons, the control of the level of zeolite-like ordering and its effect on hydrogen storage properties. *Carbon* **2011,** *49* (3), 844-853.
49. Sevilla, M.; Alam, N.; Mokaya, R., Enhancement of hydrogen storage capacity of zeolite-templated carbons by chemical activation. *The Journal of Physical Chemistry C* **2010,** *114* (25), 11314-11319.
50. Höller, H.; Wirsching, U., Zeolite formation from fly ash. *Fortschritte der mineralogie* **1985,** *63* (1), 21-43.
51. Musyoka, N. M.; Petrik, L. F.; Hums, E. In *Synthesis of zeolite A, X and P from a South African coal fly ash*, Advanced Materials Research, Trans Tech Publ: 2012; pp 1757-1762.
52. Golecki, I., Rapid vapor-phase densification of refractory composites. *Materials Science and Engineering: R: Reports* **1997,** *20* (2), 37-124.
53. Bowes, C. L.; Malek, A.; Ozin, G. A., Chemical vapor deposition topotaxy in porous hosts. *Chemical Vapor Deposition* **1996,** *2* (3), 97-103.
54. Kyotani, T.; Tsai, L.-f.; Tomita, A., Formation of ultrafine carbon tubes by using an anodic aluminum oxide film as a template. *Chemistry of materials* **1995,** *7* (8), 1427-1428.
55. Kyotani, T.; Tsai, L.-f.; Tomita, A., Preparation of ultrafine carbon tubes in nanochannels of an anodic aluminum oxide film. *Chemistry of Materials* **1996,** *8* (8), 2109-2113.
56. Li, W.; Xie, S.; Qian, L. X.; Chang, B.; Zou, B.; Zhou, W.; Zhao, R.; Wang, G., Large-scale synthesis of aligned carbon nanotubes. *Science* **1996,** *274* (5293), 1701-1703.
57. Ohring, M., *Materials science of thin films*. Elsevier: 2001.
58. Benelmekki, M.; Erbe, A., Nanostructured thin films–background, preparation and relation to the technological revolution of the 21st century. In *Frontiers of Nanoscience*, Elsevier: 2019; Vol. 14, pp 1-34.
59. Chen, Z.; Deng, S.; Wei, H.; Wang, B.; Huang, J.; Yu, G., Activated carbons and amine-modified materials for carbon dioxide capture—a review. *Frontiers of Environmental Science & Engineering* **2013,** *7* (3), 326-340.
60. Ma, X.; Li, L.; Chen, R.; Wang, C.; Li, H.; Wang, S., Heteroatom-doped nanoporous carbon derived from MOF-5 for CO2 capture. *Applied Surface Science* **2018,** *435*, 494-502.
61. Hou, P.-X.; Orikasa, H.; Itoi, H.; Nishihara, H.; Kyotani, T., Densification of ordered microporous carbons and controlling their micropore size by hot-pressing. *Carbon* **2007,** *45* (10), 2011-2016.
62. Annamalai, P.; Musyoka, N. M.; Ren, J.; Langmi, H. W.; Mathe, M.; Bessarabov, D.; Petrik, L. F., Electrospun zeolite-templated carbon composite fibres for hydrogen storage applications. *Research on Chemical Intermediates* **2017,** *43* (7), 4095-4102.
63. Molefe, L. Y.; Musyoka, N. M.; Ren, J.; Langmi, H. W.; Mathe, M.; Ndungu, P. G., Polymer-Based Shaping Strategy for Zeolite Templated Carbons (ZTC) and Their Metal Organic Framework (MOF) Composites for Improved Hydrogen Storage Properties. *Frontiers in chemistry* **2019,** *7*, 864.
64. Akcil, A.; Koldas, S., Acid Mine Drainage (AMD): causes, treatment and case studies. *Journal of cleaner production* **2006,** *14* (12-13), 1139-1145.
65. Johnson, D. B.; Hallberg, K. B., Acid mine drainage remediation options: a review. *Science of the total environment* **2005,** *338* (1-2), 3-14.
66. Macingova, E.; Luptakova, A., Recovery of metals from acid mine drainage. *Chemical Engineering* **2012,** *28*, 109-114.
67. Xiao, Y.; Guo, X.; Huang, H.; Yang, Q.; Huang, A.; Zhong, C., Synthesis of MIL-88B (Fe)/Matrimid mixed-matrix membranes with high hydrogen permselectivity. *RSC advances* **2015,** *5* (10), 7253-7259.

68. Sun, J.; Yu, G.; Huo, Q.; Kan, Q.; Guan, J., Epoxidation of styrene over Fe (Cr)-MIL-101 metal–organic frameworks. *RSC advances* **2014,** *4* (72), 38048-38054.
69. Yang, S. J.; Kim, T.; Im, J. H.; Kim, Y. S.; Lee, K.; Jung, H.; Park, C. R., MOF-derived hierarchically porous carbon with exceptional porosity and hydrogen storage capacity. *Chemistry of Materials* **2012,** *24* (3), 464-470.
70. Tang, J.; Salunkhe, R. R.; Liu, J.; Torad, N. L.; Imura, M.; Furukawa, S.; Yamauchi, Y., Thermal conversion of core–shell metal–organic frameworks: a new method for selectively functionalized nanoporous hybrid carbon. *Journal of the American Chemical Society* **2015,** *137* (4), 1572-1580.
71. Liu, B.; Shioyama, H.; Akita, T.; Xu, Q., Metal-organic framework as a template for porous carbon synthesis. *Journal of the American Chemical Society* **2008,** *130* (16), 5390-5391.
72. Salunkhe, R. R.; Kaneti, Y. V.; Kim, J.; Kim, J. H.; Yamauchi, Y., Nanoarchitectures for metal–organic framework-derived nanoporous carbons toward supercapacitor applications. *Accounts of chemical research* **2016,** *49* (12), 2796-2806.
73. Van Tran, T.; Nguyen, D. T. C.; Le, H. T.; Bach, L. G.; Vo, D.-V. N.; Dao, T.-U. T.; Lim, K. T.; Nguyen, T. D., Effect of thermolysis condition on characteristics and nonsteroidal anti-inflammatory drugs (NSAIDs) absorbability of Fe-MIL-88B-derived mesoporous carbons. *Journal of Environmental Chemical Engineering* **2019,** *7* (5), 103356.
74. Van Tran, T.; Nguyen, D. T. C.; Le, H. T. N.; Vo, D.-V. N.; Doan, V.-D.; Dinh, V.-P.; Nguyen, H.-T. T.; Nguyen, T. D.; Bach, L. G., Amino-functionalized MIL-88B (Fe)-based porous carbon for enhanced adsorption toward ciprofloxacin pharmaceutical from aquatic solutions. *Comptes Rendus Chimie* **2019,** *22* (11-12), 804-812.
75. Lee, H. J.; Cho, W.; Lim, E.; Oh, M., One-pot synthesis of magnetic particle-embedded porous carbon composites from metal–organic frameworks and their sorption properties. *Chemical Communications* **2014,** *50* (41), 5476-5479.
76. Qin, P.; Han, L.; Zhang, X.; Li, M.; Li, D.; Lu, M.; Cai, Z., MIL-101 (Fe)-derived magnetic porous carbon as sorbent for stir bar sorptive-dispersive microextraction of sulfonamides. *Microchimica Acta* **2021,** *188* (10), 1-11.
77. Iijima, S., Helical microtubules of graphitic carbon. *nature* **1991,** *354* (6348), 56-58.
78. Tran, K. Y.; Heinrichs, B.; Colomer, J.-F.; Pirard, J.-P.; Lambert, S., Carbon nanotubes synthesis by the ethylene chemical catalytic vapour deposition (CCVD) process on Fe, Co, and Fe–Co/Al2O3 sol–gel catalysts. *Applied Catalysis A: General* **2007,** *318*, 63-69.
79. Kong, J.; Cassell, A. M.; Dai, H., Chemical vapor deposition of methane for single-walled carbon nanotubes. *Chemical physics letters* **1998,** *292* (4-6), 567-574.
80. Laurent, C.; Flahaut, E.; Peigney, A.; Rousset, A., Metal nanoparticles for the catalytic synthesis of carbon nanotubes. *New Journal of Chemistry* **1998,** *22* (11), 1229-1237.
81. Dong, Z.; Li, B.; Cui, C.; Qian, W.; Jin, Y.; Wei, F., Catalytic methane technology for carbon nanotubes and graphene. *Reaction Chemistry & Engineering* **2020,** *5* (6), 991-1004.
82. Marina Filchakova, V. S. Single-walled carbon nanotubes: structure, properties, applications, and health & safety 2021. https://tuball.com/articles/single-walled-carbon-nanotubes (accessed 13 may 2021).
83. Salvetat, J.-P.; Bonard, J.-M.; Thomson, N.; Kulik, A.; Forro, L.; Benoit, W.; Zuppiroli, L., Mechanical properties of carbon nanotubes. *Applied Physics A* **1999,** *69* (3), 255-260.
84. Treacy, M. J.; Ebbesen, T. W.; Gibson, J. M., Exceptionally high Young's modulus observed for individual carbon nanotubes. *nature* **1996,** *381* (6584), 678-680.
85. Pipes, R.; Frankland, S.; Hubert, P.; Saether, E., Self-consistent physical properties of carbon nanotubes in composite materials. **2002**.
86. Ding, B.; Guo, D.; Wang, Y.; Wu, X.; Fan, Z., Functionalized graphene nanosheets decorated on carbon nanotubes networks for high performance supercapacitors. *Journal of Power Sources* **2018,** *398*, 113-119.
87. Zhang, L. L.; Zhao, X., Carbon-based materials as supercapacitor electrodes. *Chemical Society Reviews* **2009,** *38* (9), 2520-2531.
88. Berber, S.; Kwon, Y.-K.; Tománek, D., Unusually high thermal conductivity of carbon nanotubes. *Physical review letters* **2000,** *84* (20), 4613.
89. Hone, J., Carbon nanotubes: thermal properties. *Dekker Encyclopedia of Nanoscience and nanotechnology* **2004,** *7*, 603-610.

90. Zhao, N.; He, C.; Jiang, Z.; Li, J.; Li, Y., Fabrication and growth mechanism of carbon nanotubes by catalytic chemical vapor deposition. *Materials Letters* **2006,** *60* (2), 159-163.
91. Rice, F., The thermal decomposition of organic compounds from the standpoint of free radicals. I. Saturated hydrocarbons. *Journal of the American Chemical Society* **1931,** *53* (5), 1959-1972.
92. Kim, M.; Rodriguez, N.; Baker, R., The interaction of hydrocarbons with copper・ nickel and nickel in the formation of carbon filaments. *Journal of Catalysis* **1991,** *131* (1), 60-73.
93. Charlier, J.-C.; Iijima, S., Growth mechanisms of carbon nanotubes. *Carbon Nanotubes* **2001**, 55-81.
94. Ding, F.; Rosén, A.; Bolton, K., Molecular dynamics study of the catalyst particle size dependence on carbon nanotube growth. *The Journal of chemical physics* **2004,** *121* (6), 2775-2779.
95. Gohier, A.; Ewels, C.; Minea, T.; Djouadi, M., Carbon nanotube growth mechanism switches from tip-to base-growth with decreasing catalyst particle size. *Carbon* **2008,** *46* (10), 1331-1338.
96. Kumar, M., Carbon nanotube synthesis and growth mechanism. *Carbon Nanotubes-Synthesis, Characterisation, Applications* **2011**, 147-170.
97. Baddour, C. E.; Briens, C., Carbon nanotube synthesis: a review. *International journal of chemical reactor engineering* **2005,** *3* (1).
98. Arora, N.; Sharma, N., Arc discharge synthesis of carbon nanotubes: Comprehensive review. *Diamond and related materials* **2014,** *50*, 135-150.
99. Mhlanga, S. D.; Mondal, K. C.; Carter, R.; Witcomb, M. J.; Coville, N. J., The effect of synthesis parameters on the catalytic synthesis of multiwalled carbon nanotubes using Fe-Co/CaCO3 catalysts. *South African Journal of Chemistry* **2009,** *62*, 67-76.
100. Ando, Y.; Zhao, X., Synthesis of carbon nanotubes by arc-discharge method. *New diamond and frontier carbon technology* **2006,** *16* (3), 123-138.
101. Harris, P. J., Solid state growth mechanisms for carbon nanotubes. *Carbon* **2007,** *45* (2), 229-239.
102. Tessonnier, J. P.; Su, D. S., Recent progress on the growth mechanism of carbon nanotubes: a review. *ChemSusChem* **2011,** *4* (7), 824-847.
103. Prasek, J.; Drbohlavova, J.; Chomoucka, J.; Hubalek, J.; Jasek, O.; Adam, V.; Kizek, R., Methods for carbon nanotubes synthesis. *Journal of Materials Chemistry* **2011,** *21* (40), 15872-15884.
104. Journet, C.; Picher, M.; Jourdain, V., Carbon nanotube synthesis: from large-scale production to atom-by-atom growth. *Nanotechnology* **2012,** *23* (14), 142001.
105. Guo, T.; Nikolaev, P.; Thess, A.; Colbert, D. T.; Smalley, R. E., Catalytic growth of single-walled manotubes by laser vaporisation. *Chemical physics letters* **1995,** *243* (1-2), 49-54.
106. Rafique, M. M. A.; Iqbal, J., Production of carbon nanotubes by different routes-a review. *Journal of encapsulation and adsorption sciences* **2011,** *1* (02), 29.
107. Scott, C. D.; Arepalli, S.; Nikolaev, P.; Smalley, R. E., Growth mechanisms for single-wall carbon nanotubes in a laser-ablation process. *Applied Physics A* **2001,** *72* (5), 573-580.
108. Maghsoodi, S.; Khodadadi, A.; Mortasavi, Y., A novel continuous process for synthesis of carbon nanotubes using iron floating catalyst and MgO particles for CVD of methane in a fluidised bed reactor. *Applied Surface Science* **2010,** *256* (9), 2769-2774.
109. José-Yacamán, M.; Miki-Yoshida, M.; Rendon, L.; Santiesteban, J., Catalytic growth of carbon microtubules with fullerene structure. *Applied physics letters* **1993,** *62* (6), 657-659.
110. Kathyayini, H.; Nagaraju, N.; Fonseca, A.; Nagy, J., Catalytic activity of Fe, Co and Fe/Co supported on Ca and Mg oxides, hydroxides and carbonates in the synthesis of carbon nanotubes. *Journal of Molecular Catalysis A: Chemical* **2004,** *223* (1-2), 129-136.
111. Zeng, X.; Sun, X.; Cheng, G.; Yan, X.; Xu, X., Production of multi-wall carbon nanotubes on a large scale. *Physica B: Condensed Matter* **2002,** *323* (1-4), 330-332.
112. Perez-Cabero, M.; Rodrıguez-Ramos, I.; Guerrero-Ruız, A., Characterisation of carbon nanotubes and carbon nanofibers prepared by catalytic decomposition of acetylene in a fluidised bed reactor. *Journal of catalysis* **2003,** *215* (2), 305-316.
113. Hou, P.-X.; Liu, C.; Cheng, H.-M., Purification of carbon nanotubes. *carbon* **2008,** *46* (15), 2003-2025.
114. Ismail, A.; Goh, P. S.; Tee, J. C.; Sanip, S. M.; Aziz, M., A review of purification techniques for carbon nanotubes. *Nano* **2008,** *3* (03), 127-143.

115. Zhao, N.; He, C.; Li, J.; Jiang, Z.; Li, Y., Study on purification and tip-opening of CNTs fabricated by CVD. *Materials Research Bulletin* **2006,** *41* (12), 2204-2209.
116. Dong, C.; Campell, A. S.; Eldawud, R.; Perhinschi, G.; Rojanasakul, Y.; Dinu, C. Z., Effects of acid treatment on structure, properties and biocompatibility of carbon nanotubes. *Applied Surface Science* **2013,** *264*, 261-268.
117. Mohanapriya, S.; Lakshminarayanan, V., Simultaneous purification and spectrophotometric determination of nickel present in as-prepared single-walled carbon nanotubes (SWCNT). *Talanta* **2007,** *71* (1), 493-497.
118. Delpeux, S.; Szostak, K.; Frackowiak, E.; Béguin, F., An efficient two-step process for producing opened multi-walled carbon nanotubes of high purity. *Chemical physics letters* **2005,** *404* (4-6), 374-378.
119. Ajayan, P.; Ebbesen, T.; Ichihashi, T.; Iijima, S.; Tanigaki, K.; Hiura, H., Opening carbon nanotubes with oxygen and implications for filling. *Nature* **1993,** *362* (6420), 522-525.
120. Park, Y. S.; Choi, Y. C.; Kim, K. S.; Chung, D.-C.; Bae, D. J.; An, K. H.; Lim, S. C.; Zhu, X. Y.; Lee, Y. H., High yield purification of multiwalled carbon nanotubes by selective oxidation during thermal annealing. *Carbon* **2001,** *39* (5), 655-661.
121. Bonard, J. M.; Stora, T.; Salvetat, J. P.; Maier, F.; Stöckli, T.; Duschl, C.; Forró, L.; de Heer, W. A.; Châtelain, A., Purification and size-selection of carbon nanotubes. *Advanced Materials* **1997,** *9* (10), 827-831.
122. Shelimov, K. B.; Esenaliev, R. O.; Rinzler, A. G.; Huffman, C. B.; Smalley, R. E., Purification of single-wall carbon nanotubes by ultrasonically assisted filtration. *Chemical physics letters* **1998,** *282* (5-6), 429-434.
123. Abatemarco, T.; Stickel, J.; Belfort, J.; Frank, B. P.; Ajayan, P.; Belfort, G., Fractionation of multiwalled carbon nanotubes by cascade membrane microfiltration. *The Journal of Physical Chemistry B* **1999,** *103* (18), 3534-3538.
124. Jiang, Y.; Song, H.; Xu, R., Research on the dispersion of carbon nanotubes by ultrasonic oscillation, surfactant and centrifugation respectively and fiscal policies for its industrial development. *Ultrasonics sonochemistry* **2018,** *48*, 30-38.
125. Fagan, J. A.; Becker, M. L.; Chun, J.; Hobbie, E. K., Length fractionation of carbon nanotubes using centrifugation. *Advanced Materials* **2008,** *20* (9), 1609-1613.
126. Yu, A.; Bekyarova, E.; Itkis, M. E.; Fakhrutdinov, D.; Webster, R.; Haddon, R. C., Application of centrifugation to the large-scale purification of electric arc-produced single-walled carbon nanotubes. *Journal of the American Chemical Society* **2006,** *128* (30), 9902-9908.
127. Montoro, L. A.; Rosolen, J. M., A multi-step treatment to effective purification of single-walled carbon nanotubes. *Carbon* **2006,** *44* (15), 3293-3301.
128. Epp, J., X-ray diffraction (XRD) techniques for materials characterisation. In *Materials characterisation using nondestructive evaluation (NDE) methods*, Elsevier: 2016; pp 81-124.
129. Bunaciu, A., E. g. Udriştioiu and HY Aboul-Enein. *Crit. Rev. Anal. Chem* **2015,** *45*, 289-299.
130. Gabbott, P., *Principles and applications of thermal analysis*. John Wiley & Sons: 2008.
131. Zhou, W.; Wang, Z. L., *Scanning microscopy for nanotechnology: techniques and applications*. Springer science & business media: 2007.
132. Vladár, A. E.; Postek, M. T., The scanning electron microscope. In *Handbook of Charged Particle Optics*, CRC Press: 2017; pp 437-496.
133. Vernon-Parry, K., Scanning electron microscopy: an introduction. *III-Vs Review* **2000,** *13* (4), 40-44.
134. Wang, H.; Wu, Y.; Lassiter, B.; Nehl, C. L.; Hafner, J. H.; Nordlander, P.; Halas, N. J., Symmetry breaking in individual plasmonic nanoparticles. *Proceedings of the National Academy of Sciences* **2006,** *103* (29), 10856-10860.
135. Madsen, J.; Susi, T., The abTEM code: transmission electron microscopy from first principles. *Open Research Europe* **2021,** *1* (24), 24.
136. Sigle, W., Analytical transmission electron microscopy. *Annual Review of Materials Research* **2005,** *35* (1), 239-314.
137. Susi, T.; Madsen, J.; Ludacka, U.; Mortensen, J. J.; Pennycook, T. J.; Lee, Z.; Kotakoski, J.; Kaiser, U.; Meyer, J. C., Efficient first principles simulation of electron scattering factors for transmission electron microscopy. *Ultramicroscopy* **2019,** *197*, 16-22.

138. Malac, M.; Hettler, S.; Hayashida, M.; Kano, E.; Egerton, R. F.; Beleggia, M., Phase plates in the transmission electron microscope: operating principles and applications. *Microscopy* **2021,** *70* (1), 75-115.
139. Hodkiewicz, J.; Scientific, T., Characterising carbon materials with Raman spectroscopy. *Thermo Scientific Application Note* **2010,** *51946*.
140. Long, D. A., Raman spectroscopy. *New York* **1977,** *1*.
141. Auner, G. W.; Koya, S. K.; Huang, C.; Broadbent, B.; Trexler, M.; Auner, Z.; Elias, A.; Mehne, K. C.; Brusatori, M. A., Applications of Raman spectroscopy in cancer diagnosis. *Cancer and Metastasis Reviews* **2018,** *37* (4), 691-717.
142. Bardestani, R.; Patience, G. S.; Kaliaguine, S., Experimental methods in chemical engineering: specific surface area and pore size distribution measurements—BET, BJH, and DFT. *The Canadian Journal of Chemical Engineering* **2019,** *97* (11), 2781-2791.
143. Hwang, N.; Barron, A. R., BET surface area analysis of nanoparticles. *The Connexions project* **2011**, 1-11.
144. Bermeo, M.; Vega, L. F.; Abu-Sahra, M. R.; Khaleel, M., Critical assessment of the performance of next-generation carbon-based adsorbents for CO2 capture focused on their structural properties. *Science of The Total Environment* **2022,** *810*, 151720.
145. Gaslain, F. O.; Parmentier, J.; Valtchev, V. P.; Patarin, J., First zeolite carbon replica with a well resolved X-ray diffraction pattern. *Chemical communications* **2006,** (9), 991-993.
146. Musyoka, N. M.; Ren, J.; Langmi, H. W.; North, B. C.; Mathe, M., A comparison of hydrogen storage capacity of commercial and fly ash-derived zeolite X together with their respective templated carbon derivatives. *international journal of hydrogen energy* **2015,** *40* (37), 12705-12712.
147. Xia, Y.; Yang, Z.; Mokaya, R., CVD Nanocasting Routes to Zeolite-Templated Carbons for Hydrogen Storage. *Chemical Vapor Deposition* **2010,** *16* (10-12), 322-328.
148. Yang, Z.; Xia, Y.; Sun, X.; Mokaya, R., Preparation and hydrogen storage properties of zeolite-templated carbon materials nanocast via chemical vapor deposition: effect of the zeolite template and nitrogen doping. *The Journal of Physical Chemistry B* **2006,** *110* (37), 18424-18431.
149. Gholipour, F.; Mofarahi, M., Adsorption equilibrium of methane and carbon dioxide on zeolite 13X: Experimental and thermodynamic modeling. *The Journal of Supercritical Fluids* **2016,** *111*, 47-54.
150. Pour, A. A.; Sharifnia, S.; NeishaboriSalehi, R.; Ghodrati, M., Performance evaluation of clinoptilolite and 13X zeolites in CO2 separation from CO2/CH4 mixture. *Journal of Natural Gas Science and Engineering* **2015,** *26*, 1246-1253.
151. Silva, J. A.; Schumann, K.; Rodrigues, A. E., Sorption and kinetics of CO2 and CH4 in binderless beads of 13X zeolite. *Microporous and Mesoporous Materials* **2012,** *158*, 219-228.
152. Kareem, F. A. A.; Shariff, A.; Ullah, S.; Mellon, N.; Keong, L., Adsorption of pure and predicted binary (CO2: CH4) mixtures on 13X-Zeolite: Equilibrium and kinetic properties at offshore conditions. *Microporous and Mesoporous Materials* **2018,** *267*, 221-234.
153. Mulgundmath, V.; Tezel, F.; Saatcioglu, T.; Golden, T., Adsorption and separation of CO2/N2 and CO2/CH4 by 13X zeolite. *The Canadian Journal of Chemical Engineering* **2012,** *90* (3), 730-738.
154. Nishihara, H.; Yang, Q.-H.; Hou, P.-X.; Unno, M.; Yamauchi, S.; Saito, R.; Paredes, J. I.; Martínez-Alonso, A.; Tascón, J. M.; Sato, Y., A possible buckybowl-like structure of zeolite templated carbon. *Carbon* **2009,** *47* (5), 1220-1230.
155. Leyva-García, S.; Nueangnoraj, K.; Losano-Castello, D.; Nishihara, H.; Kyotani, T.; Morallon, E.; Cazorla-Amorós, D., Characterisation of a zeolite-templated carbon by electrochemical quartz crystal microbalance and in situ Raman spectroscopy. *Carbon* **2015,** *89*, 63-73.
156. Bokobsa, L.; Bruneel, J.-L.; Couzi, M., Raman spectroscopy as a tool for the analysis of carbon-based materials (highly oriented pyrolitic graphite, multilayer graphene and multiwall carbon nanotubes) and of some of their elastomeric composites. *Vibrational Spectroscopy* **2014,** *74*, 57-63.
157. Lee, S.-K.; Park, H.; Yoon, J. W.; Kim, K.; Cho, S. J.; Maurin, G.; Ryoo, R.; Chang, J.-S., Microporous 3D Graphene-like Zeolite-Templated Carbons for Preferential Adsorption of Ethane. *ACS Applied Materials & Interfaces* **2020,** *12* (25), 28484-28495.
158. Lowell, S.; Shields, J. E.; Thomas, M. A.; Thommes, M., *Characterisation of porous solids and powders: surface area, pore size and density*. Springer Science & Business Media: 2012; Vol. 16.
159. Song, X.; Xu, R.; Wang, K., The structural development of zeolite-templated carbon under pyrolysis. *Journal of Analytical and Applied Pyrolysis* **2013,** *100*, 153-157.

160. Musyoka, N. M.; Ren, J.; Annamalai, P.; Langmi, H. W.; North, B. C.; Mathe, M.; Bessarabov, D., Synthesis of a hybrid MIL-101 (Cr)/ZTC composite for hydrogen storage applications. *Research on Chemical Intermediates* **2016,** *42* (6), 5299-5307.
161. Furukawa, H.; Ko, N.; Go, Y. B.; Aratani, N.; Choi, S. B.; Choi, E.; Yasaydin, A. Ö.; Snurr, R. Q.; O'Keeffe, M.; Kim, J., Ultrahigh porosity in metal-organic frameworks. *Science* **2010,** *329* (5990), 424-428.
162. Düren, T.; Millange, F.; Férey, G.; Walton, K. S.; Snurr, R. Q., Calculating geometric surface areas as a characterisation tool for metal− organic frameworks. *The Journal of Physical Chemistry C* **2007,** *111* (42), 15350-15356.
163. Jedrzejewska, A.; Costa, S.; Cendrowski, K.; Kalenczuk, R.; Mijowska, E., Synthesis and characterisation of iron-filled multi-walled nanotubes. *Materials Science-Poland* **2011,** *29* (4), 299-304.
164. Siddheswaran, R.; Manikandan, D.; Avila, R. E.; Jeyanthi, C. E.; Mangalaraja, R. V., Formation of carbon nanotube forest over spin-coated Fe2O3 reduced thin-film by chemical vapor deposition. *Fullerenes, Nanotubes and Carbon Nanostructures* **2015,** *23* (5), 392-398.
165. Yang, Z.-F.; Li, L.-Y.; Hsieh, C.-T.; Juang, R.-S., Co-precipitation of magnetic Fe3O4 nanoparticles onto carbon nanotubes for removal of copper ions from aqueous solution. *Journal of the Taiwan Institute of Chemical Engineers* **2018,** *82*, 56-63.
166. Costa, S.; Borowiak-Palen, E.; Kruszynska, M.; Bachmatiuk, A.; Kalenczuk, R., Characterisation of carbon nanotubes by Raman spectroscopy. *Materials Science-Poland* **2008,** *26* (2), 433-441.
167. Sharma, D. K.; Bagotia, N., Production of graphene and carbon nanotubes using low cost carbon-based raw materials and their utilisation in the production of polycarbonate/ethylene methyl acrylate-based nanocomposites. *Indian Journal of Engineering and Materials Sciences (IJEMS)* **2021,** *27* (6), 1127-1135.
168. Dresselhaus, M. S.; Dresselhaus, G.; Saito, R.; Jorio, A., Raman spectroscopy of carbon nanotubes. *Physics reports* **2005,** *409* (2), 47-99.
169. Serrano-Lotina, A.; Dasa, L., Highly stable and active catalyst for hydrogen production from biogas. *Journal of power sources* **2013,** *238*, 81-86.
170. Ismagilov, Z.; Yashnik, S.; Shikina, N.; Matus, E.; Efimova, O.; Popova, A.; Nikitin, A., Effect of acid treatment on the functionalisation of surface, structural and textural properties of carbon nanotubes taunit. *Eurasian Chemico-Technological Journal* **2019,** *21* (4), 291-302.
171. Ordoñez Casanova, E. G.; Trejo Mandujano, H. A.; Aguirre, M. R., Microscopy and Spectroscopy Characterisation of Carbon Nanotubes Grown at Different Temperatures Using Cyclohexanol as Carbon Source. *Journal of Spectroscopy* **2019,** *2019*.
172. Ma, M.; Bétard, A.; Weber, I.; Al-Hokbany, N. S.; Fischer, R. A.; Metzler-Nolte, N., Iron-based metal–organic frameworks MIL-88B and NH2-MIL-88B: high quality microwave synthesis and solvent-induced lattice "breathing". *Crystal growth & design* **2013,** *13* (6), 2286-2291.
173. Bauer, S.; Serre, C.; Devic, T.; Horcajada, P.; Marrot, J.; Férey, G.; Stock, N., High-throughput assisted rationalisation of the formation of metal organic frameworks in the iron (III) aminoterephthalate solvothermal system. *Inorganic chemistry* **2008,** *47* (17), 7568-7576.
174. Gecgel, C.; Simsek, U. B.; Gozmen, B.; Turabik, M., Comparison of MIL-101 (Fe) and amine-functionalized MIL-101 (Fe) as photocatalysts for the removal of imidacloprid in aqueous solution. *Journal of the Iranian Chemical Society* **2019,** *16* (8), 1735-1748.
175. Thanh, H. T. M.; Phuong, T. T. T.; Le Hang, P. T.; Toan, T. T. T.; Tuyen, T. N.; Mau, T. X.; Khieu, D. Q., Comparative study of Pb (II) adsorption onto MIL–101 and Fe–MIL–101 from aqueous solutions. *Journal of environmental chemical engineering* **2018,** *6* (4), 4093-4102.
176. Farisabadi, A.; Moradi, M.; Hajati, S.; Kiani, M. A.; Espinos, J. P., Controlled thermolysis of MIL-101 (Fe, Cr) for synthesis of FexOy/porous carbon as negative electrode and Cr2O3/porous carbon as positive electrode of supercapacitor. *Applied Surface Science* **2019,** *469*, 192-203.
177. Li, J.; Zhang, Y., A simple purification for single-walled carbon nanotubes. *Physica E: Low-dimensional Systems and Nanostructures* **2005,** *28* (3), 309-312.
178. Wang, C.; Chang, J.; Amatosa, T. A.; Guo, Y.; Lin, F.; Yen, Y., Carbon Nanotubes Grown Using Solid Polymer Chemical Vapor Deposition in a Fluidised Bed Reactor with Iron (III) Nitrate, Iron (III) Chloride and Nickel (II) Chloride Catalysts. *Inventions* **2018,** *3* (1), 18.
179. Donohue, M.; Aranovich, G., Classification of Gibbs adsorption isotherms. *Advances in colloid and interface science* **1998,** *76*, 137-152.